EXPERIMENTAL INVESTIGATION ON THE OUT-OF-PLANE BEHAVIOUR OF CONCRETE MASONRY INFILLED FRAMES

by

Chongyang Wang

Submitted in partial fulfilment of the requirements
for the degree of Master of Applied Science

at

Dalhousie University
Halifax, Nova Scotia
October 2017

To Parents and Wife

爱你们

TABLE OF CONTENTS

LIST OF TABLES

LIST OF FIGURES

ABSTRACT

Previous studies on the masonry infilled frame have shown that masonry infills that are built in contact with their bounding frames display greater out-of-plane strengths than conventional flexural walls, and this increased capacity is attributed to a mechanism referred to as arching action. The literature review, however, yielded limited scientific information on analysis and design of these infills considering various geometric and material parameters of masonry infilled frames. Although some methods were developed to estimate the out-of-plane strength of infills, their efficacy has not been thoroughly assessed. For design, the Canadian standard CSA S304-14 permits the use of first principle mechanics for the out-of-plane strength calculation but without providing specific equations. The American masonry standard MSJC 2013 adopts a semi-empirical equation for out-of-plane strength calculation for masonry infills of simple conditions.

As an integral part of an on-going research on out-of-plane behaviour of masonry infills, this study was motivated to augment the existing experimental database on out-of-plane behaviour and strength of masonry infills by expanding on the variations on the parameters, and to assess the efficacy of existing analytical methods for infill out-of-plane strength calculation. A total of five scaled masonry infilled frame specimens including four masonry infilled RC frames and one masonry infilled steel frame were tested to failure under uniformly distributed out-of-plane loading. Parameters considered for the RC frame specimens included infill opening (door opening), prior in-plane damage, and gaps at either frame-to-beam or frame-to-column interfaces. The steel frame specimen was designed as a control specimen. The experimental results were presented and discussed in terms of load vs. displacement response, cracking pattern, and failure mode for each specimen and the effect of parameters was studied. The existing analytical methods for out-of-plane strength calculation were examined using the available test results.

Experimental results showed that all studied parameters have a significant effect on the out-of-plane behaviour and strength of infills. It was found that the reduction in the out-of-plane strength and the prior in-plane damage level is in a more or less linear relationship. The infill-top beam gap is more detrimental to the infill strength than the infill-column gap. The presence of door opening resulted in more reduction in ultimate strength than a window opening of the same size.

The existing methods for “regular” infills was shown to provide inconsistently strength estimate for specimens with RC frames vs. steel frames. None was able to provide accurate estimates for both materials. For “irregular” infills (opening, gap, in-plane damage), the methods by Dawe and Seah (1989) and MSJC 2013 for interfacial gap consideration performed reasonably well while the methods for infill openings and prior in-plane damage produced resulted in significant disparity with the experimental results.

LIST OF ABBREVIATIONS AND SYMBOLS USED

Abbreviations

ASTM	American Society for Testing and Materials
CMUs	Concrete masonry units
COV	Coefficient of variation
CSA	Canadian Standards Association
FEMA	Federal Emergency Management Agency
IF-RC-DO	Reinforced concrete infilled frame with door opening
IF-RC-ID	Reinforced concrete infilled frame with prior in-plane damage
IF-RC-TG	Reinforced concrete infilled frame with top gap
IF-RC-SG	Reinforced concrete infilled frame with side gap
IF-S	Steel infilled frame
LVDT	Linear variable differential transformer
MSJC	Masonry Society Joint Committee
NBCC	National Building Code of Canada
RC	Reinforced concrete
URM	Unreinforced masonry

Symbols

A_o	Area of opening in infill panel
A_p	Area of infill panel without opening
A_w	Effective area of the effective throat the weld
C	Internal thrust force
C_h, C_v	Horizontal, vertical clamping compressive force
D	Size of fillet weld
E	Modulus of elasticity
E_b, E_{bb}	Modulus of elasticity of bounding beam
E_c, E_{bc}	Modulus of elasticity of bounding column
E_f	Modulus of elasticity of bounding frame
E_m	Modulus of elasticity of masonry
EI	Flexural stiffness of bounding frame
E_fI_f	Flexural stiffness of the weakest member of the bounding frame
f_c	Maximum stress at contact surface after arching action is enabled
f'_c	Compressive strength of concrete
f'_j	Compressive strength of mortar

f'_m	Compressive strength of masonry
f_{tn}	Flexural tensile strength of masonry normal to bed joints
f_{tp}	Flexural tensile strength of masonry parallel to bed joints
f_u	Ultimate stress of steel
f_y	Yield stress of steel
F_{app}	Applied load of infilled frame under in-plane loading
F_{cr}	First crack load of the infilled frame under in-plane loading
F_r	Modification factor that depend on whether or not the opening is blast-resisting
g	Maximum gap that could exit at the infill-bounding frame interaction
g_o	Axial shortening of the infill
G	Shear modulus
G_b, G_c	Shear modulus of bounding beam, bounding column
GJ	Torsional stiffness of the bounding frame
G_fJ_f	Torsional stiffness of weakest member of the bounding frame
h, $h_{inf,}$	Height of the infill
h_{eo}	Effective height of the infill with opening
h_o	Height of the opening

H	Height of the infill
I_b, I_{bb}	Moment of inertia of bounding beam
I_c, I_{bc}	Moment of inertia of bounding column
I_m	Effective moment of inertia of infill
J_b, J_c	Torsional constant of bounding beam, bounding column
K_{cr}	Slope of the line connecting origin and point having the first crack
K_{ini}	Slope of tangent line of initial linear portion of the load vs. displacement curve
K_{ult}	Slope of the line connecting origin and point having the ultimate load
l, l_{inf}	Length of the infill
l_{eo}	The effective length of the infill with opening
l_o	Length of the opening
L	Length of the infill
M_{rh}	Horizontal bending moment resistant
M_{rv}	Vertical bending moment resistant
M_w	Strength reduction factor for multi-orientation fillet welds to account for ductility incompatibility of the individual weld segments
M_{yh}	Horizontal flexural resisting moment

M_{yv}	Vertical flexural resisting moment
P_{ana}	Out-of-plane strength of the infill obtained from analytical method
P_{cr}	First crack pressure of the infill under out-of-plane loading
P_{ini}	Pressure at end of the initial linear portion of the load vs. displacement curve
P_{fail}	Pressure corresponding to the failure moment of infill
P_{ult}	Ultimate pressure of the infill under out-of-plane loading
q	Applied out-of-plane loading
q'	Resistance of the infill without opening
q_{cr}	Out-of-plane load at the occurrence of boundary crushing of infill
q_{max}	Out-of-plane load at the occurrence of transverse instability of infill
q_{ult}	Ultimate out-of-plane resistance of infill
R	Out-of-plane ductility factor
R_{in}	Prior in-plane damage reduction factor
R_1	A reduction factor accounting for prior in-plane damage
R_2	A reduction factor accounting for bounding frame stiffness
S_m	Effective section modulus of infill
t, t_{inf}	Thickness of the infill

t_e	Effective thickness of the infill
V_r	Shear resistance of fillet weld
w, w_f	Applied out-of-plane load
w_d	Oven-dry weight of masonry unit
w_i	Immersed weight of masonry unit
w_r	Received weight of masonry unit
w_s	Saturated weight of masonry unit
W	Width of infill
x_{yh}, x_{yv}	Horizontal, vertical arching out-of-plane displacement
X_u	Ultimate strength as rated by the electrode classification number
α, α_{arch}	A measure of relative stiffness of the bounding column
β, β_{arch}	A measure of relative stiffness of the bounding beam
γ	A factor that accounts for depth of compression with value of 0.9
δ	Displacement of the infilled frame under in-plane loading
δ_{app}	Displacement at applied load of the infilled frame under in-plane loading
δ_{cr}	First crack displacement of the infilled frame under in-plane loading
δ_{ult}	Displacement at ultimate load of the infilled frame under in-plane loading

Δ_{ana}	Out-of-plane displacement of the infill obtained from analytical method
Δ_{cr}	First crack displacement of the infill under out-of-plane loading
Δ_{exp}	Experimental Out-of-plane displacement of infill
Δ_{fail}	Displacement at failure load of the infill under out-of-plane loading
Δ_{g}	Out-of-plane displacement caused by the exiting gap
Δ_{ini}	Displacement at end of the initial linear portion of the load vs. displacement curve
Δ_{0}	Midspan deflection of the infill in one-way arching condition
Δ_{ult}	Displacement at ultimate load of the infill under out-of-plane loading
$\Delta_{0.6ult}$	Displacement at 60% of ultimate load of the infill under out-of-plane loading
ε_m	Strain of the infill corresponding to axial shortening
θ	Angle whose tangent is the infill height-to-length aspect ratio
λ, λ_2	A reduction factor accounting for slenderness ratio of infill
Φ_m	Resistance factor for masonry
Φ_w	Resistance factor for fillet weld

ACKNOWLEDGEMENTS

I would like to first and foremost show my deepest gratitude to my supervisor, Dr. Yi Liu, who has provided me with valuable guidance in every stage of my studies at Dalhousie University. Without her enlightening instruction, impressive kindness and patience, I could not have completed my dissertation. Her keen and vigorous academic observation enlightens me not only in this dissertation but also in my future study.

I would extend my thanks to my committee members, Dr. Hany El-Naggar and Dr. Navid Bahrani, for taking the time to review this thesis and providing valuable feedback.

I would like to thank the departmental technicians Mr. Brian Kennedy, Mr. Brian Liekens, Mr. Blair Nickerson, and the mason Gerry Hubley for their assistance and contribution during the experiment.

My thanks also go to the Canadian Concrete Masonry Products Association for providing financial assistance.

Lastly, I would like to express my thanks to my parents and my wife for their valuable encouragement, spiritual support, and unconditional love during my study.

CHAPTER 1 INTRODUCTION

1.1 BACKGROUND OF MASONRY INFILLS

The use of masonry as a construction material dates back ten thousand years ago (Drysdale and Hamid 2005). Due to its durability and versatility, masonry has remained as one of the primary materials used in building construction either on its own or in combination with concrete and steel materials. A masonry infill is one example that masonry is used with other structural materials. Masonry walls built inside either a concrete or steel frame are referred to as masonry infills. As shown in Figure 1.1, they are commonly used either as exterior walls to complete building envelopes or as interior partition walls. The previous studies have shown that the presence of infills will significantly affect the behaviour of the bounding frame and a proper design for infilled frames needs to consider the interaction between the infill and the frame for all loading conditions. Previous research conducted from 1960s to 1990s showed that when lateral loading is applied to the infilled system, the infill is shown to increase the strength, stiffness and ductility of frames to a great extent. When the infill is subjected to out-of-plane loading, the bounding frame is shown to provide a boundary support that leads to increases in the out-of-plane strength of infills. Despite the research evidence on the benefit of infill-frame interaction, due to the complexity of the system consisting of two different materials where each could have various geometric and

material properties, the research findings have not been translated into practice. For industry practice, the masonry infills are often not considered as structural elements, and the lateral load resisting relies on other steel or concrete elements. Thus, the infills are commonly isolated from the bounding frames in construction so that they do not partake in load sharing with the frame. To correct the disconnect between the research findings and industry practice, since 2000 there is a renewed interest in the research community to address both the in-plane and out-of-plane behaviour of masonry infills where varying geometric and material parameters are included through systematic studies.

(a) (b)

Figure 1.1 Application of Masonry Infilled Frame

(a) Reinforced concrete frame structures with brick masonry infills (word house encyclopedia); (b) Steel frame structures with concrete masonry infills (word house encyclopedia)

1.2 MASONRY INFILLS UNDER OUT-OF-PLANE LOADING

The infilled frames have been studied since 1960s, but most research focused on the behaviour and strength of infilled frames under in-plane loading. A comprehensive

literature review on the in-plane behaviour of infills can be found in Chen (2016). On the contrary, the literature review yielded limited scientific information on the out-of-plane behaviour and strength of infilled frames and even within the few available studies, the number of parameters and their variations are all limited in comparison. The Canadian masonry standard CSA S304-14 (2014) and American masonry standard MSJC 2013 contain design provisions for the stiffness and strength of infills under in-plane loading, albeit for the simple situations of infills. In the case of out-of-plane loading, the CSA S304-14 provides no design equations or explicit guidelines but a statement permitting the use of first principle mechanics for analysis. The MSJC 2013, on the other hand, provides a semi-empirical equation for calculation of infills' out-of-plane strength based on the methods initially proposed by Dawe and Seah (1989) and later modified by Flanagan and Bennett (1999). However, the efficacy of the equation in application of various situations of infills and bounding frames has not been thoroughly examined.

Among the exiting studies on the out-of-plane behaviour of infills, the general findings indicate that the masonry infills under certain conditions can resist much larger out-of-plane loading than that predicted by conventional elastic or flexural analysis. The mechanism for this capacity increase is commonly referred to as arching action. Under the out-of-plane loading, the flexural behaviour contributes to the main out-of-plane load capacity for infills until first major cracking occurs usually at the midheight where moment is maximum. After

cracking, masonry is separated into two segments. Further displacement causes the segments to rotate with respect to each other and also butt against the boundary provided by frame members thus creating thrust forces at each end. Once arching action is enabled, the out-of-plane strength of the wall is believed to be dependent on the compressive strength of masonry rather than its tensile strength. It was found that the out-of-plane load capacity of masonry infills was several times that predicted by flexural analysis (Gabrielsen et al. 1975). Existing studies on this arching action focused on the effects of several geometric properties of the infilled frame such as the aspect ratio and slenderness ratio of the infill, and the bounding frame rigidity. Several analytical methods have also been proposed for the calculation of out-of-plane strength of infills. However, the existing methods were mainly developed based on a limited number of data points covering a limited range of variation of parameters, and their application in a wide range of infilled frame situations is not verified.

More research is in need to provide reliable experimental results that could be used to further understand the behaviour and validate the existing methods. Furthermore, in-plane and out-of-plane behaviour may have some level of interaction in the event of earthquake. It is conceivable that the in-plane damage sustained in the infill could affect its out-of-plane strength and vice versa. However, the potential interaction of in-plane and out-of-plane behaviour of masonry infills has received little research attention.

A multi-phased research program is being conducted at Dalhousie University to investigate the out-of-plane behaviour and strength of masonry infills bounded by frames. As an extension of a previous study (Sepasdar 2017), this study is to further the investigation to include both reinforced concrete (RC) and steel frames as bounding frames, and also expanded the range of several influential parameters.

1.3 RESEARCH OBJECTIVES

This study involved an experimental investigation of the out-of-plane behaviour and strength of masonry infills with a focus on the effect of infill opening, frame-to-infill interfacial gaps, and prior in-plane damage. The objectives of this study include the following:

1. To analyze the effect of several key parameters including infill opening, frame-to-infill interfacial gaps, and prior in-plane damage on the out-of-plane behaviour and strength of infilled RC frames.
2. To investigate the difference of out-of-plane behaviour and strength between steel and RC infilled frames.
3. To compare the results of this experimental study with values estimated based on the existing analytical methods.
4. To present appropriate conclusions and recommendations that obtained from the

results of this experimental study.

1.4 DOCUMENT ORGANIZATION

The thesis consists of six chapters. Chapter 1 introduces the objectives and scope of this thesis. Chapter 2 presents a brief literature review of previous studies on out-of-plane behaviour of infilled frame, analytical methods and design codes in North America for infilled frames under out-of-plane loading. Chapter 3 provides a detailed description of the experimental program including construction of masonry infilled frames, test set-up and procedure, and component tests of the materials. Chapter 4 contains discussion of the results obtained from the experimental program. Chapter 5 presents the comparison between experimental results and existing methods. Chapter 6 provides the summary and conclusions of the research, and recommendation for future research.

CHAPTER 2 LITERATURE REVIEW

2.1 INTRODUCTION

The primary objective of this research is to investigate the effect of several parameters on the out-of-plane behaviour and strength of masonry infills. The following sections present a summary of the available literature on the out-of-plane behaviour of masonry infills with a focus on the effect of identified influential parameters.

2.2 GENERAL BEHAVIOUR

As mentioned previously, the out-of-plane resistance of masonry infills bounded by frames is derived largely by the arching action rather than conventional flexural behaviour. The arching action phenomenon was first analyzed by McDowell et al. (1956). This model assumes that after the development of tension cracking at the supports and mid-height of an infill where maximum moments occur under the out-of-plane load, the wall acts as two rigid segments, with each segment rotating about its end until either the masonry crushes or the two segments snap through. Figure 2.1 illustrates the proposed load transfer mechanism through arching action. Rotation enabled by three hinges after cracking will cause the rigid segments to push against either the rigid supports or each other, generating internal thrust forces (T) to resist the out-of-plane load. Using an idealized masonry material stress-strain relationship, the out-of-plane load can be estimated using equilibrium

between the moment caused by internal thrust load and the external applied moment at the mid height. This mechanism, relying on thrust forces generated at two boundaries (top and bottom) with the frame, can then be considered as one-way arching action.

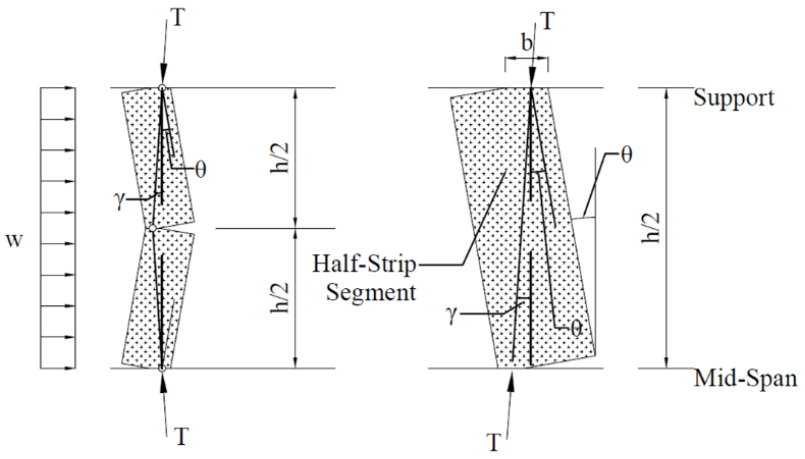

Figure 2.1 Idealized Model for Arching Action (Abrams et al., 1996)

Most analytical models were developed based on the one-way arching mechanism as described above. Several studies (Dawe and Seah 1989; Angel 1994; Henderson et al. 2003) showed that two-way arching action can also develop and can result in a substantially higher ultimate load than one-way arching action. However, they also pointed out that the interfacial gap due to wall shrinkage and settlement will affect the arching action and thus the out-of-plane strength of infills. It has also been shown that development of arching action enhanced the stability of infills even after the ultimate capacity was achieved (Flanagan and Bennett 1993), and slipping or overturning of masonry infills is less significant than that of flexural masonry walls due to the improved stability of infills

(Bennett et al. 1996; Dafnis et al. 2002). A sample calculation on both arching and flexural analysis of an infill is presented in APPENDIX A to demonstrate the capacity difference.

2.3 EXPERIMENTAL STUDIES ON PARAMETERS

Previous studies have identified several geometric and material parameters that are influential in the consideration of arching action and out-of-plane strength of masonry infills. They are slenderness of infills, gaps between infills and frames, strength of masonry, frame rigidity, and infill opening.

2.3.1 Slenderness Ratio of Infills

Anderson (1984) tested masonry wall panels subjected to out-of-plane loading applied through hydraulic jacks. It was found that the out-of-plane strength of masonry panels decreased with increases in the slenderness ratio of panels. For the masonry panels with small slenderness ratio, the failure mode was governed by crushing due to the development of arching action. However, for slenderness ratios in the range of 35-40, the failure of masonry panels was governed by instability.

Angel (1994) tested eight masonry infilled RC frames that consisted of either clay brick or concrete masonry block infills to investigate the effect of slenderness ratio on the out-of-plane strength of infilled frames. His study indicated that if the slenderness ratio of infills was reduced in half (h/t ratios of 34 to 17), the out-of-plane strength of the infills increased

by more than seven times. For the infills with a slenderness ratio larger than 30, arching action had significantly less effect on the out-of-plane resistance of masonry infills.

2.3.2 Gaps between Infills and Frames

A gap may be existent due to defective workmanship, wall shrinkage and settlement, or an intentional movement joint placed between the infill and frame. Most studies agreed that gaps at the wall boundaries not only significantly influence the development of arching action, but also the out-of-plane strength and behaviour of masonry infills.

Gabrielsen et al. (1975) tested masonry walls having a top gap between the wall panel and an abutment under a uniform blast load. The gaps of 0.1 inch (2.54 mm) and 0.2 inch (5.08 mm) were considered. It was found that the gapped infills were still considerably stronger than either cantilevered walls or walls pinned on two opposite edges due to the forming of arching action, but the gapped walls only resisted 1/6 to 1/8 of the load that sustained by infills without gaps.

Gabrielsen and Kaplan (1976) showed that the development of arching action was different in the infills with tight rigid supports (without gap) and with small gaps at the top wall boundaries. A symmetrical three-hinged arch was formed in an infill with tight rigid supports, while the infill with gaps needed to displace more in order to engage the support thus creating an unsymmetrical arch as shown in Figure 2.2.

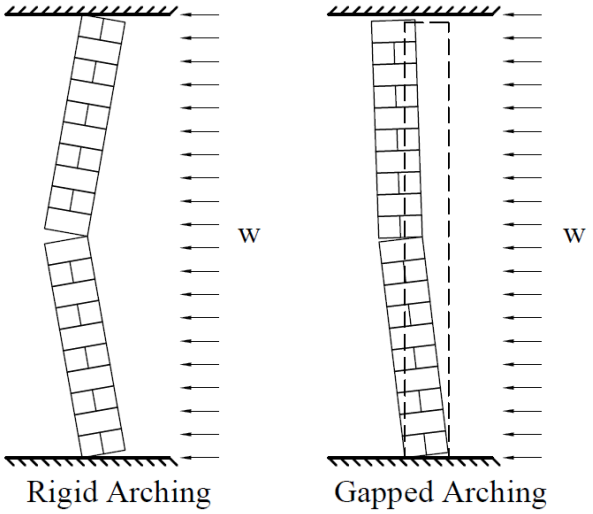

Figure 2.2 The Differences in Motion between Rigid and Gapped Arching (Gabrielsen and Kaplan, 1976)

Dafnis et al. (2002) conducted a shaking table test to study the out-of-plane arching behaviour of full scale masonry walls with a 3 mm gap between the top abutment and the infill. It was found that during the dynamic loading, the gapped specimen experienced a larger deformation than the non-gapped counterpart before the arching action developed and the out-of-plane capacity was smaller.

Drysdale and Hamid (2005) investigated the development of arching action in gapped infills using mechanics of rigid body movement. They concluded that the maximum gap that could exist was controlled by the diagonal length between the compression forces at the hinges, and the maximum gap was expressed as:

$$g \leq \frac{4(\gamma t)^2}{l} \qquad [2\text{-}1]$$

where l is the length of infills, and γ=0.9.

Additionally, they also proposed the following equation for calculating the infill out-of-plane displacement, Δ_g, taking into account of the gap size, g.

$$\Delta_g = \frac{g(l - g)}{4\gamma t} \qquad [2\text{-}2]$$

2.3.3 Compressive Strength of Masonry

Abrams et al. (1996) tested clay brick infilled RC frames subjected to out-of-plane load applied through an air bag. The out-of-plane strength of masonry infills was shown to increase as the compressive strength of masonry increased. The out-of-plane strength of the infill with a larger compressive strength of masonry (11 MPa) was more than doubled the strength of the infill with a lower compressive strength (5.6 MPa). An experimental study by Moghaddam and Goudarzi (2010) performed on masonry infilled RC frames showed that the higher masonry strength, the smaller out-of-plane deflection and the out-of-plane strength of masonry panels increased linearly with an increase in the compressive strength of masonry.

2.3.4 Frame Rigidity

Experiments conducted by Monk (1958) and Gabrielsen and Wilton (1974) showed qualitatively that the out-of-plane strength of infills bounded by flexible frames was less than that of the infills bounded by rigid frames.

Dawe and Seah (1989) investigated masonry infilled steel frames having different frame stiffness, in particular column stiffness, under uniform pressure applied through an air bag. It was found that both the flexural stiffness and torsional stiffness of frame columns had an effect on the out-of-plane strength of infills and they in turn proposed an equation to include the effect of both to calculate the out-of-plane strength of infills. This method formed the basis for the provision in the American masonry standard MSJC for infill design which is discussed later.

Angel (1994) studied the effect of stiffness of bounding frames on the out-of-plane strength of infills using numerical simulations. They concluded that the out-of-plane strength of infilled frame can be benefited by using stiffer frame members. However, the increase in out-of-plane strength is insignificant when the flexural stiffness (EI) of the frame exceeds $2.6x10^{13}$ N-mm^2. He developed a flexural stiffness reduction factor based on the flexural stiffness of the frame to modify the strength of infill bounding by less stiff frames.

2.3.5 Infill Opening

Experiments conducted by Gabrielsen et al. (1975) showed that the infill opening did not significantly decrease the out-of-plane strength of masonry panel with the development of arching action, and in his study, the infill opening actually increased the out-of-plane strength.

Dawe and Seah (1989) tested the specimens consisting of a 3.6 m x 2.8 m masonry infilled steel frame with a 1.6 m x 1.2 m central opening (19% of infill area). Comparing with the out-of-plane strength of infill specimen without opening, a reduction of 9.4% was observed and the deflection of the infill was significantly smaller than the solid masonry infill.

Akhoundi et al. (2016) investigated a brick masonry infilled frame having a center opening of 13% area of the infill under uniform out-of-plane pressure. The test results showed that the infill with opening did not show significant reduction in its out-of-plane strength.

2.3.6 Prior In-Plane Damage

In recent years, the interaction of in-plane and out-of-plane behaviour, in particular, the effect of damage sustained from in-plane loading on the out-of-plane strength of the infill and vice versa, became a topic of interest. This is in recognition that if masonry infills are incorporated into the lateral load resisting system, the potential damage caused by resisting in-plane lateral load may have an effect on the out-of-plane strength.

Angel (1994) investigated the effect of in-plane damage caused by lateral loading on the out-of-plane strength of infilled RC frames. It was found that the out-of-plane strength decreased in accordance with the magnitude of in-plane damage, and he developed an out-of-plane strength reduction factor in terms of the ratio of maximum in-plane applied displacement to the twice in-plane displacement at which the first crack occurred.

Porto et al. (2013) conducted out-of-plane tests on full scale clay masonry infilled RC frames with various levels of prior damage defined by in-plane deformation of the frame. They found that the out-of-plane strength of the masonry infilled frames can be related to the in-plane drift. Compared with the specimen with 0.5% in-plane drift, a 1.2% in-plane drift resulted in 39% and 19% reductions in the initial stiffness and out-of-plane strength respectively.

Furtado et al. (2016) tested three full scale clay masonry infilled RC frames with in-plane damages under cyclic out-of-plane loading. The specimen was loaded laterally to a 15 mm displacement which was twice the displacement at the ultimate load. Compared with the specimen with in-plane damage, the ultimate out-of-plane strength for undamaged specimen was four times higher and the displacement was also greater. It was also shown that the failure mode of the infilled frame under out-of-plane load was depended on the previous in-plane damage. Comparing with the specimen without prior in-plane damage, the development of arching action was not significant for the specimen with prior in-plane damage, and no cracking occurred in the middle of the infill.

2.4 ANALYTICAL METHODS

Several analytical methods have been developed by various researchers to compute the out-of-plane strength of masonry infills. Aside from the method based on first principle

mechanics, other methods are empirical or semi-empirical in nature, developed mainly using curve-fitting on either experimental data or numerical simulation results.

The methodology presented for arching action by McDowell et al. (1956) was adopted in the British Standards "Code of practice for use of masonry" (BS 5628 2005) for infill out-of-plane strength calculation. Figure 2.3 illustrates the first principle of mechanics using this method. As expressed below, this equation applies to the infills after cracking occurs.

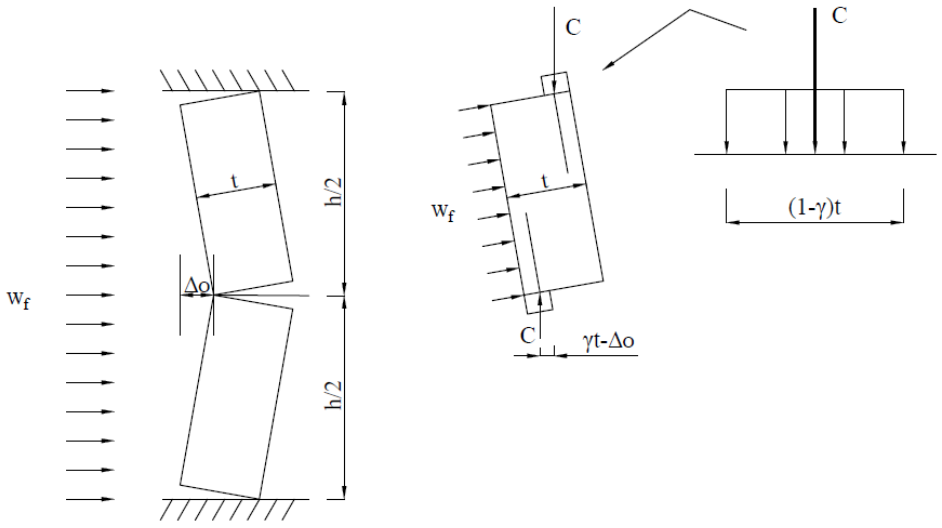

Figure 2.3 Arching Action in Mechanics of Arching (Drysdale and Hamid, 2005)

$$w_f = \frac{8C}{h^2}(\gamma t - \Delta_0) \qquad [2\text{-}3]$$

where γ=0.9, Δ_0 is the wall deflection, t and h are thickness and height of the infill. The term C is essentially the thrust force from masonry segments being compressed against each other and against the frame member and is given as:

$$C = \emptyset_m 0.85 f'_j (0.1t) \qquad [2\text{-}4]$$

where f'_j is the compressive strength of the mortar joint at contact surface. It is assumed that the contact length for developing thrust force is 0.1t. When a top gap exists, the wall deflection expressed in Eqn [2-2] can be used in the place of Δ_0 provided that the gap size satisfies the limit determined by Eqn [2-1].

Klinger et al. (1996) proposed an analytical method that considers two-way arching based on the geometry of the cracking pattern as shown in Figure 2.4 as follows:

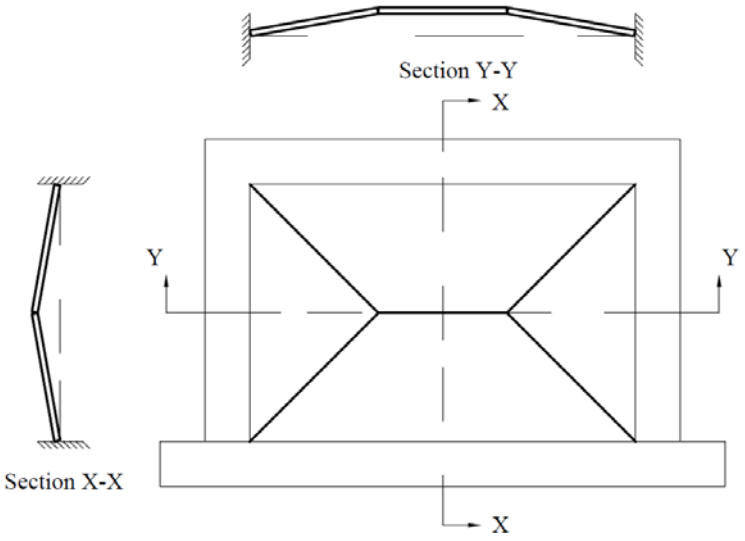

Figure 2.4 Idealized Deflected Shape of a Typical Infill under Out-of-Plane Loading

$$q = \frac{8}{h^2 l}\left\{M_{yv}[(l-h) + h\ln(2)] + M_{yh}\left(\frac{x_{yv}}{x_{yh}}\right)\ln\left(\frac{1}{1-h/2}\right)l\right\} \qquad [2\text{-}5]$$

where M_{yv} is calculated as

$$M_{yv} = \frac{0.85f'_m}{4}\left(t - x_{yv}\right)^2 \qquad [2\text{-}6]$$

where x_{yv} is the maximum vertical deflection of the infill panel at the ultimate load and is calculated as

$$x_{yv} = \frac{tf'_m}{1{,}000E\left[1 - \frac{h}{2\sqrt{(h/2)^2 + t^2}}\right]} \qquad [2\text{-}7]$$

The term M_{yh} in Eqn [2-5] is calculated from Eqn [2-6] by replacing x_{yv} with x_{yh}, and x_{yh} is calculated from Eqn [2-7] by substituting h with l.

Based on experimental results, Dawe and Seah (1989) proposed two sets of equations to evaluate the out-of-plane strength of infills bounded by steel frames. The effect of frame stiffness and boundary supports on the out-of-plane behaviour of infills was taken into consideration. The method showed that the inclusion of arching action in yield line analysis improved the capacity prediction over that predicted by the conventional yield line theory. The ultimate uniform out-of-plane pressure q_{ult} (kPa), that an infill can resist is estimated as:

1. For a panel supported on three sides and free at the top

$$q_{ult} = 800(f'_m)^{0.75}t^2\alpha/L^{2.5} \qquad [2\text{-}8]$$

where

$$\alpha = \frac{1}{H}(EI_c H^2 + GJ_c tH)^{0.25} \leq 75 \quad [2\text{-}9]$$

2. For a panel supported on four sides

$$q_{ult} = 800(f'_m)^{0.75} t^2 \{\alpha/L^{2.5} + \beta/H^{2.5}\} \quad [2\text{-}10]$$

where

$$\alpha = \frac{1}{H}(EI_c H^2 + GJ_c tH)^{0.25} \leq 50 \quad [2\text{-}11]$$

$$\beta = \frac{1}{L}(EI_b L^2 + GJ_b tL)^{0.25} \leq 50 \quad [2\text{-}12]$$

In Eqn [2-8] to [2-12], f'_m is the compressive strength of masonry (kPa), t is the thickness of the panel (mm), L is the length of the panel (mm), H is the height of the panel (mm), E and G are the Young's modulus (MPa) and shear modulus (MPa) of the frame members respectively, I_c and I_b are moments of inertia (mm^4) of columns and beam respectively, and J_c and J_b are torsional constants (mm^4) of columns and beam respectively.

Angel (1994) proposed an analytical method based on experimental and numerical results where the infill slenderness ratio, frame stiffness, and potential in-plane damage are considered. The out-of-plane strength of infills is expressed as:

$$q = \frac{2f'_m}{(\frac{h}{t})} R_1 R_2 \lambda \quad [2\text{-}13]$$

where R_1 is the reduction factor for prior in-plane loading damage, as defined in Eqn [2-

14]; R_2 is the reduction factor to account for the effect of frame stiffness, as defined in Eqn [2-15]. λ is used to account for the slenderness effect of the infill for value of h/t between 10 and 30, as defined in Eqn [2-16].

$$R_1 = \left[1.08 - 0.015\left(\frac{h}{t}\right) - 0.00049\left(\frac{h}{t}\right)^2 + 0.000013\left(\frac{h}{t}\right)^3\right]^{\frac{\delta}{2\delta_{cr}}} \left(\frac{\delta}{2\delta_{cr}} > 0.5\right)$$
$$R_1 = 1 \left(\frac{\delta}{2\delta_{cr}} \leq 0.5\right) \qquad [2\text{-}14]$$

where δ and δ_{cr} are the maximum in-plane horizontal displacement of the infill prior to the out-of-plane loading and the in-plane horizontal displacement of the infill at first cracking load, respectively.

$$R_2 = 0.357 + 7.14 \times 10^{-8} EI \ (2.0 \times 10^6 < EI < 9.0 \times 10^6)$$
$$R_2 = 1 \ (EI \geq 9.0 \times 10^6) \qquad [2\text{-}15]$$

where the unit of EI is kip-in^2.

$$\lambda = 0.154 \exp\left(-0.0985 \frac{h}{t}\right) \qquad [2\text{-}16]$$

Flanagan and Bennett (1999) modified the work of Dawe and Seah (1989), and presented the following equations to calculate the out-of-plane capacity of masonry infills. For most practical frames, the GJ_ctH and GJ_btL terms in the method proposed by Dawe and Seah (1989) are much smaller than EI_cH^2 and EI_bL^2 terms. Thus, Flanagan and Bennett eliminated the torsional terms (GJ_ctH and GJ_btL) and expressed the capacity in the imperial units.

$$q_{ult} = 4.1(f'_m)^{0.75}t^2\left(\frac{\alpha}{l^{2.5}} + \frac{\beta}{h^{2.5}}\right) \quad [2\text{-}17]$$

α and β are shown in Eqn [2-18a] and [2-18b], respectively.

$$\alpha = \frac{1}{h}(E_c I_c h^2)^{0.25} \leq 50 \quad [2\text{-}18a]$$

$$\beta = \frac{1}{l}(E_b I_b l^2)^{0.25} \leq 50 \quad [2\text{-}18b]$$

If the h/t is less than 8, the thickness of the infill (t) should be used as a value of 1/8 of the infill height in Eqn [2-17] and [2-18]. They also suggested that the formula given in FEMA 356 be used to determine the deflection of the infill panel with the value of h/t less than 25 at the ultimate load, Δ_{ult}, as shown in Eqn [2-19].

$$\frac{\Delta_{ult}}{h} = \frac{0.002\left(\frac{h}{t}\right)}{1 + \sqrt{1 - 0.002\left(\frac{h}{t}\right)^2}} \quad [2\text{-}19]$$

Moghaddam and Goudarzi (2010) proposed the following two equations to calculate the out-of-plane strength of infills considering both boundary crushing (q_{cr}) in relation to the panel slenderness ratio, the compressive strength, and elasticity modulus of the masonry and the boundary stiffness; and transverse instability (q_{max}) that resulted from large transverse deflection of the infill as failure modes.

$$q_r = \min \begin{Bmatrix} q_{cr} = \left[0.85 - \left(0.12 + \frac{0.045}{\alpha}\right)\frac{f'_m}{E_m}\lambda^2\right]\frac{f'_m}{\lambda^2} \\ q_{max} = \frac{0.18E_m}{\left(0.12 + \frac{0.045}{\alpha}\right)\lambda^4} \end{Bmatrix} \text{(in kPa)} \qquad [2\text{-}20]$$

where λ is the slenderness ratio (h/t) of infill, α is the ratio of the support stiffness to the vertical in-plane stiffness of the panel, and is expressed as:

$$\alpha = \frac{K}{(E_m tl/h)} \qquad [2\text{-}21]$$

where K is the stiffness of the top beam and can be calculated using Eqn [2-22], which considers the infilled frame has a fixed-end beam.

$$K = \frac{384E_f I_b}{l^3} \qquad [2\text{-}22]$$

where E_f is the modulus of elasticity of bounding frame of infill (MPa), I_b is the moment of inertia of beam of infilled frame (mm^4), and l is the infill length (mm).

2.4.1 CSA S304-14

The Canadian masonry design standard CSA S304-14 does not provide any explicit provisions for the determination of the out-of-plane strength of infills. It, however, permits the use of first principle mechanics to calculate the out-of-plane strength considering arching action.

2.4.2 MSJC 2013

The American masonry standard MSJC 2013 adopts the arching action model to determine the out-of-plane capacity of masonry infills. The proposed equation is based on the work originally done by Dawe and Seah (1989) and later modified by Flanagan and Bennett (1999).

$$q_{ult} = 729(f'_m)^{0.75} t_{inf}^{\ 2} \left(\frac{\alpha_{arch}}{l_{inf}^{\ 2.5}} + \frac{\beta_{arch}}{h_{inf}^{\ 2.5}}\right) \quad [2\text{-}23]$$

α_{arch} and β_{arch} are shown in Eqn [2-24a] and [2-24b], respectively.

$$\alpha_{arch} = \frac{1}{h_{inf}} (E_{bc} I_{bc} h_{inf}^{\ 2})^{0.25} \leq 50 \quad [2\text{-}24a]$$

$$\beta_{arch} = \frac{1}{l_{inf}} (E_{bb} I_{bb} l_{inf}^{\ 2})^{0.25} \leq 50 \quad [2\text{-}24b]$$

where I_{bc} and I_{bb} are the moment of inertia of the frame columns and frame beams, respectively; t_{inf} shall not be larger than $1/8h_{inf}$.

The effect of interfacial gaps between the infill and the bounding frame is also considered in MSJC 2013. When a side gap exits, α_{arch} shall be taken as zero. When a top gap exists, β_{arch} shall be taken as zero.

2.4.3 FEMA 356 (2000)

Federal Emergency Management Agency FEMA 356 (2000) provides the following

equation for the out-of-plane strength calculation for infills. The equation is based on the method proposed by Angel (1994). It is noted that Eqn [2-25] is formulated in imperial units, and works only for infills without prior in-plane cracking (Misir et al. 2015).

$$q_{ult} = \frac{0.7f'_m\lambda_2}{(\frac{h_{inf}}{t_{inf}})} \times 144 \qquad [2\text{-}25]$$

where λ_2 is the slenderness parameter as defined in Table 2.1.

Table 2.1 Values of λ_2

h/t	5	10	15	25
λ_2	0.129	0.06	0.034	0.013
Interpolation shall be used				

FEMA 356 states that if all of the following conditions exist, the arching action should be considered.

1. The panel is in full contact with the bounding frame components.
2. The stiffness of frame members in term of E_fI_f, should exceed the value of $1.03x10^{13}$ N-mm^2.
3. The frame components have sufficient strength to resist thrusts from arching of an infill.
4. The slenderness ratio of the infill (h_{inf}/t_{inf}) should not be larger than 25.

CHAPTER 3 EXPERIMENTAL PROGRAM

3.1 GENERAL

As mentioned earlier, this study is an integral part of an on-going research on the behaviour and strength of concrete masonry infilled frames under out-of-plane loading. The overall research framework is to quantify the arching action on the strength of masonry infills covering a range of geometric and material parameters. The first phase of this research was conducted by Sepasdar (2017) on RC frames with the main parameters being the infill opening, and prior in-plane damage. As the second phase, this study is to augment the results from the phase one with more variables and also further experimental testing to include steel bounding frames. A total of five infilled frame specimens were tested in this study including four masonry infilled RC frames and one masonry infilled steel frame. Parameters considered included the infill opening, prior in-plane damage, and interfacial gaps for RC frame specimens. The steel frame specimen served as a control specimen to be compared with the RC frame control specimen tested by Sepasdar (2017).

In addition to the infilled frames, the experimental program also included the component tests to determine material properties of concrete masonry units (CMUs), mortar, masonry prisms, concrete cylinders and steel rebars used in the RC frame and steel sections used in the steel frame. The following sections present detailed descriptions of the infilled frame

specimens, test set-up, and test procedures as well as component tests.

3.2 INFILLED FRAME SPECIMENS

A summary of the infilled frame specimens is presented in Table 3.1. All the masonry infills were fabricated with the same geometry but with different parameters. They included four infilled RC frame specimens and one infilled steel frame specimen. Four RC frame specimens included one with a central door opening of 17.6% of the infill area (IF-RC-DO), one with prior in-plane damage (IF-RC-ID), and two with frame-to-infill interfacial gaps. The gapped specimens included one having a 10 mm frame-to-beam gap (IF-RC-TG) and one having a 5 mm frame-to-column gaps at both frame-column interfaces (IF-RC-SG). It is noted that Sepasdar's study included a specimen with a window opening of 17.4% of the infill area and two specimens (IF-D1 and IF-D2) sustained prior in-plane damage at varying degrees. Specimen IF-D1 was subjected to in-plane loading until occurrence of a major diagonal crack (107.4 kN and in-plane displacement of 6.5 mm, $\delta_{app}/h = 0.66\%$) and specimen IF-D2 reached the ultimate in-plane strength of the infill (139.3 kN and in-plane displacement of 26.4 mm, $\delta_{app}/h = 2.71\%$), respectively. Specimen IF-RC-ID in this study was designed to experience an in-plane displacement of about 13.4 mm ($\delta_{app}/h = 1.37\%$), which was considered at a stage somewhere in between. In this study, specimens 1 and 2 were used to augment the results obtained by Sepasdar while specimens 3, 4, and 5 were with new parameters.

Table 3.1 Summary of Infilled Frame Specimen

Number	Specimen ID	Gap	Opening-to-Infill Area	Prior In-Plane Damage (δ_{app}/h)	Bounding Frames
			Current Study		
1	IF-RC-DO	N/A	Door 17.6%	N/A	RC
2	IF-RC-ID	N/A	N/A	Diagonal Cracking (δ_{app}/h =1.37%)	RC
3	IF-RC-TG	10 mm Top Gap	N/A	N/A	RC
4	IF-RC-SG	5 mm Side Gap (each side)	N/A	N/A	RC
5	IF-S	N/A	N/A	N/A	Steel
			Sepasdar (2017)		
6	IF-ND	N/A	N/A	N/A	RC
7	IF-W-ND	N/A	Window 17.4%	N/A	RC
8	IF-D1	N/A	N/A	Diagonal Cracking (δ_{app}/h =0.66%)	RC
9	IF-D2	N/A	N/A	Loaded to Ultimate (δ_{app}/h =2.71%)	RC

In order to compare the results with those obtained by Sepasdar (2017), the geometry and reinforcement details of specimens were kept the same between the two studies. Figure 3.1 and Figure 3.2 respectively show the dimensions of the RC frame specimens and steel frame specimen. The custom made half-scale standard 200 mm masonry blocks were used to construct the infill panels in the running bond. Figure 3.3 shows that the average dimensions of stretchers and half blocks in the experimental program. The half bocks were cut from stretcher blocks. The geometry of the infill and CMUs yields a height-to-length aspect ratio of 0.73, and a height-to-thickness slenderness of 10.89 for all infills. All the infills were unreinforced and ungrounded except for the specimen (IF-RC-DO) with a center door opening where the masonry blocks surrounding the door opening were grouted in accordance with CSA A179-14.

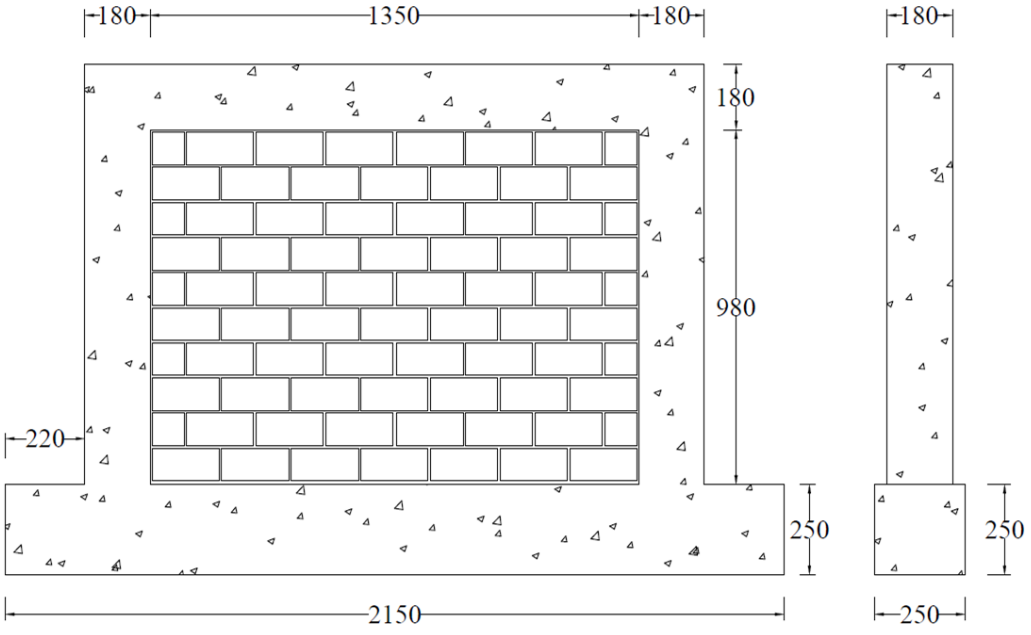

Figure 3.1 Details of RC Infilled Frame Specimens (unit: mm)

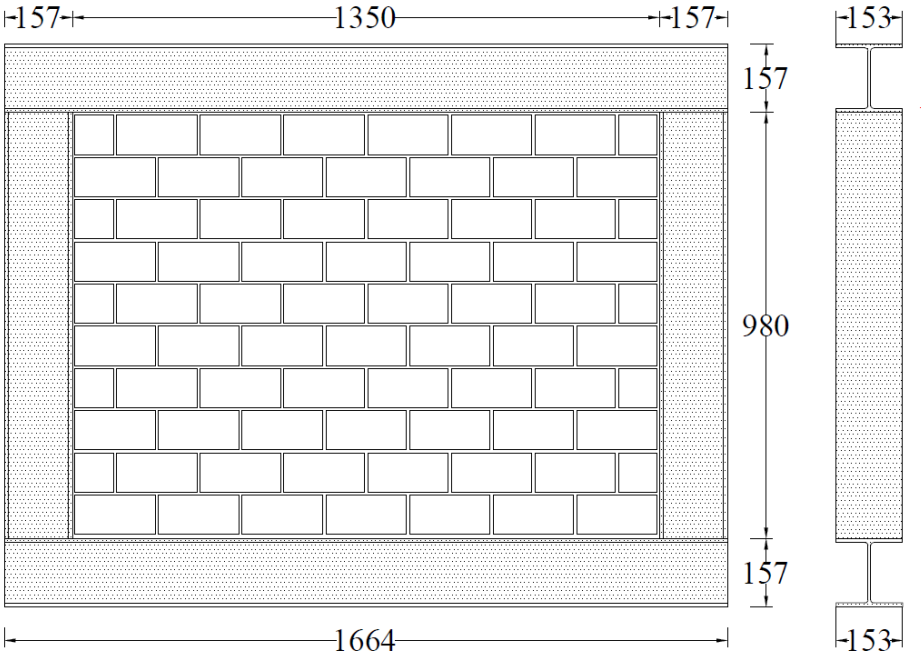

Figure 3.2 Details of Steel Infilled Frame Specimen (unit: mm)

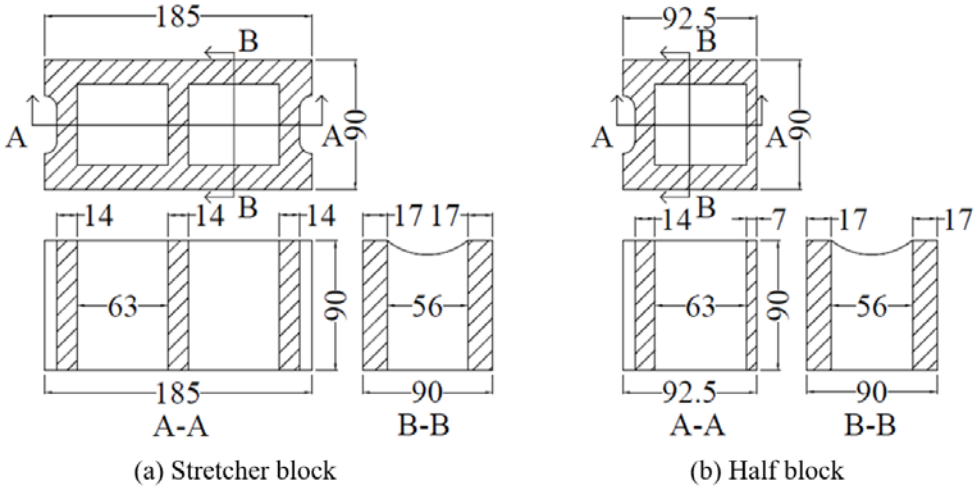

Figure 3.3 Details of Half-Scaled CMUs (unit: mm)

The RC frame was designed in accordance with CAN/CSA A23-3 (2014) and the reinforcement detailing including size, spacing, arrangement of longitudinal bars and stirrups complied with requirements to provide ductility and avoid brittle shear failure. A detailed drawing of reinforcement is shown in Figure 3.4. The frame top beam and columns

had 180 mm square cross-section reinforced with 4-10M longitudinal deformed rebars and 10M stirrups at 100 mm center-to-center spacing. The base beam of the frame had a 250 mm square cross-section reinforced with 4-15M longitudinal deformed rebars and 10M stirrups at 100 mm center-to-center spacing. To strengthen the intersection at the top beam and columns, four 300 mm by 300 mm 10M L-shaped rebars were added at each top beam-column corner.

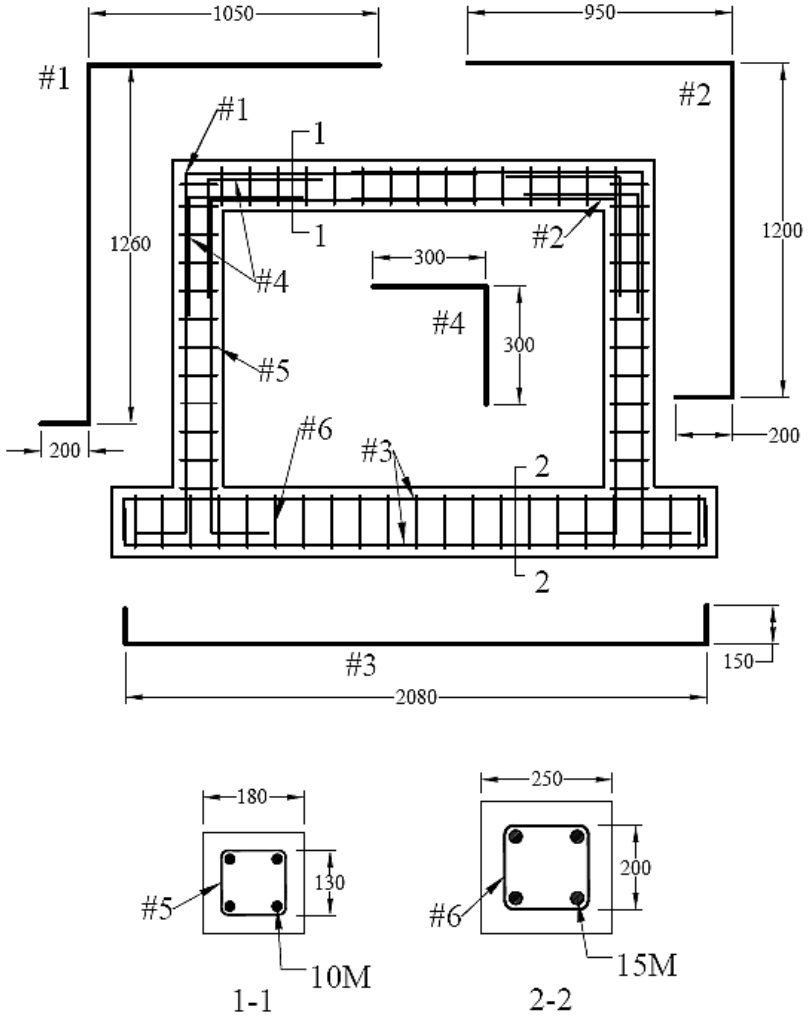

Figure 3.4 Details of Reinforcement in RC frame

3.2.1 Construction of RC Frames

Construction of RC frames began with forming steel reinforcement into “cages”. The formwork was then constructed using plywood boards cut to specified geometry (Figure 3.5). The reinforcement cage was carefully positioned inside the formwork (Figure 3.6) resting on plastic chairs which were used to achieve the 25 mm concrete cover (Figure 3.7). Six holes on the frame beams were designed to be used for installing a reaction frame to the RC frame. The PVC tubes were placed in the top and base beams for this purpose (Figure 3.8). The ready-mix concrete with a specified compressive strength of 25 MPa and a maximum aggregate size of 12 mm was used for the RC frames. The strength of 25 MPa was used to maintain the comparability between this study and the previous study. The casting of concrete occurred in July of 2016. The concrete was provided by a local ready-mix company and when the concrete arrived on site, the slump test was conducted in accordance with ASTM C143/C143M (2015) Standard Test Method for Slump of Hydraulic-Cement Concrete. The slump test showed a falling height of 160 mm which met the workability of fresh concrete.

A vibrator was used to ensure that the concrete was free of air bubbles during pouring (Figure 3.9). The surface was leveled and smoothed with a masonry trowel after thorough vibration (Figure 3.10). Alongside pouring concrete frames, concrete cylinders were also cast to be used in the determination of concrete properties in accordance with ASTM

C39/C39M (2016) Standard Test Method for Compressive Strength of Cylindrical Concrete Specimens. All RC frame specimens and concrete cylinders were moisture cured for 14 days, and then followed by air curing until the testing day. The formwork was removed at the 14th day after pouring.

Figure 3.5 Overview of Formwork

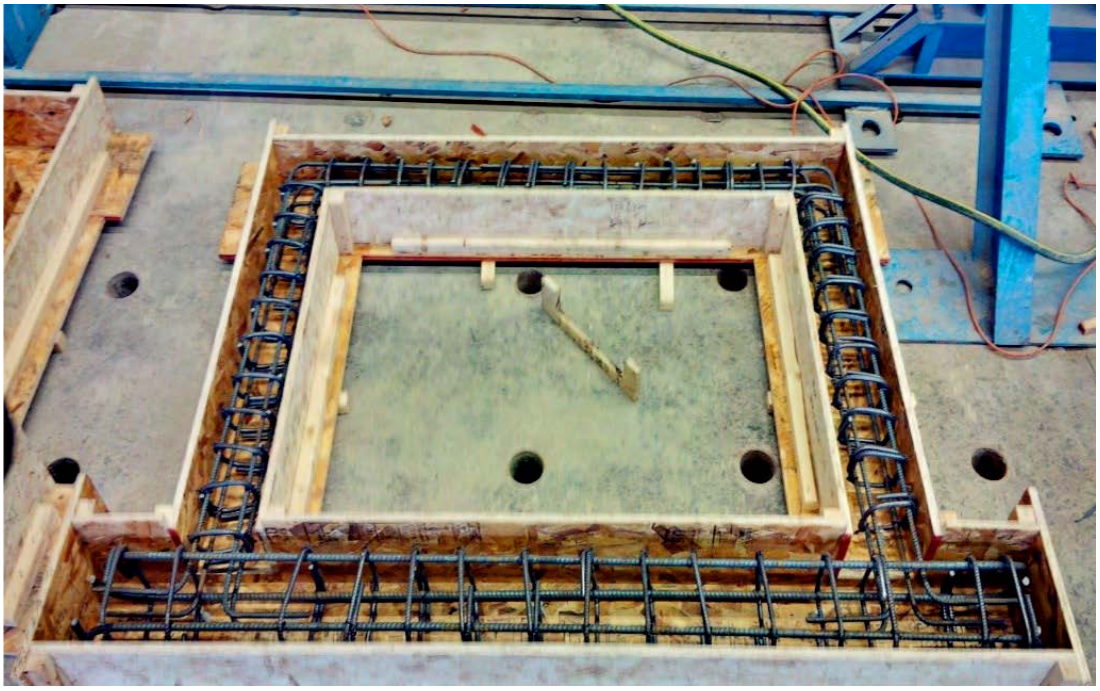

Figure 3.6 Overview of Formwork and Reinforcement Cage

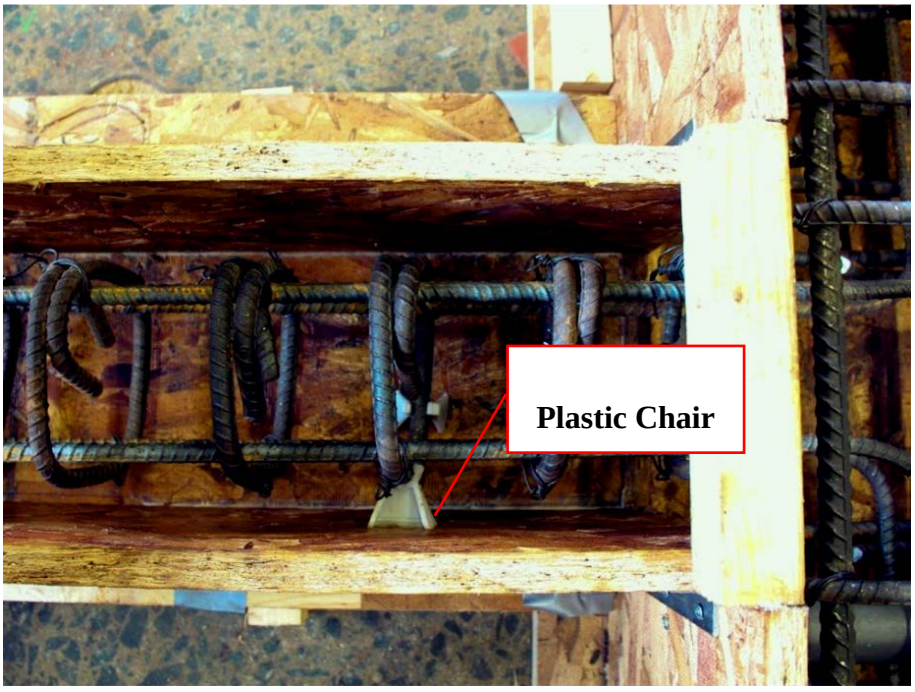

Figure 3.7 Details of Reinforcement

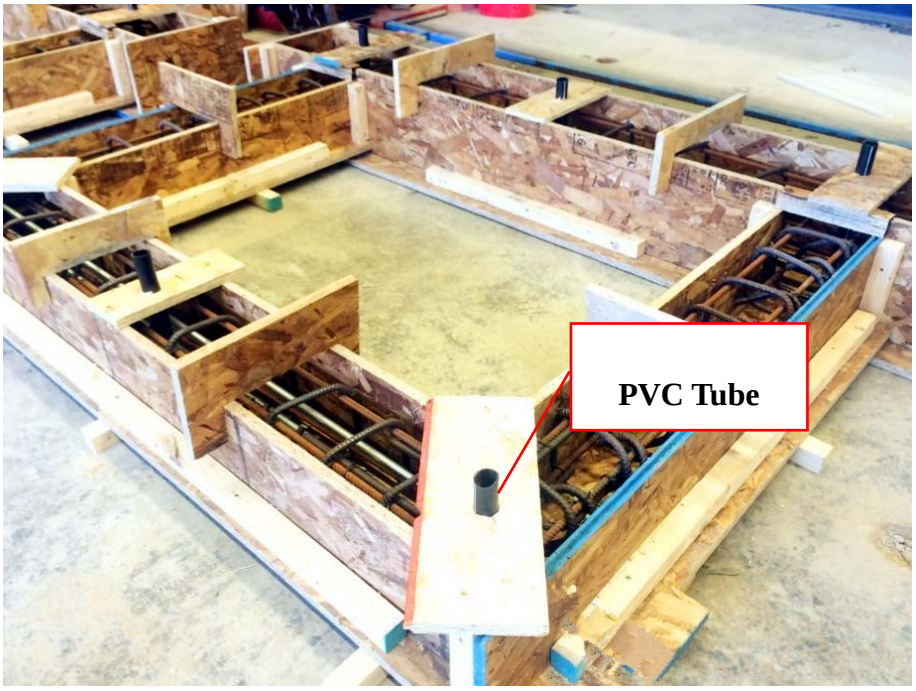

Figure 3.8 Formwork with Reinforcement and PVC Tubes

Figure 3.9 Concrete Casting and Vibrating

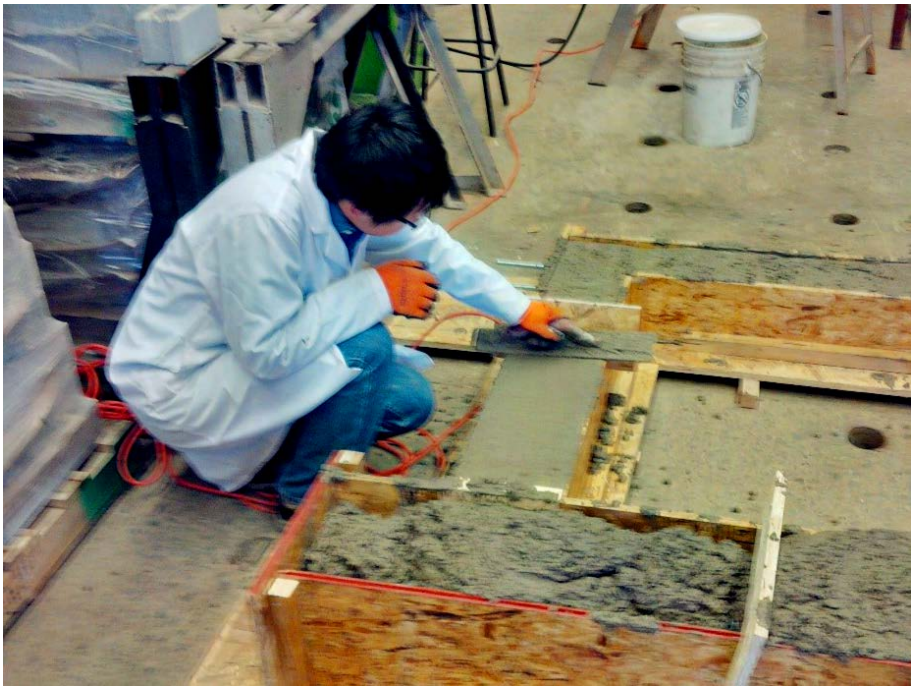

Figure 3.10 Concrete Surface Smoothing with Trowel

3.2.2 Fabrication of Steel Bounding Frames

Steel section W150X30 (G40.21 350W) was used for both beams and columns for the steel frame. Four members were weld-connected using a 6 mm fillet weld to form the frame. As shown in Figure 3.11 and Figure 3.12, the weld was placed along the web of the column on both sides at the beam-column connection. An analysis as shown in APPENDIX B indicates that a 6 mm fillet weld on both sides of the column web is sufficient to resist the load which may be exerted onto the frame by the infill under out-of-plane loading.

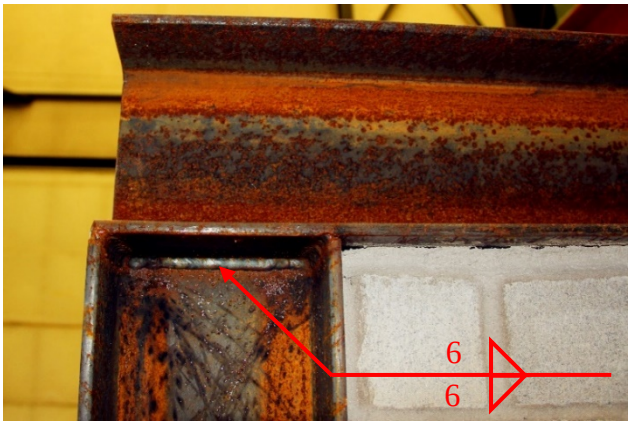

Figure 3.11 Details of Top Beam-Column Interaction

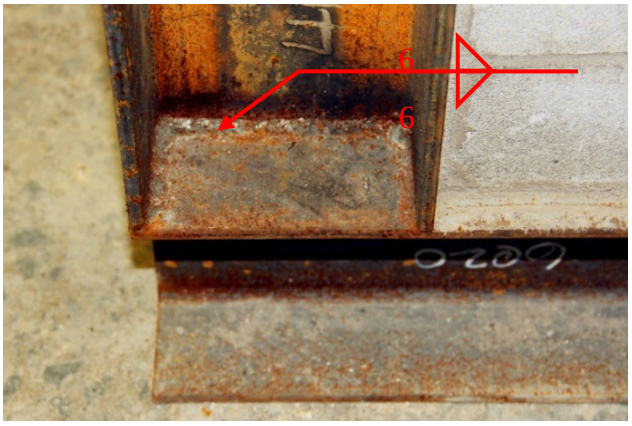

Figure 3.12 Details of Base Beam-Column Interaction

3.2.3 Construction of Masonry Infill Walls

The masonry infill walls were constructed in the Heavy Structures Laboratory at Dalhousie University by a certified mason to the standard of construction practice. Built in two batches, the specimens IF-RC-ID and IF-RC-DO were built on 29th March 2017, and the specimens IF-RC-TG, IF-RC-SG and IF-S were built on 30th March 2017. Figure 3.13 shows the process of fabrication of masonry infill walls. Main procedures and points of interest are described in the following. Before construction of masonry infills, the stretcher blocks were

cut into half blocks (Figure 3.13 a). The mason carefully marked the reference lines on the frame to achieve the specified mortar thickness between the CMUs and between the infill and bounding frame (Figure 3.13 b). The mortar was only applied on the face shell of CMUs for both the bed joints and head joints (Figure 3.13 c). At each course, a level and plumb were used to ensure that the wall was levelled and built square within the frame (Figure 3.13 d). For the specimen with door opening (IF-RC-DO), the block cells were grouted surrounding the door opening as shown in Figure 3.13 (e). A temporary shoring was placed after construction and removed after 48 hours. For the specimens with gaps (IF-RC-TG and IF-RC-SG), thickness of the mortar was adjusted to achieve the specified gaps. Along with construction of the walls, masonry prisms and mortar cubes were built and cured under the same moisture condition for 28 days, and then cured under the same air condition until the day of testing.

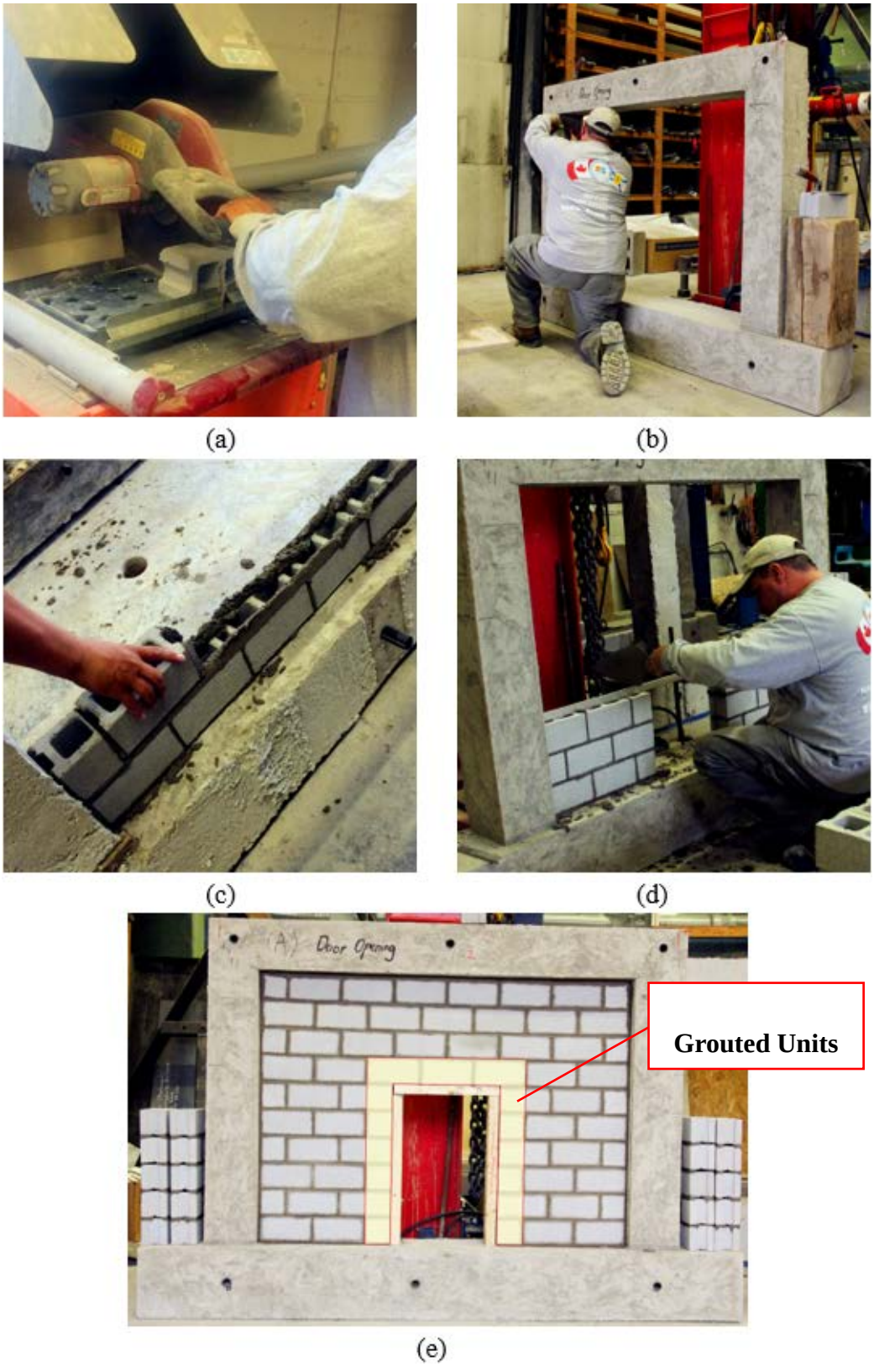

Figure 3.13 Construction of Masonry Infills

3.3 OUT-OF-PLANE TEST SET-UP

For both RC and steel frame specimens, the out-of-plane load was applied to the masonry infills using an air bag through a self-equilibrating system as shown in Figure 3.14. The air bag was housed in a reaction frame which was in turn connected to the bounding frame through high strength threaded rods. The reaction frame was comprised of a 15 mm thick Douglas Fir Plywood board stiffened with steel HSS sections as shown in Figure 3.15. For the RC infilled frame specimen, the bottom beam of the frame was clamped down with W steel beams which were in turn secured to the strong floor using threaded steel rods as shown in Figure 3.16 (a) and Figure 3.17. For the steel infilled frame specimen, the bottom beam of the frame was welded to two W steel beams which were bolt-connected to the strong floor using high strength steel rods as shown in Figure 3.16 (b) and Figure 3.18.

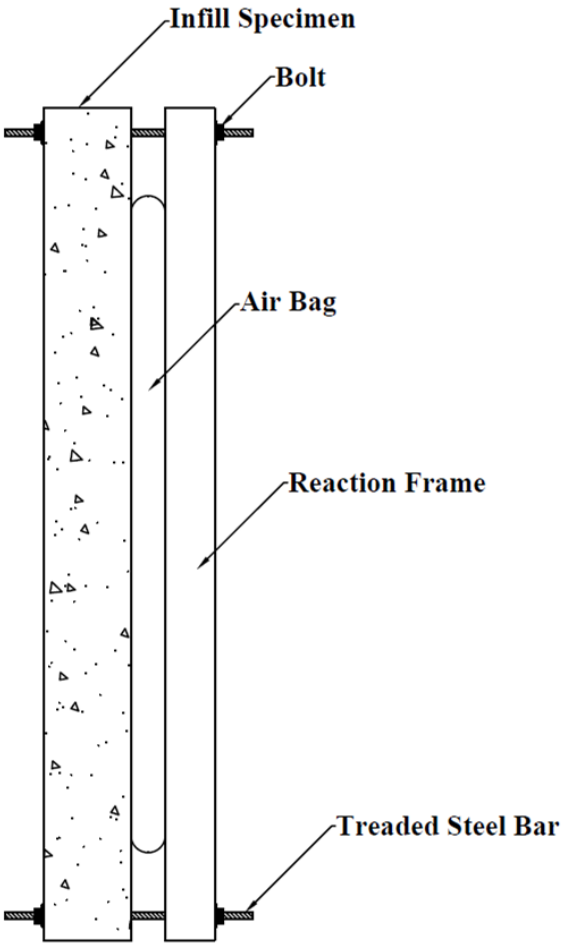

Figure 3.14 Schematic Top View of the Air Bag Loading Arrangement

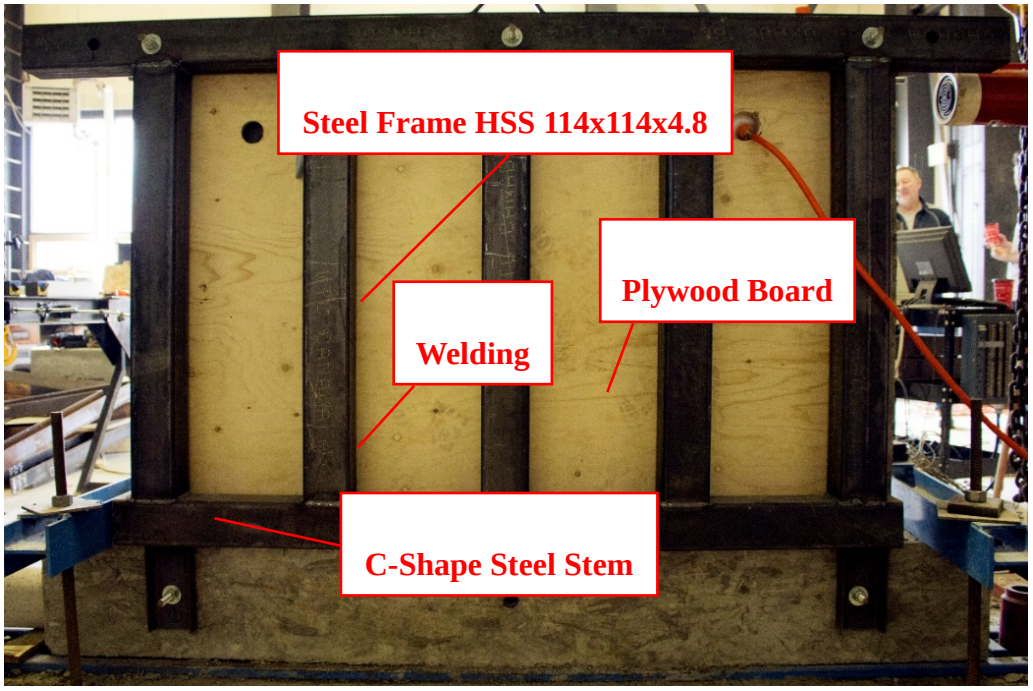

Figure 3.15 Details of Reaction Frame

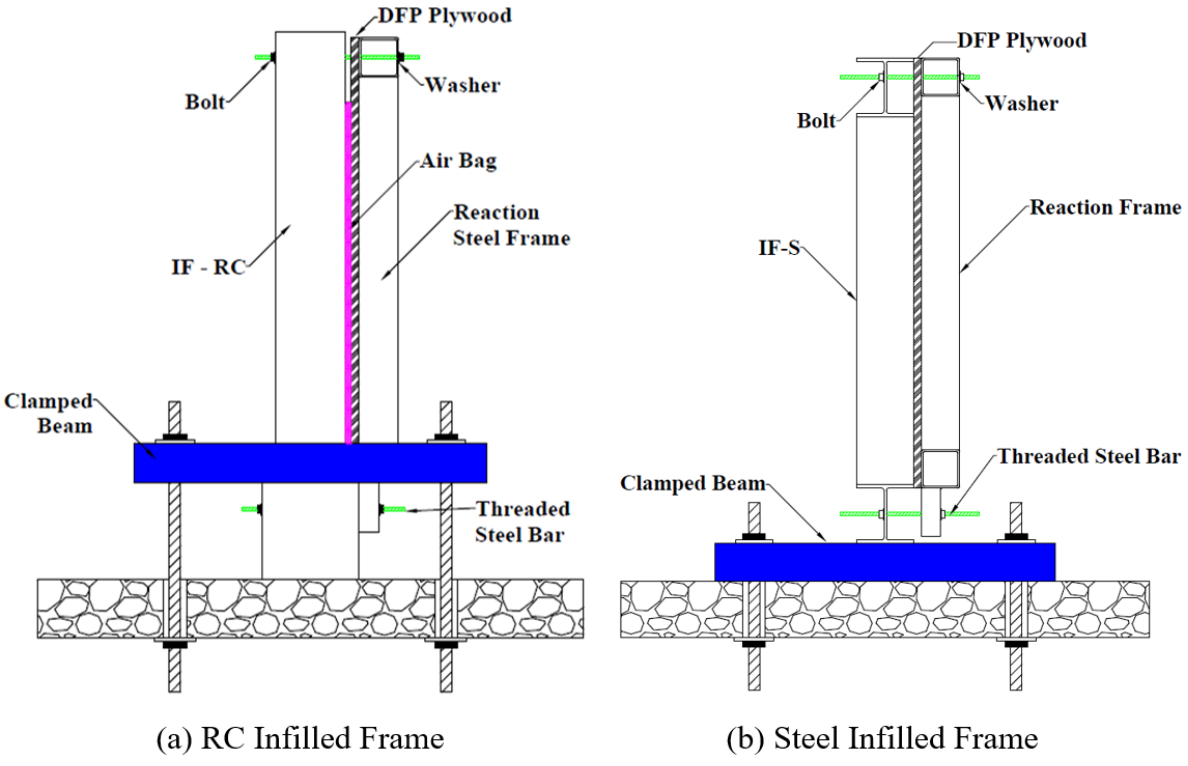

Figure 3.16 Schematic Side View of Test Set-up for Infilled Frame Specimen

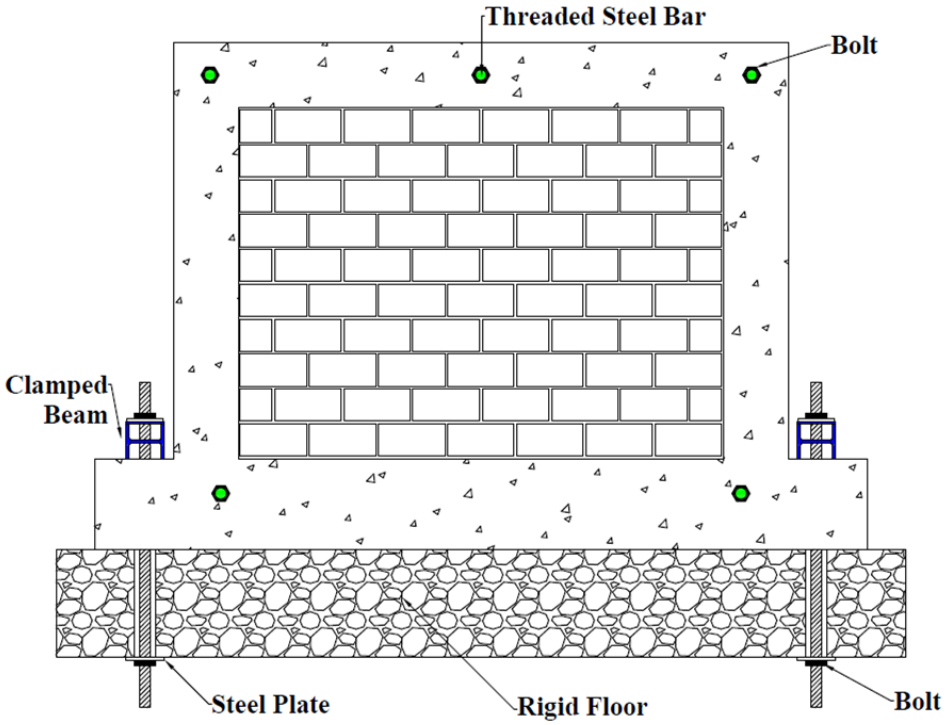

Figure 3.17 Schematic Front View of Test Set-up for RC Infilled Frame Specimen

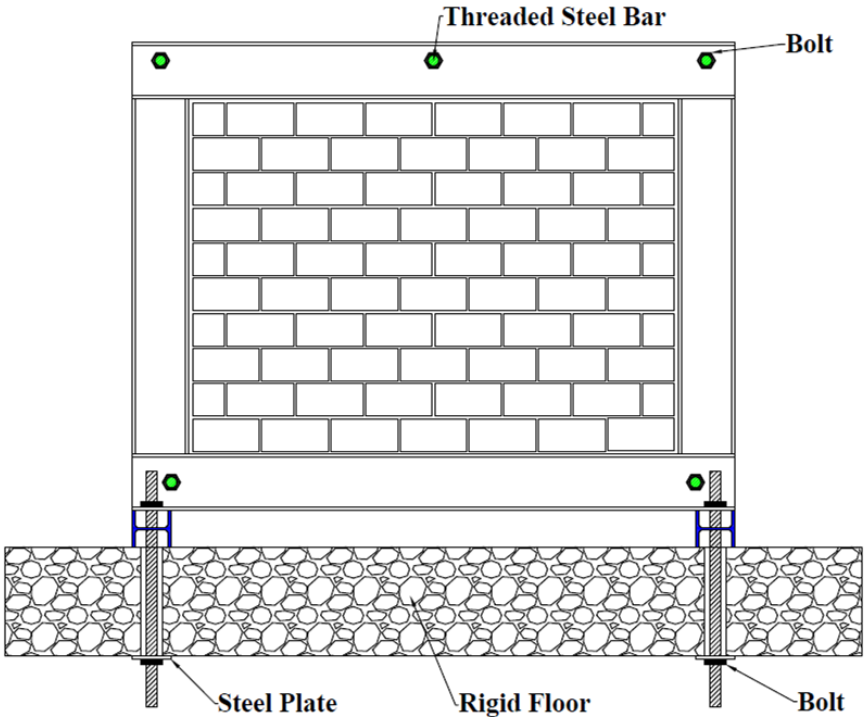

Figure 3.18 Schematic Front View of Test Set-up for Steel Infilled Frame Specimen

The airbag was inflated by an air compressor and the pressure in the air bag was measured and recorded using a pressure transducer as shown in Figure 3.19. A pressure gauge was also used during the test to monitor the consistency between two devices.

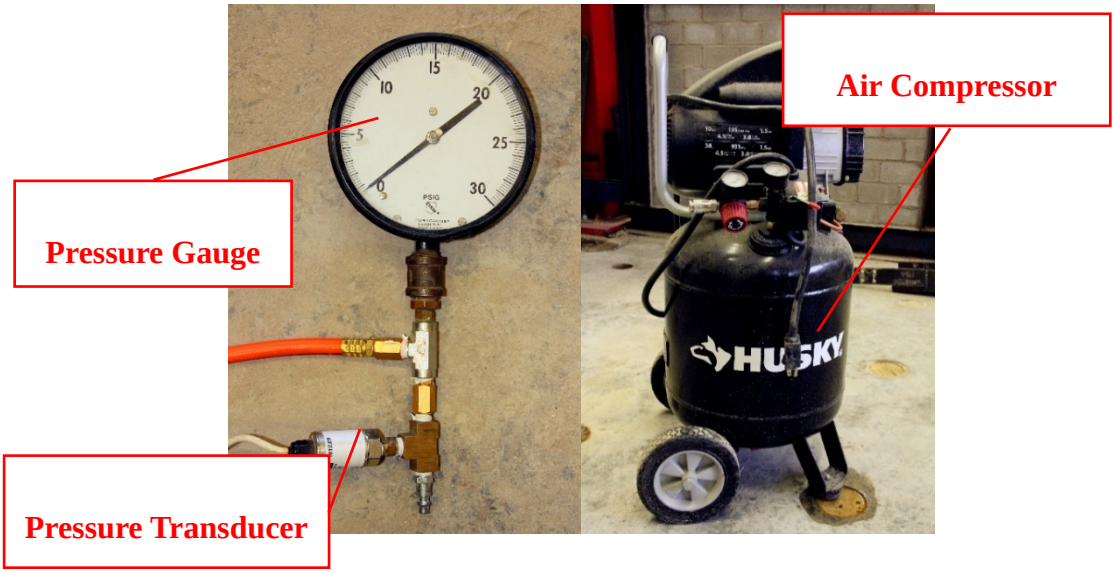

Figure 3.19 Pressure Transducer and Air Compressor

Six linear variable differential transformers (LVDTs) were used to measure and record the out-of-plane displacements of infills. For the specimens IF-S, IF-RC-TG and IF-RC-SG, the LVDTs position was shown in Figure 3.20 (a). One LVDT was used to measure the out-of-plane displacement at the center of the infill; four LVDTs were used to measure the out-of-plane displacement at the center of top, bottom, right and left half of the infill respectively; One LVDT was used to measure the out-of-plane displacement at the very top (directly below the interface) of infill. For the specimens IF-RC-ID, the location of LVDTs was the same as IF-RC-TG except for the LVTD that measured the displacement at the very top of infill was placed at the center of the top left quarter of the infill to measure the out-

of-plane displacement along the diagonal cracking caused by in-plane lateral load as shown in Figure 3.20 (b). For the specimens IF-RC-DO, three LVDTs were used to measure the out-of-plane displacement of the center of each side and the top left corner of the opening respectively as shown in Figure 3.20 (c).

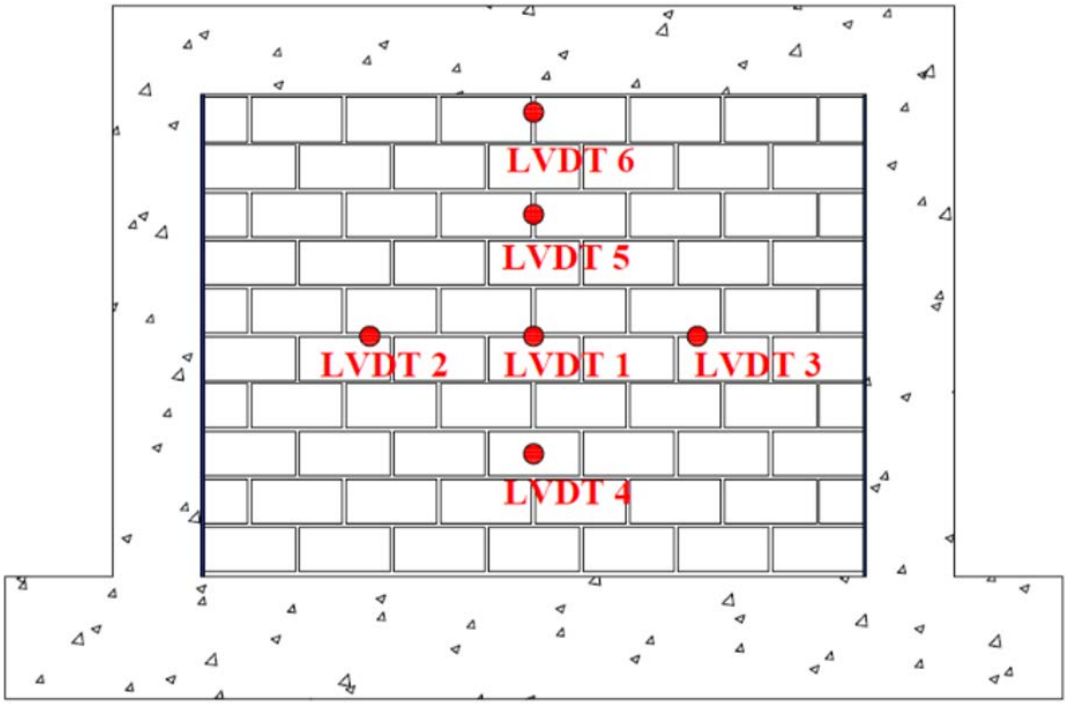

(a) Specimens IF-S, IF-RC-TG and IF-RC-SG

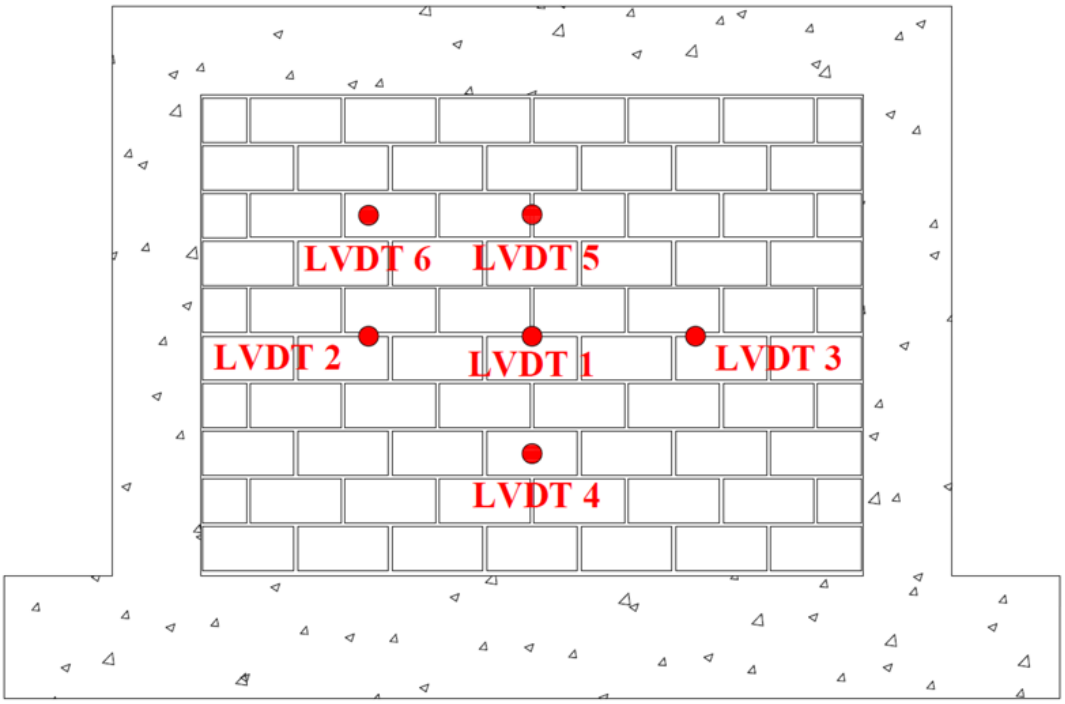

(b) Specimens IF-RC-ID

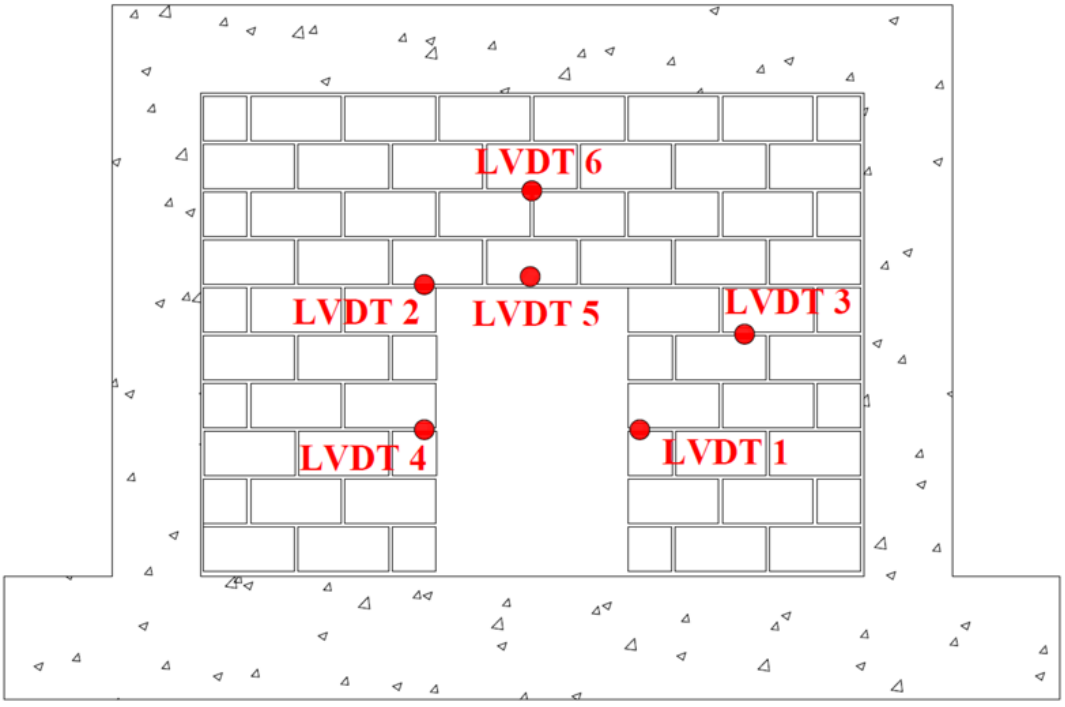

(c) Specimens IF-RC-DO

Figure 3.20 LVDTs Position

3.4 IN-PLANE TEST SET-UP

For specimen IF-RC-ID, the prior damage caused by in-plane lateral load was required before application of the out-of-plane load. A picture and schematic view of the in-plane test setup were shown in Figure 3.21 and Figure 3.22 respectively. A hydraulic actuator with a capacity of 250 kN was used to apply the in-plane lateral load monotonically, and the hydraulic actuator was bolted to the column of an independent reaction frame. A load cell was attached to the actuator to measure and record the applied in-plane load as shown in Figure 3.23. A steel plate was placed between the load cell and the specimen to ensure a uniform distribution of the concentrate load and to prevent crushing of the concrete.

Figure 3.21 In-Plane Test Setup

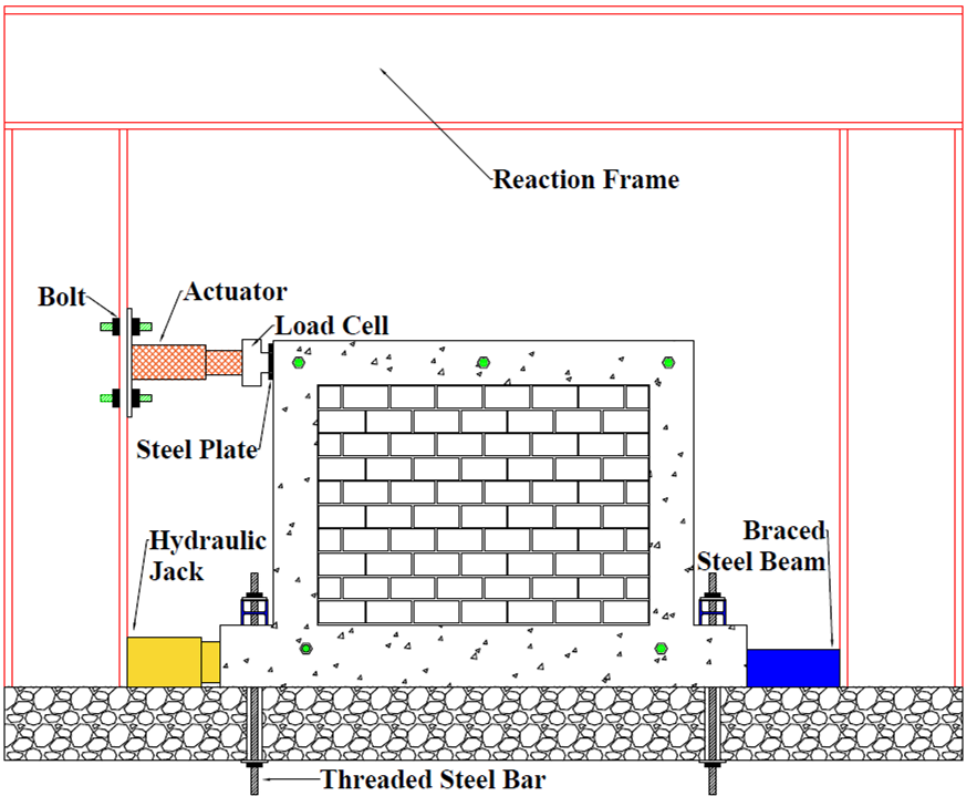

Figure 3.22 Schematic View of In-plane Test Setup

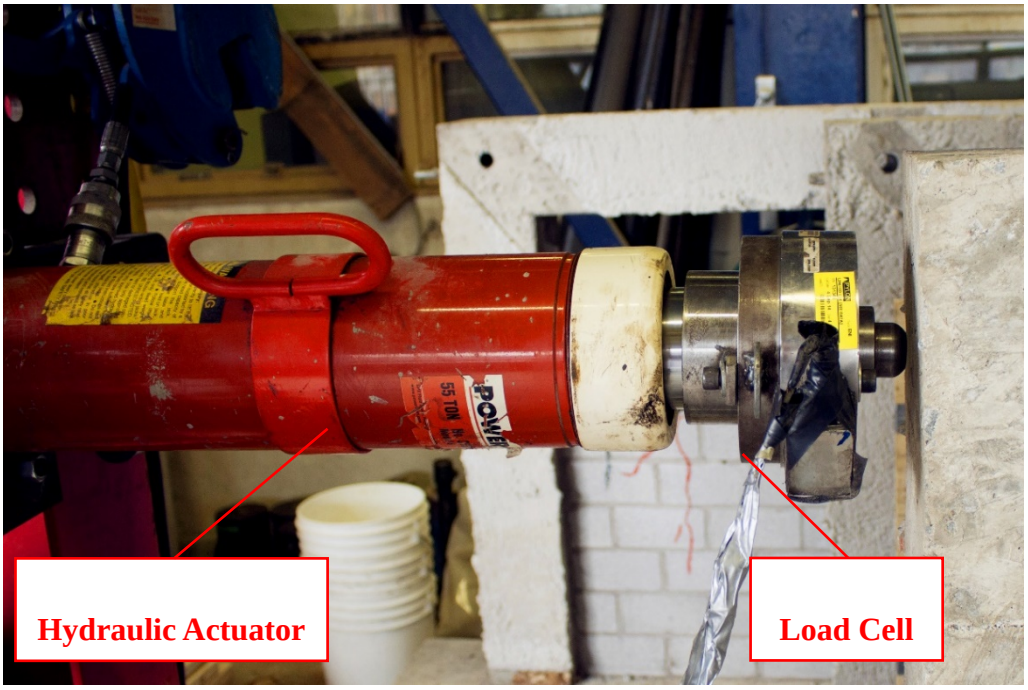

Figure 3.23 Hydraulic Actuator Connection to Test Specimen

To provide the fixity of the frame base, the base beam of the frame was clamped down to the floor with two W steel beams, in the same way as the out-of-plane test setup. The base beam was further braced against any potential sliding using a hydraulic jack against the column of the reaction frame as shown in Figure 3.24.

Two LVDTs were used to measure the in-plane displacements of the infill where LVDT 1 and LVDT 2 were mounted at the center line of the top and base beams of the specimen respectively as shown in Figure 3.25 and Figure 3.26.

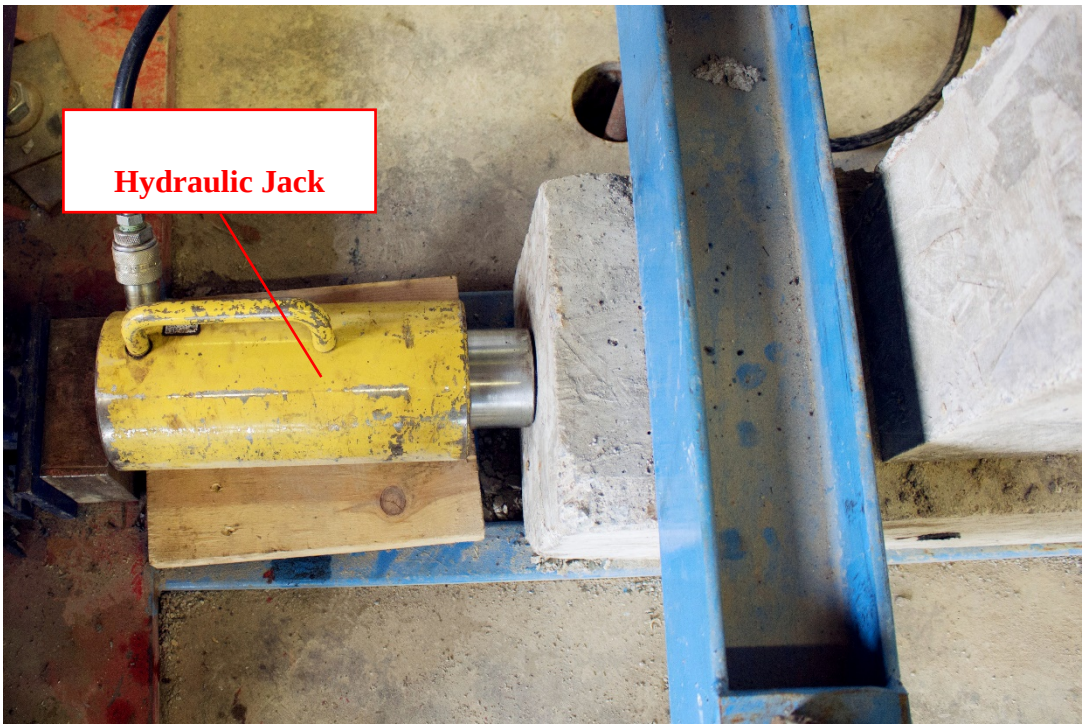

Figure 3.24 Hydraulic Jack Bracing the Base of Specimen

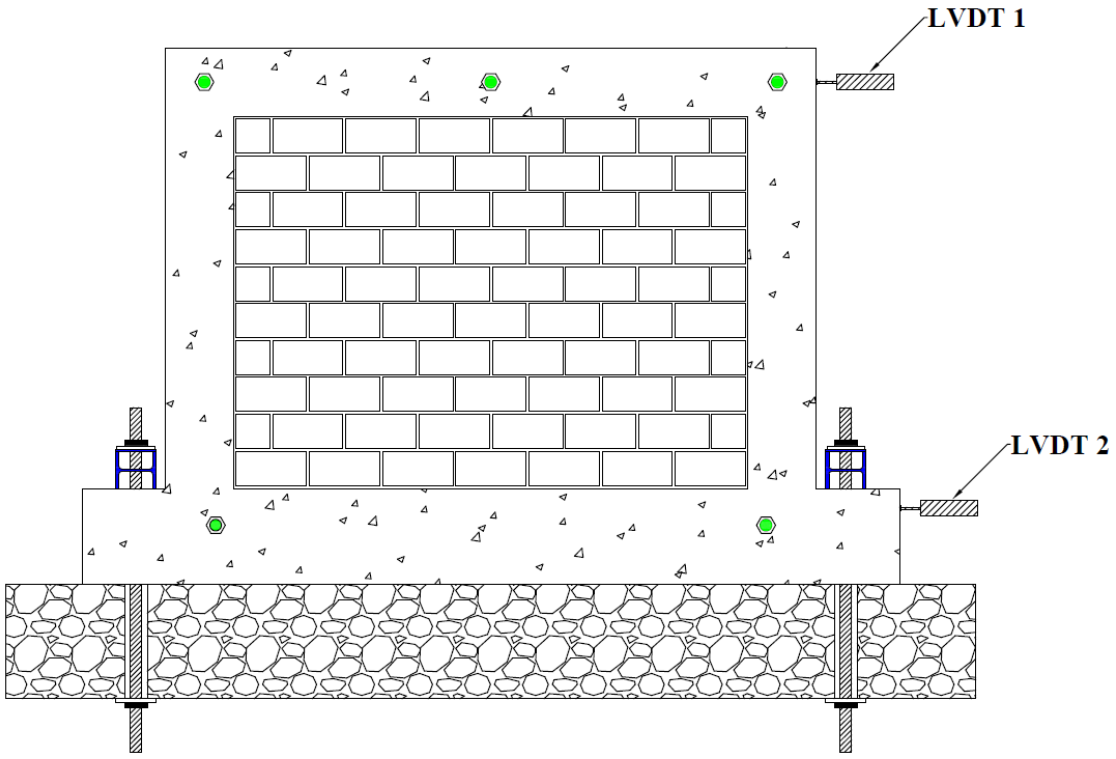

Figure 3.25 Schematic View of Placement of LVDT 1 and LVDT 2

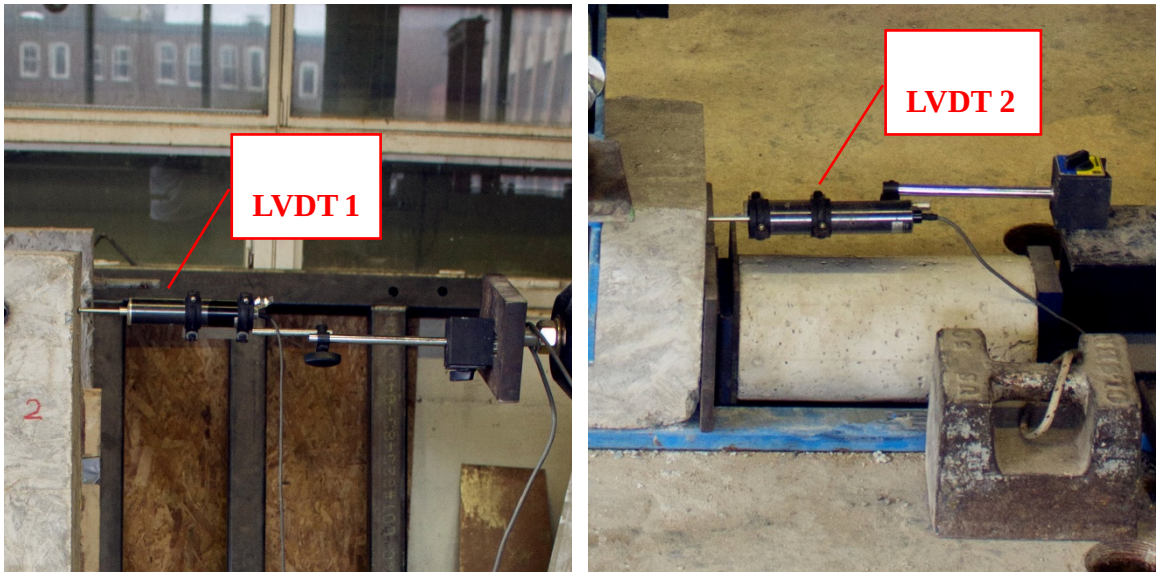

Figure 3.26 Placement of LVDT 1 and LVDT 2

3.5 OUT-OF-PLANE TEST PROCEDURE

After careful positioning of the test specimen, the air bag assembly and measuring devices were mounted and checked to ensure that they worked properly and zeroed for initial recording. The air bag pressure was applied gradually at a rate of 1.5 kPa per minute until the failure of the specimen. The pressure and out-of-plane displacement readings were recorded at a 0.1 second interval using an electronic data acquisition system. During each test, the cracking load, ultimate load, cracking pattern and failure mode were recorded and marked when necessary.

3.6 IN-PLANE TEST PROCEDURE

For specimen IF-RC-ID which was intended to have sustained prior in-plane damage, once the specimen was positioned in place and clamped to the strong floor. The in-plane lateral load was applied gradually at a rate of 6 kN per minute until the desired in-plane displacement was reached. The in-plane load and displacement readings were recorded at 0.1 second intervals using an electronic data acquisition system. The cracking load and cracking pattern were noted.

3.7 COMPONENT TESTS

Concurrent with the testing of infilled frame specimens, specimen material tests were carried out to obtain the material properties of CMUs, mortar, masonry prims, concrete,

reinforcing steel rebar and steel sections. The test setup and procedures of those tests are described in the following sections.

3.7.1 CMUs

Both physical properties and compressive strength of masonry blocks were determined according to ASTM C140/C140M (2016). The physical properties tested included the 24-hour percentage adsorption, density, and moisture content. Six randomly selected blocks were used in the test. A universal Instron was used to determine the compressive strength of the block. As shown in Figure 3.27, a masonry block with fiberboard capping on two end surfaces is positioned to be tested.

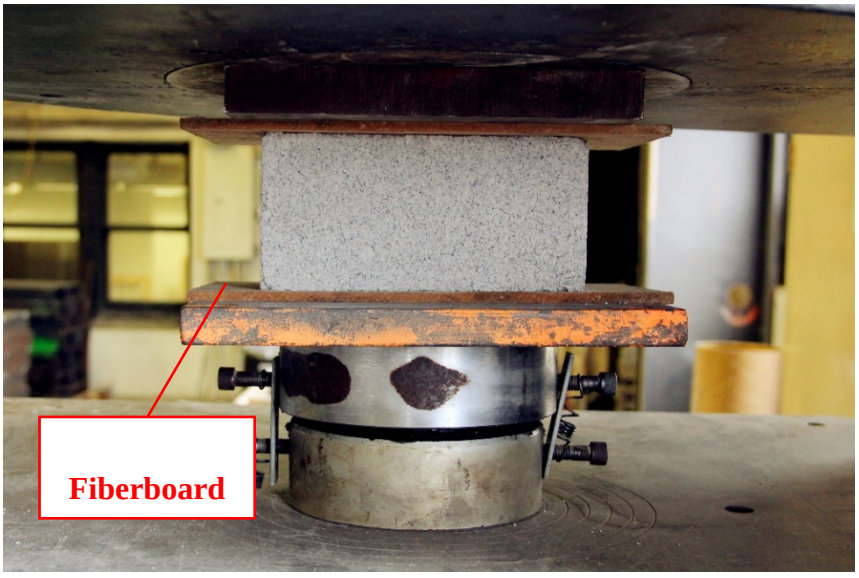

Figure 3.27 Compression Test Set-up for CMUs

3.7.2 Mortar

Type N mortar was used for the fabrication of masonry infill walls. The Type N mortar was obtained on site by mixing Portland cement, type N masonry cements, and sand in a volumetric proportion of 1:2:4 respectively in accordance with industry practice. Two batches of mortar (Batch A and Bath B) were needed to construct the infilled frame specimens and mortar cubes. Six 50 mm mortar cubes were cast in a non-absorbent mould for each batch as shown in Figure 3.28. The mortar cubes were demoulded after 72 hours of air-curing, and then cured in hydrated lime water for 28 days. The compressive strength of mortar cubes was obtained using the universal Instron testing machine as shown in Figure 3.29. The constructing and testing of mortar cubes were carried out in accordance with the ASTM C270 (2014) Standard Specification for Mortar for Unit Masonry.

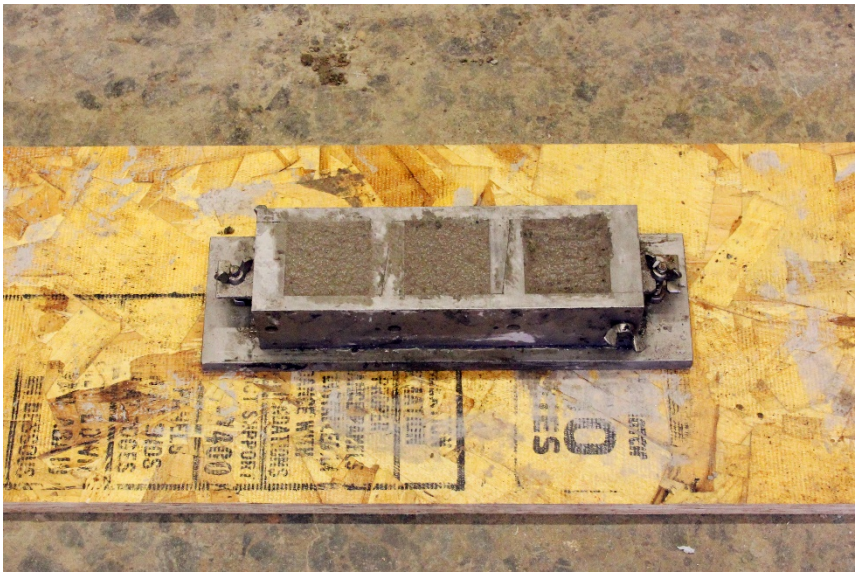

Figure 3.28 Mortar Cubes in the Mould

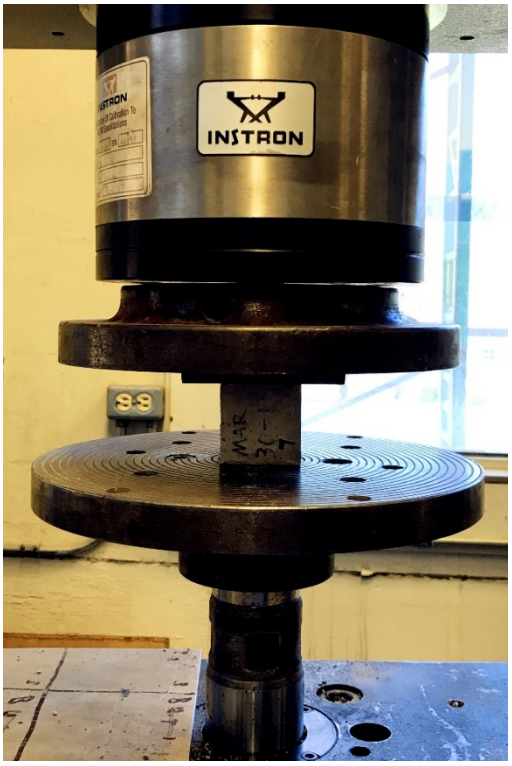

Figure 3.29 Compression Test Set-up for Mortar Cubes

3.7.3 Masonry Prisms

A total of fifteen 5-course high hollow masonry prisms were constructed alongside the masonry infill walls. To better reflect the masonry strength in real wall construction, prisms incorporating both head and bed joints were constructed as illustrated in Figure 3.30. They were cured under the same condition as the infilled frame specimens. The compression test was conducted in accordance with the ASTM C1314 (2016) Standard Test Method for Compressive Strength of Masonry Prisms. The prisms were fiberboard capped, similar to the CMUs, and were tested in the universal Instron testing machine as illustrated in Figure 3.31.

Figure 3.30 Construction of Masonry Prisms

Figure 3.31 Compression Test Set-up for 5-Course Masonry Prisms

3.7.4 Concrete

The frames were cast in two batches on the July 15th 2016 and July 19th 2016 respectively. For each batch, six 100×200 mm and three 150×300 mm cylinders were also poured. The small cylinders were tested on the 14th day and 28th day for compressive strength. The large cylinders were tested on the day of testing the frame specimens to obtain both compressive strength and modulus of elasticity of the concrete. All the testing procedures were performed in accordance with the ASTM C39/C39M (2016) Standard Test Method for Compressive Strength of Cylindrical Concrete Specimens. The test setup is shown in Figure 3.32.

Figure 3.32 Compression Test Set-up for Concrete Cylinder

3.7.5 Reinforcing Steel

The properties of steel reinforcement in the RC frames were obtained from a study by Hu (2015) in the same research team. Hu's research was on the in-plane test of masonry infilled RC frames and the rebars used in both studies were from the same batch. The randomly selected 10M rebars were cut and milled into three steel coupons with dimension details shown in Figure 3.33. They were tested in the universal Instron testing machine to obtain the stress-strain relationship of reinforcing steel in accordance with the ASTM E8 (2008) Standard Test Methods for Tension Testing of Metallic Materials as shown in Figure 3.34.

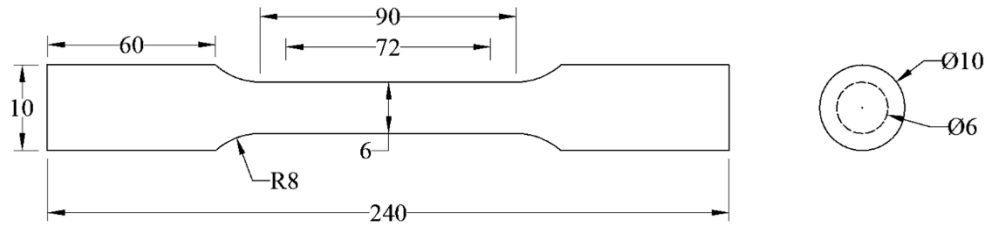

Figure 3.33 Details of Steel Coupon (Hu, 2015)

Figure 3.34 Tension Test Set-up for Reinforcing Steel Coupon (Hu, 2015)

3.7.6 Steel Frame

Five steel coupons were cut from the steel section stock consisting of 2 from the flange and 3 from the web. The coupons were milled in accordance with the ASTM Standard A370 (2012) for specimens with a gauge length of 50 mm as shown in Figure 3.35. The coupons were tested in the universal Instron testing machine as shown in Figure 3.36 to obtain the yield and tensile strength as well as the elastic modulus of the steel in accordance with the ASTM E8 (2008) Standard Test Methods for Tension Testing of Metallic Materials.

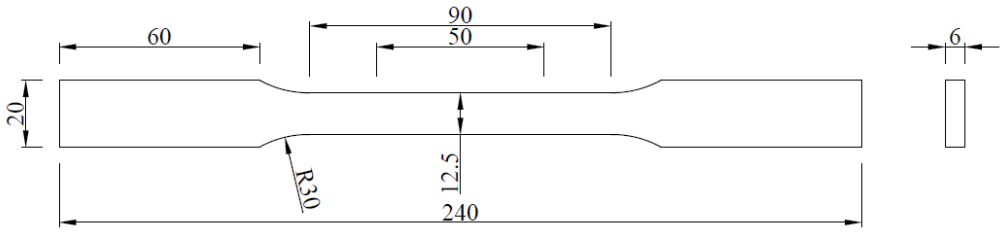

Figure 3.35 Details of Steel Frame Coupon

Figure 3.36 Tension Test Set-up for Steel Frame Coupons

CHAPTER 4 EXPERIMENTAL RESULTS

4.1 INTRODUCTION

This chapter presents the test results and discussion from component and infilled frame tests. The component test provides the physical and mechanical properties of CMUs, mortar and masonry prisms of infill; and concrete, reinforcing steel, steel section of frames. The results of infilled frame tests present the behaviour, strength and failure pattern of infilled frames under out-of-plane loading. The effect of parameters is also evaluated in this chapter.

4.2 MASONRY COMPONENT TEST RESULTS

4.2.1 CMUs

Six randomly selected CMUs were used to determine the physical properties of CMUs including net area, weight, absorption rate, moisture content, and density in accordance with ASTM C140/C140M (2016). The received weight (w_r) was measured for each selected CMUs with actual moisture content in the air. The CMU was then completely immersed in water for 24 hours, and the immersed weight (w_i) of the CMU was measured. The CMU was then removed from the water and surfaced dried, and the weight at this point was counted as saturated weight (w_s). The CMU was dried in an oven at 100℃ for 24 hours, and then oven-dry weight (w_d) was measured. Using formulas specified in ASTM

C140/C140M, the following physical properties of CMUs were determined and shown in Table 4.1. The average moisture content of CMUs was 12.6% with a COV of 10.1%; the average absorption rate of CMUs was 6.5% with a COV of 7.9%; the average absorption of CMUs was 137.4 kg/m^3 with a COV of 7.1%; and average density of CMUs was 2120.4 kg/m^3 with a COV of 1.4%. According to CAN/CSA A165(2015) Standard on Concrete Masonry Units, standard 200 mm hollow masonry block should have a density greater than 2000 kg/m^3, moisture content less than 45%, and absorption below 175 kg/m^3. Table 4.1 shows that the physical properties of CMUs used in this study meet the required criterion and are comparable to standard CMUs.

Table 4.1 Physical Properties of CMUs

ID	Received Weight (g)	Immersed Weight (g)	Saturated Weight (g)	Oven-Dry Weight (g)	Absorption		Moisture Content (%)	Density (kg/m^3)
					(kg/m^3)	(%)		
C1	1662.2	969.5	1749.5	1648.4	129.6	6.1	13.6	2113.3
C2	1662.5	968.3	1746.9	1648.5	126.4	6.0	14.2	2117.3
C3	1583.9	931.1	1680.3	1571.8	144.8	6.9	11.2	2098.0
C4	1589.1	936.2	1688.9	1575.4	150.8	7.2	12.1	2093.0
C5	1593.4	943.8	1687.1	1581.5	142.1	6.7	11.3	2127.7
C6	1660.5	988.7	1746.9	1647.6	131.0	6.0	13.0	2173.0
				Avg.	137.4	6.5	12.6	2120.4
				COV (%)	7.1	7.9	10.1	1.4

Table 4.2 shows the results of compressive strength. The net area with the average value of 9128 mm^2 was used to calculate compressive strength, as shown in Figure 4.1. The average compressive strength of the CMUs was 12.5 MPa with a COV of 7.1%. The typical

compressive failure mode of CMUs was conical shear, as illustrated in Figure 4.2.

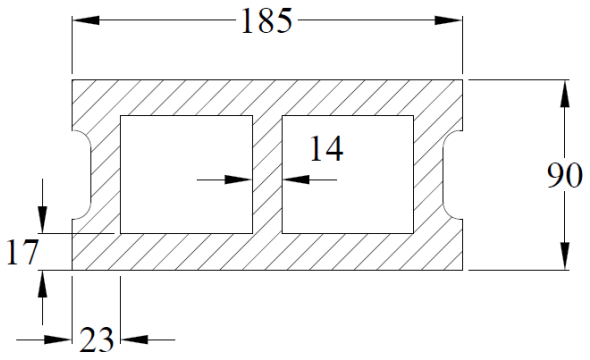

Figure 4.1 Net Area of CMUs

Table 4.2 Compressive Test Results of CMUs

Masonry Unit ID	Ultimate Load (kN)	Compressive Strength (MPa)
1	111.2	12.2
2	114.0	12.5
3	118.6	13.0
4	105.7	11.6
5	126.8	13.9
6	105.6	11.6
	Avg. (MPa)	12.5
	COV (%)	7.1

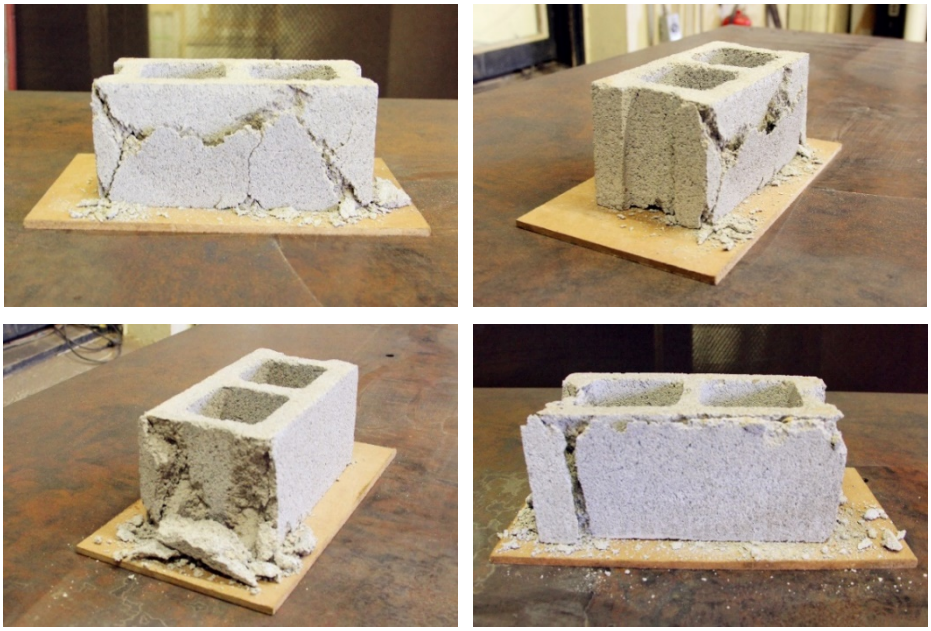

Figure 4.2 Typical Compressive Failure Mode of CMUs

4.2.2 Mortar

Two batches of mortar (batch A and batch B) were used to construct masonry infills where specimens IF-RC-DO and IF-RC-ID were made of batch A mortar, and specimens IF-RC-TG, IF-RC-SG and IF-S were made of batch B mortar. The dimensions and compressive strength of mortar cubes are shown in Table 4.3. Batch A mortar had an average compressive strength of 10.4 MPa with a COV of 4.1%, and Batch B mortar had an average compressive strength of 7.6 MPa with a COV of 6.5%. According to the specified provisions in CSA S304-14, the compressive strengths of mortar were greater than the limit of 5.0 MPa, and the COVs of both batches of mortar satisfied the COV limit of 15%. A conical failure mode of mortar cubes was observed under compressive loading, as shown in Figure 4.3.

Table 4.3 Compressive Test Results of Mortar Cubes

Mortar Cubes ID	Ultimate Load (kN)	Width (mm)	Length (mm)	Area (mm^2)	Compressive Strength (MPa)
Mortar Batch A (for IF-RC-ID and IF-RC-DO)					
MA1	25.1	49.9	50.4	2515.0	10.0
MA2	25.5	50.1	50.5	2530.1	10.1
MA3	27.2	50.0	50.5	2525.0	10.8
MA4	28.1	49.9	50.8	2534.9	11.1
MA5	26.0	50.0	50.7	2535.0	10.3
MA6	26.3	50.0	50.9	2545.0	10.3
				Avg. (MPa)	10.4
				COV (%)	4.1
Mortar Batch B (for IF-RC-TG, IF-RC-SG and IF-S)					
MB1	20.4	51.0	51.1	2606.1	7.8
MB2	18.5	51.0	51.1	2606.1	7.1
MB3	20.3	51.0	51.2	2611.2	7.8
MB4	18.5	51.0	51.2	2611.2	7.1
MB5	19.6	51.1	51.2	2616.3	7.5
MB6	21.9	51.1	51.2	2616.3	8.4
				Avg. (MPa)	7.6
				COV (%)	6.5

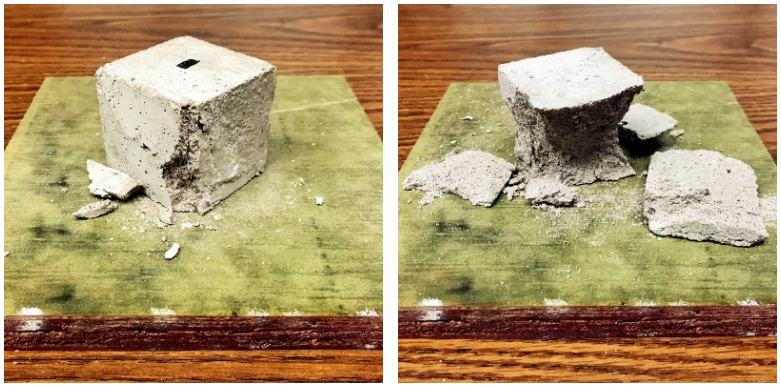

Figure 4.3 Typical Compressive Failure Mode of Mortar Cubes

4.2.3 Masonry Prisms

The prism batch A and batch B were built with mortar batch A and batch B, respectively. The mortar was only applied to the face shells of CMUs to be consistent with the construction practice. Therefore, only the face shell area as shown in Figure 4.4 was considered as the effective area of prisms (average 6290 mm^2) to determine the compressive strength. Table 4.4 presents the ultimate compressive load sustained by each prism and the corresponding compressive strength. The average compressive strength of prisms batch A was 7.9 MPa with a COV of 20.1%, and the average compressive strength of prisms batch B was 9.0 MPa with a COV of 13.5%. The masonry prisms typically exhibited face shell separation failure mode that was characterized by tensile splitting with vertical failure planes, as illustrated in Figure 4.5.

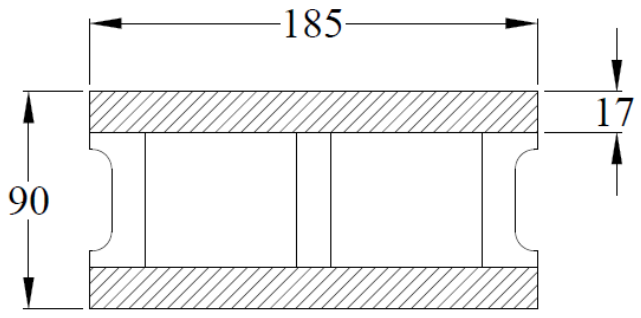

Figure 4.4 Effective Area of Masonry Prisms (mm^2)

Table 4.4 Compressive Test Results of Masonry Prisms

Prisms ID	Ultimate Load (kN)	f'_m (MPa)
Prisms Batch A (for IF-RC-ID and IF-RC-DO)		
PA1	44.9	7.1
PA2	41.7	6.6
PA3	43.9	7.0
PA4	59.3	9.4
PA5	65.6	10.4
PA6	43.6	6.9
	Avg. (MPa)	7.9
	COV (%)	20.1
Prisms Batch B (for IF-RC-TG, IF-RC-SG and IF-S)		
PB1	56.5	9.0
PB2	68.8	10.9
PB3	60.8	9.7
PB4	45.9	7.3
PB5	51.5	8.2
PB6	57.4	9.1
PB7	49.2	7.8
PB8	52.0	8.3
PB9	66.3	10.5
	Avg. (MPa)	9.0
	COV (%)	13.5

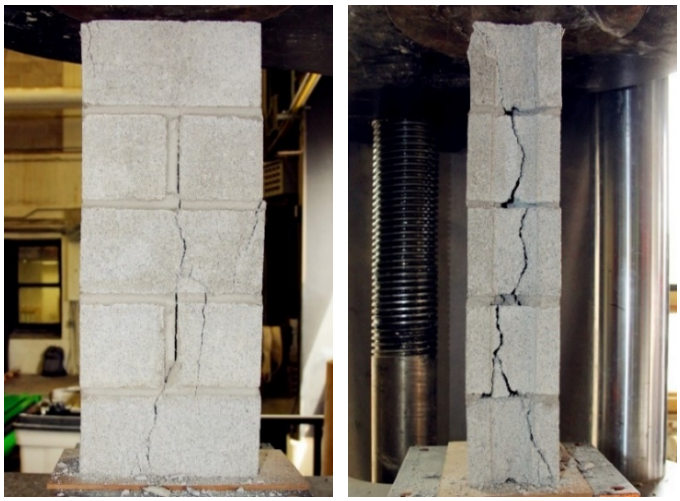

Figure 4.5 Typical Compressive Failure of Masonry Prisms

4.2.4 Steel Frame

A summary of the material properties, including the modulus of elasticity E, yield stress f_y, and ultimate stress f_u, is provided for each coupon in Table 4.5. As shown in Table 4.5, the average yield strength of steel frame coupons was 402 MPa with a COV of 5.4%, the average ultimate strength of steel frame coupons was 525 MPa with a COV of 2.6%, and the average modulus of elasticity of steel frame coupons was 201172 MPa with a COV of 4.0%.

Table 4.5 Tensile Test Results of Steel Frame Coupons

Coupons ID	Location	Yield Strength (MPa)	Ultimate Strength (MPa)	Modulus of Elasticity (MPa)
S1	Flange	378	503	198684
S2	Flange	378	524	204293
S3	Web	417	530	197475
S4	Web	421	530	213306
S5	Web	415	539	192101
Avg. (MPa)		402	525	201172
COV (%)		5.4	2.6	4.0

4.2.5 Concrete

Two batches of concrete (batch A and batch B) were used to construct RC frames where specimens IF-RC-DO, IF-RC-ID, and IF-RC-SG were made of batch A concrete, and specimen IF-RC-TG was made of batch B concrete. Table 4.6 summarizes the results of concrete strength at different days of curing. For batch A, the average 14-day strength was 24.5 MPa with a COV of 8.4%; the average compressive strength on 28-day was 35.8 MPa with a COV of 2.3%; the average compressive strength on the day of testing was 38.5 MPa with a COV of 0.7%; and the average modulus of elasticity was 16911 MPa with a COV of 2.9%. For batch B, the average 14-day strength was 29.1 MPa with a COV of 9.0%; the average compressive strength on 28-day was 36.6 MPa with a COV of 6.4%; and the average compressive strength on the day of testing was 42.4 MPa with a COV of 4.6%; and the average modulus of elasticity was 20357 MPa with a COV of 7.9%. The results showed that the strength of batch B concrete was slightly higher than the batch A concrete. A typical conical failure mode of the concrete cylinders was observed under compressive loading, as shown in Figure 4.6.

Table 4.6 Compressive Test Results of Concrete Cylinder

14 Days	Ultimate Load (kN)	f'c (MPa)	28 Days	Ultimate Load (kN)	f'c (MPa)	120 Days	Ultimate Load (kN)	f'c (MPa)	E (MPa)
Concrete Batch A (for IF-RC-DO, IF-RC-ID, and IF-RC-SG)									
A1	194.0	24.7	A4	278.8	35.5	A7	682.7	38.6	17247
A2	175.1	22.3	A5	288.2	36.7	A8	684.4	38.7	16342
A3	207.3	26.4	A6	275.7	35.1	A9	674.7	38.2	17145
Avg.		24.5			35.8			38.5	16911
COV(%)		8.4			2.3			0.7	2.9
Concrete Batch B (for IF-RC-TG)									
B1	233.9	29.8	B4	304.2	38.7	B7	781.0	44.2	19083
B2	206.2	26.2	B5	267.6	34.1	B8	755.3	42.7	22160
B3	246.0	31.3	B6	290.6	37.0	B9	712.0	40.3	19829
Avg.		29.1			36.6			42.4	20357
COV(%)		9.0			6.4			4.6	7.9

Figure 4.6 Typical Compressive Failure of Concrete Cylinder

4.2.6 Summary of Component Test Results

A summary of mechanical properties for every infilled frame component is given in Table 4.7. The properties of steel reinforcement were obtained from the previous testing program conducted by Hu (2015).

Table 4.7 Component Test Results of Infilled Frames

Component	Property (MPa)	IF-RC-ID	IF-RC-DO	IF-RC-TG	IF-RC-SG	IF-S
CMUs	Compressive Strength	12.5	12.5	12.5	12.5	12.5
Mortar	Compressive Strength	10.4	10.4	7.6	7.6	7.6
Masonry Prism	Compressive Strength	7.9	7.9	9.0	9.0	9.0
	Elastic Modulus	6715	6715	7650	7650	7650
Steel Frame Coupon	Yield Strength (Ultimate)	-	-	-	-	402 (525)
	Elastic Modulus	-	-	-	-	201172
Concrete Cylinder	Compressive Strength	38.5	38.5	42.4	38.5	-
	Elastic Modulus	16911	16911	20357	16911	-
Reinforcement (Hu 2015)	Yield Strength (Ultimate)	446 (665)	446 (665)	446 (665)	446 (665)	-
	Elastic Modulus	247357	247357	247357	247357	-

4.3 INFILLED FRAME SPECIMEN RESULTS

The following sections describe the behaviour, strength and failure pattern for each specimen. Additionally, comparison of the results with the previous study (Sepasdar 2017) is also described.

4.3.1 General Behaviour of Specimens Subjected to Out-of-Plane Loading

For ease of discussion, the following terms are defined in describing the out-of-plane behaviour. A typical pressure vs. out-of-plane displacement curve is illustrated in Figure 4.7 using specimen IF-RC-ID as an example. The LVDT with the largest recorded displacement was used in the plot. The response may be divided into four stages. Stage one is characterized by the portion with linear behaviour prior to initial cracking, and initial stiffness (K_{ini}) represents the slope of the initial linear portion of the load vs. displacement curve. Stage two started from the end of stage one to the load when the first significant cracking occurred, and cracking stiffness (K_{cr}) can be defined as the slope of the line connecting the origin and the point having the first significant crack. Stage three started from the cracking load to the ultimate load, and ultimate stiffness (K_{ult}) is defined as the slope of the line connecting the origin and the point having the ultimate load. In stage four, the load started to drop until physical failure of the infill occurred. The pressure and displacement corresponding to the ending of stage one are defined as initial load (P_{ini}) and

initial displacement (Δ_{ini}), respectively. The pressure and displacement corresponding to the first significant crack are defined as cracking load (P_{cr}) and cracking displacement (Δ_{cr}), respectively. The pressure and displacement corresponding to the maximum load are defined as ultimate load (P_{ult}) and ultimate displacement (Δ_{ult}), respectively. The pressure and displacement corresponding to the final failure of specimens are defined as failure load (P_{fail}) and failure displacement (Δ_{fail}), respectively.

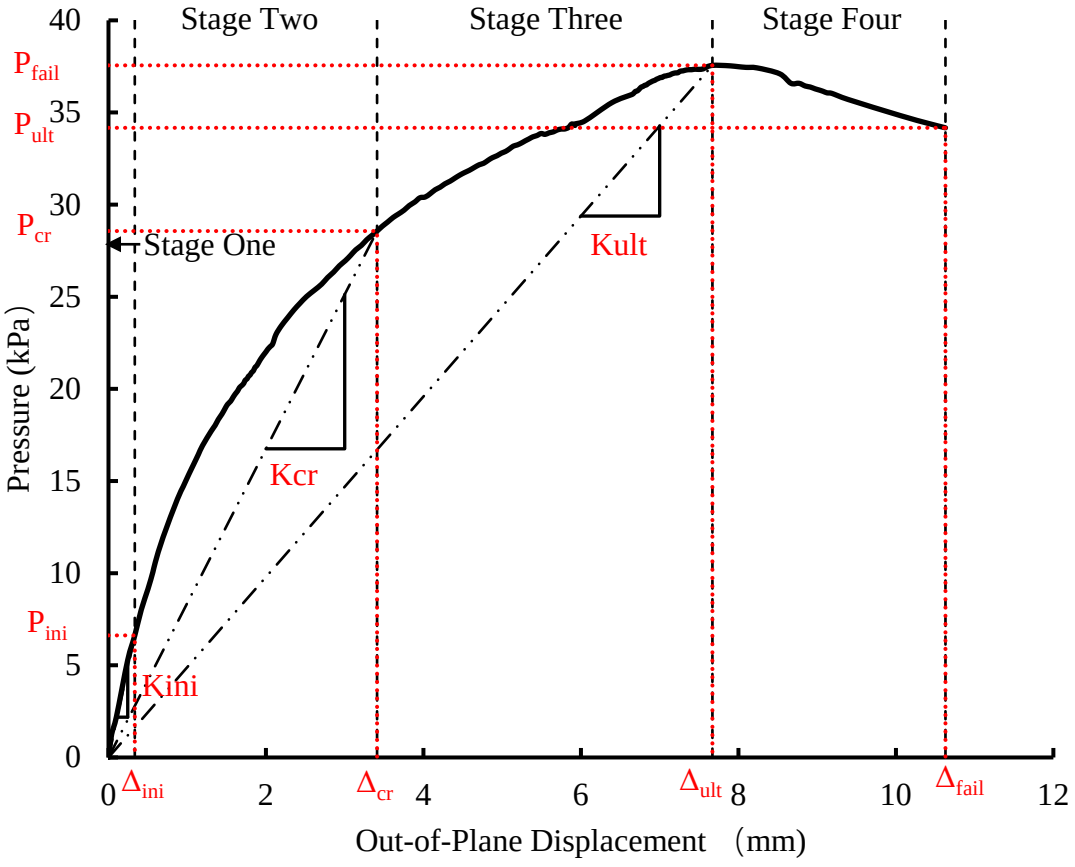

Figure 4.7 Typical Pressure vs. Out-of-Plane Displacement of Infilled Specimen

4.3.2 Specimen IF-RC-DO

This specimen had a 592 mm by 392 mm door opening at the center of infill which was covered with a 30 mm thick plywood board during the test. The pressure vs. out-of-plane displacement curve of the infill for the LVDT 5 (right above the opening, the one with the largest recorded displacement) and the cracking pattern with corresponding load are shown in Figure 4.8 and Figure 4.9, respectively.

In the first stage, small hairline cracks were observed at top corners of the opening at pressure of 7.4 kPa. The hairline cracks expanded toward the corners of the infill with a length of half block. The infill showed initial linear load vs. out-of-plane displacement behaviour up to about 15 kPa (41% of ultimate load). As the load continued to increase, a visible vertical crack began to develop at the top edge of the opening at pressure of 19.7 kPa and out-of-plane displacement of 1.2 mm. Compare with the initial stiffness, the infill had a 34% stiffness reduction at the cracking load. With the increase of pressure, the vertical crack continued to develop along the interface between the blocks and mortar, and extended to the top center of the infill at the pressure of 23.6 kPa. At a pressure of 29.2 kPa, some horizontal cracks began to develop along the top of the opening, but the initial hairline cracks did not widen significantly. The decreasing in the stiffness of the infill was accompanied by the development of cracking in stage three. At pressure of 36.2 kPa and out-of-plane displacement of 7.9 mm, the infill reached its ultimate strength. Beyond this

point, collapse of the infill suddenly occurred at the pressure of 35.4 kPa and out-of-plane displacement of 8.6 mm. At the point of collapse, two new cracks extended from the existing cracks that developed at top corners of the opening to the top and bottom boundary of the infill, and one crack developed along the left boundary of the infill.

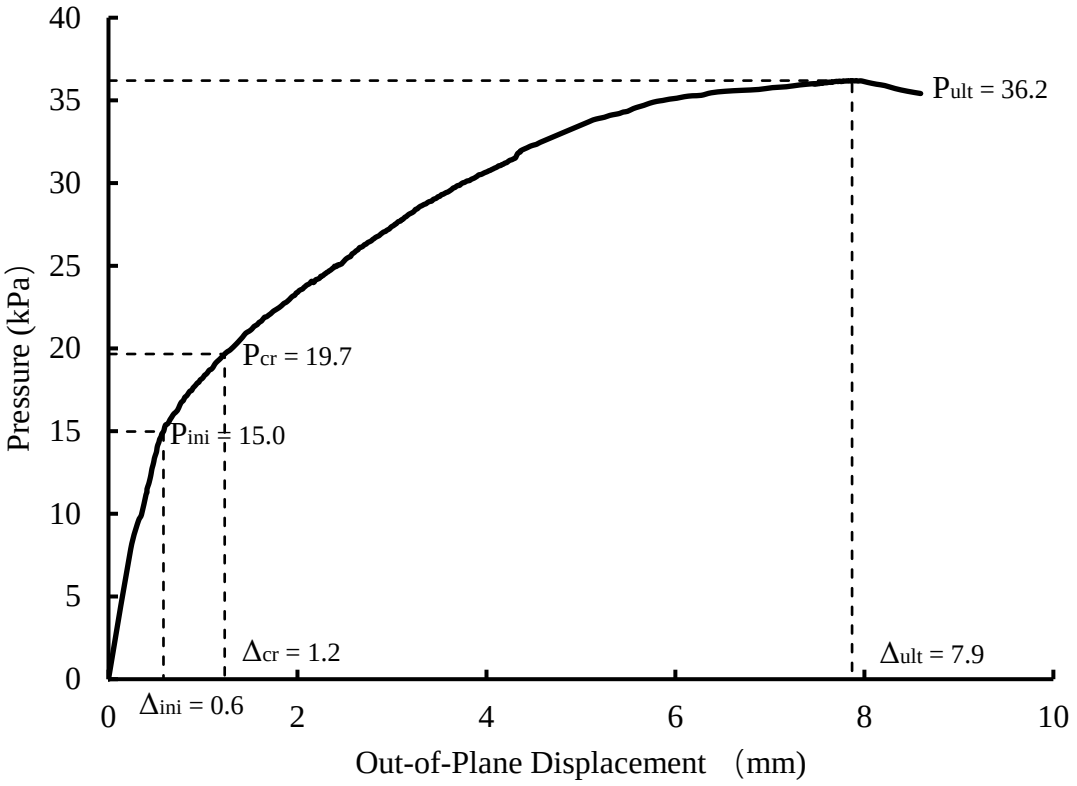

Figure 4.8 Pressure vs. Out-of-Plane Displacement of Specimen IF-RC-DO

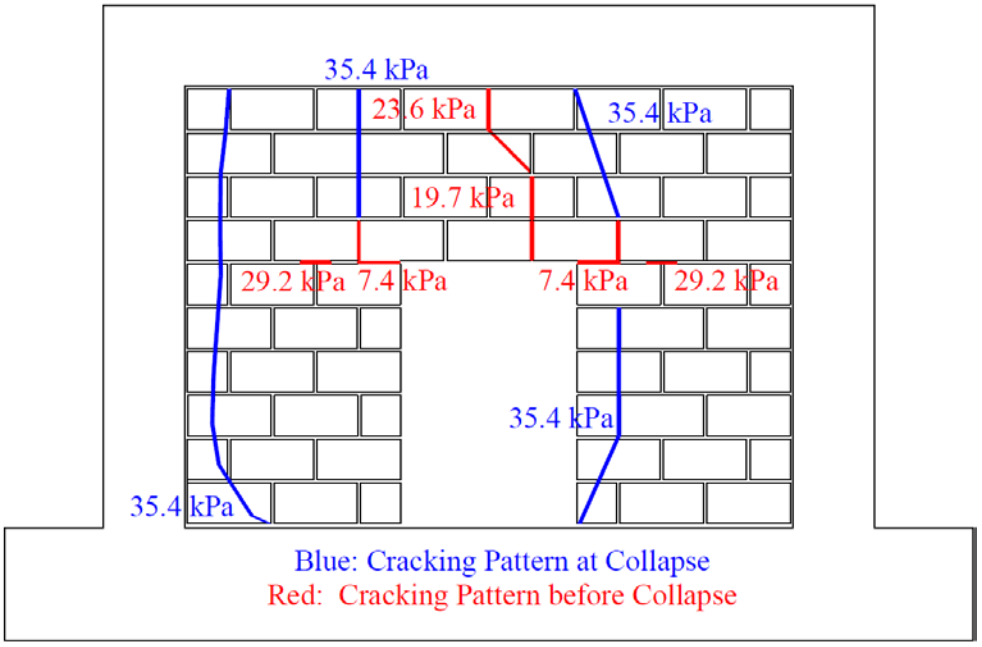

Figure 4.9 Crack Patterns of Specimen IF-RC-DO

Figure 4.10 and Figure 4.11 show the final failure at the leeward and windward of the specimen respectively. Aside from extensive cracking developed around the door opening, the entire section containing the opening collapsed on the windward side and face shell spalling was observed on the leeward side. A close-up view of the face shell spalling illustrated in Figure 4.12 showed the web shear failure of the masonry blocks. This shear type of failure was also observed in the study by Sepasdar (2017).

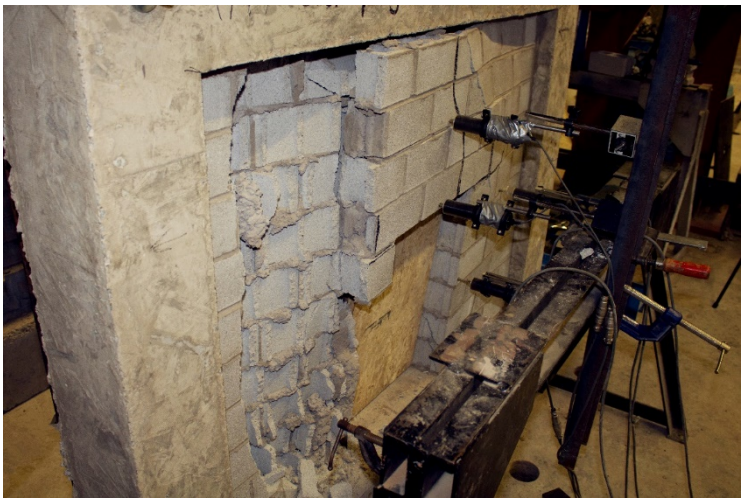

Figure 4.10 Failure Mode of Specimen IF-RC-DO on Leeward

Figure 4.11 Failure Mode of Specimen IF-RC-DO on Windward

Figure 4.12 Web Shear Failure of Masonry Units for Specimen IF-RC-DO

Figure 4.13 and Figure 4.14 plot the vertical displacement profile along the center of the infill and along the left side of the opening respectively. Figure 4.15 plots the horizontal displacement profile across the opening. It can be seen that the ultimate and failure displacements of the infill were observed along the top of the opening (LVDT 2 and LVDT 5) with the values of about 7.9 mm and 8.6 mm, respectively. Also, about 84% and 80% of ultimate out-of-plane displacement of the infill were developed after the infill reached cracking load and 60% ultimate load, respectively; and about 8% failure displacement of the infill was developed after the infill reached its ultimate strength. The fact that most displacement developed after the initial cracking supports the arching action where displacement is resulted mainly from rotation of cracked infill segments. Comparing Figures 4.14 and 4.15, the infill did not behave symmetrically with respect to center horizontal axis of the infill but relatively symmetrically with respect to center vertical axis

of the infill under out-of-plane loading. This suggests that presence of the opening introduced a weak plane along its top which moved the initial horizontal cracking to that location. Since in this case, the vertical arching is dominant and therefore the opening affects the vertical arching more than the horizontal arching.

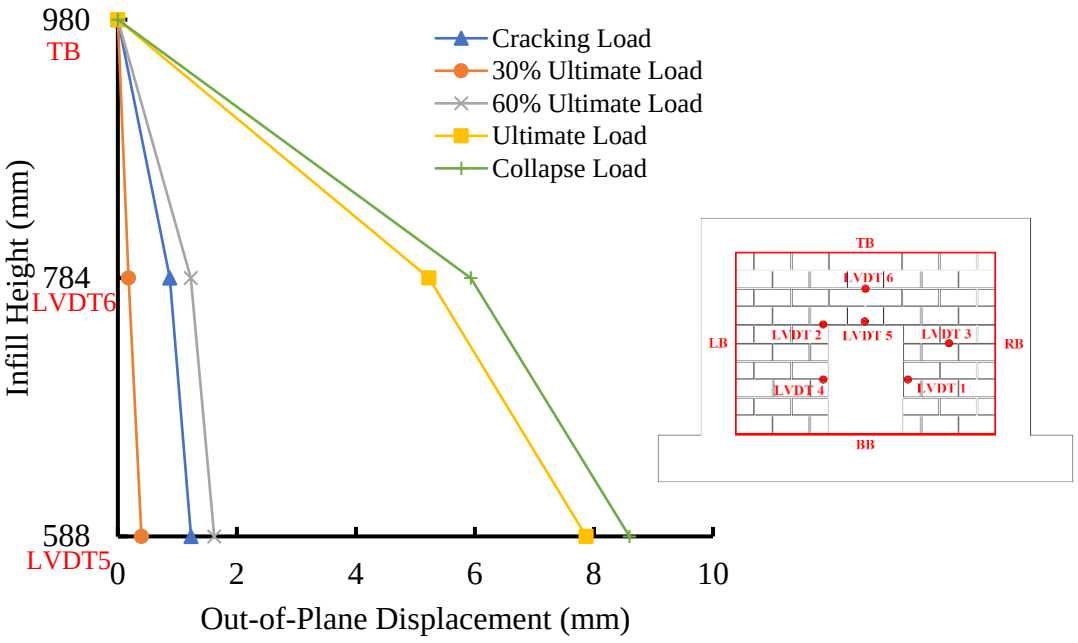

Figure 4.13 Displacement Curves of Specimen IF-RC-DO for Vertical LVDTs

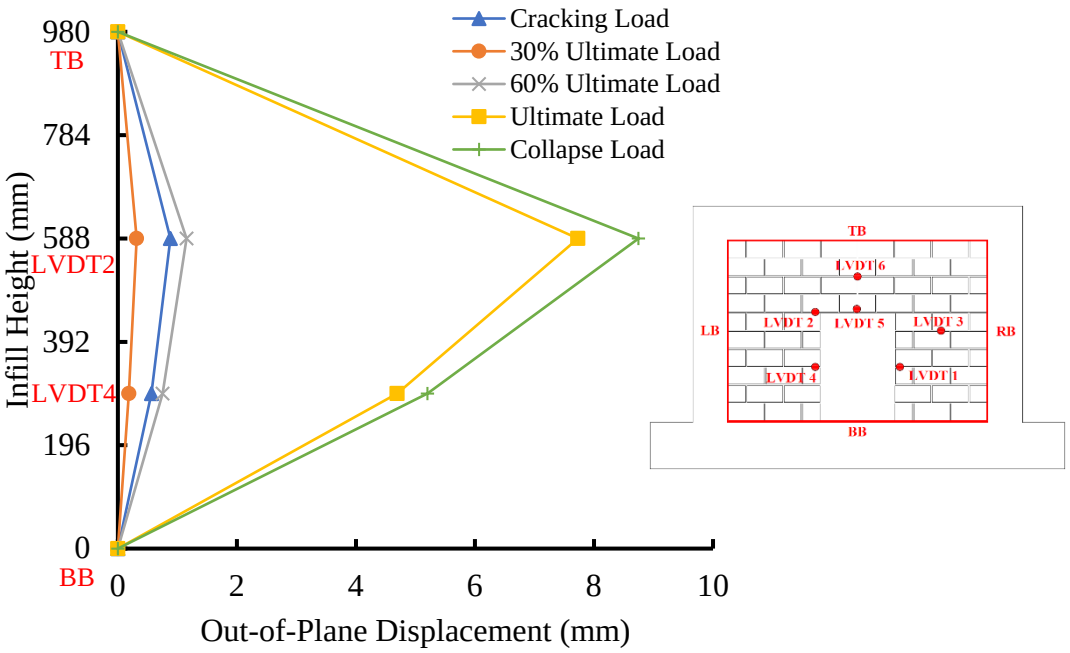

Figure 4.14 Displacement Curves of Specimen IF-RC-DO for Vertical LVDTs through Infill Center

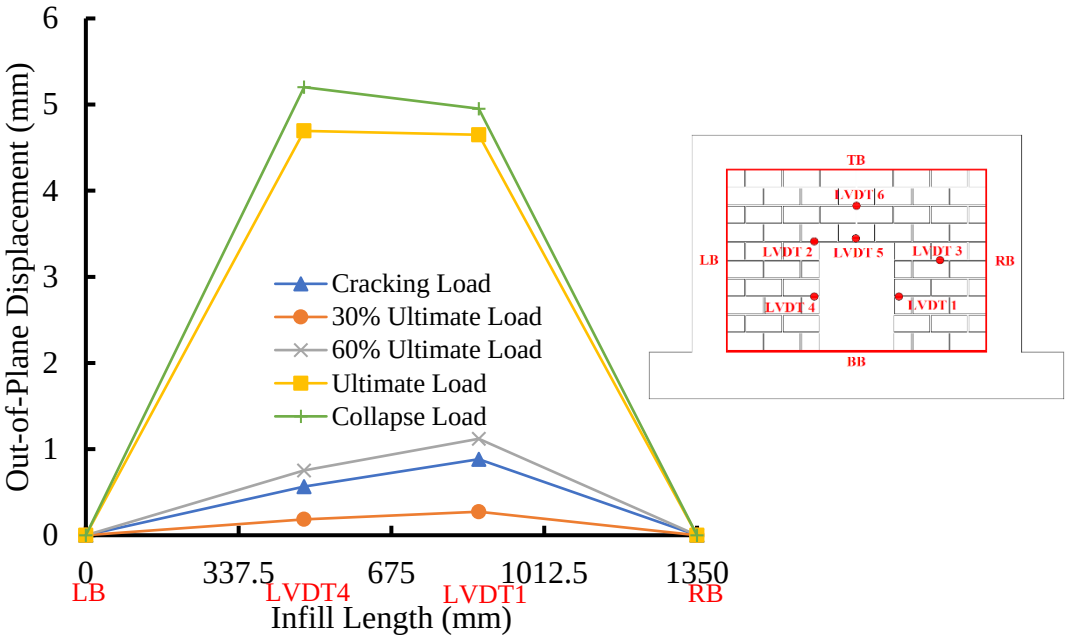

Figure 4.15 Displacement Curves of Specimen IF-RC-DO for Horizontal LVDTs

4.3.3 Specimen IF-RC-ID

This specimen was used to investigate the effect of prior in-plane damage on the out-of-plane behaviour of infilled frame. The in-plane loading was first applied to the specimen to a lateral displacement of 13.4 mm. The load vs. in-plane displacement curve, and the cracking pattern developed up to the pre-load level are presented in Figure 4.16 and Figure 4.17, respectively. The initial response of the infill was more or less liner. A hairline crack was developed at the right top corner of the infill at a load of 28 kN, beyond which point, some nonlinearity began to develop in the response. The first major diagonal crack was developed at a load of 80.7 kN with a lateral displacement of 7.2 mm. The response curve experienced a marked load drop at this point but immediately thereafter, load continued to increase. At a load of 90 to 95 kN, separation between the infill and the bounding frame was observed at the left bottom of the infill with a length of 2 blocks and shear sliding was developed at the interface with the top beam. With a further increase in load, the diagonal cracks developed more extensively as illustrated in Figure 4.17 and Figure 4.18. The cracking was shown to be either through masonry blocks or mortar joints. At the load of about 105 kN and the in-plane displacement of about 13.4 mm, the in-plane loading was removed, and the load and in-plane displacement corresponded to this point are defined as applied in-plane load (F_{app}) and applied in-plane displacement (δ_{app}), respectively. Comparing with Sepasdar's specimen IF-D1 where pre-loading was applied till

development of a major diagonal crack and this occurred at an in-plane load of 107.4 kN with a lateral displacement of 6.5 mm as shown in Figure 4.19, specimen IF-RC-ID of this study had more extensive diagonal cracking and greater in-plane displacement, signifying a more developed cracking stage.

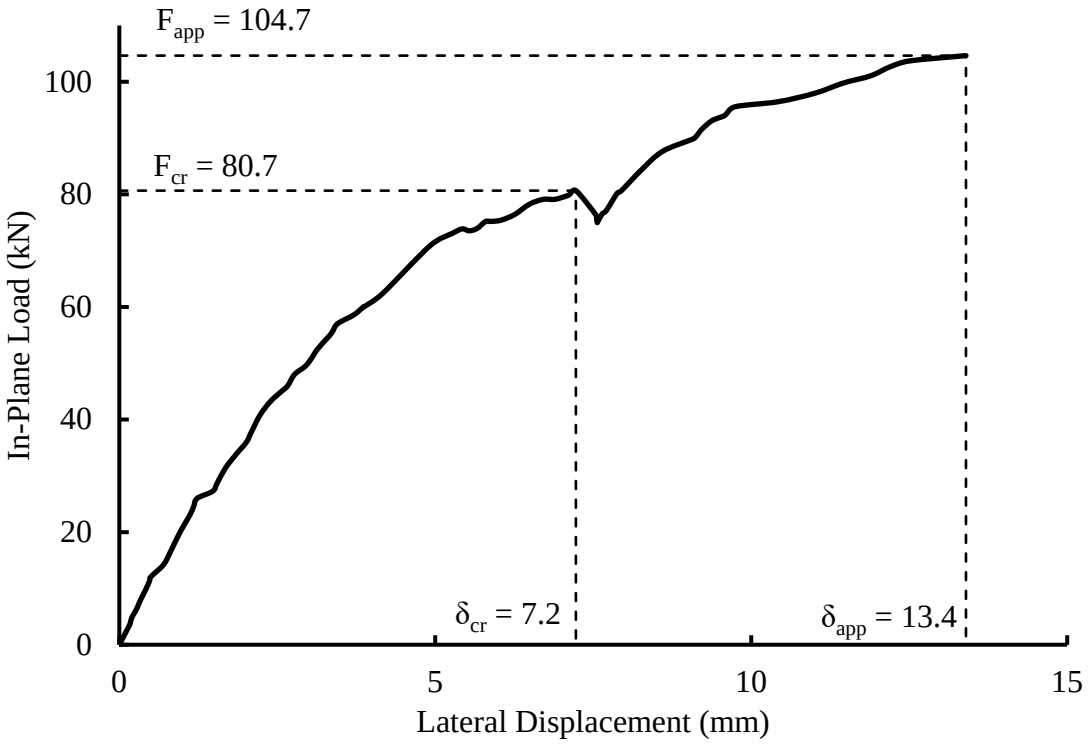

Figure 4.16 Load vs. In-Plane Displacement of Specimen IF-RC-ID

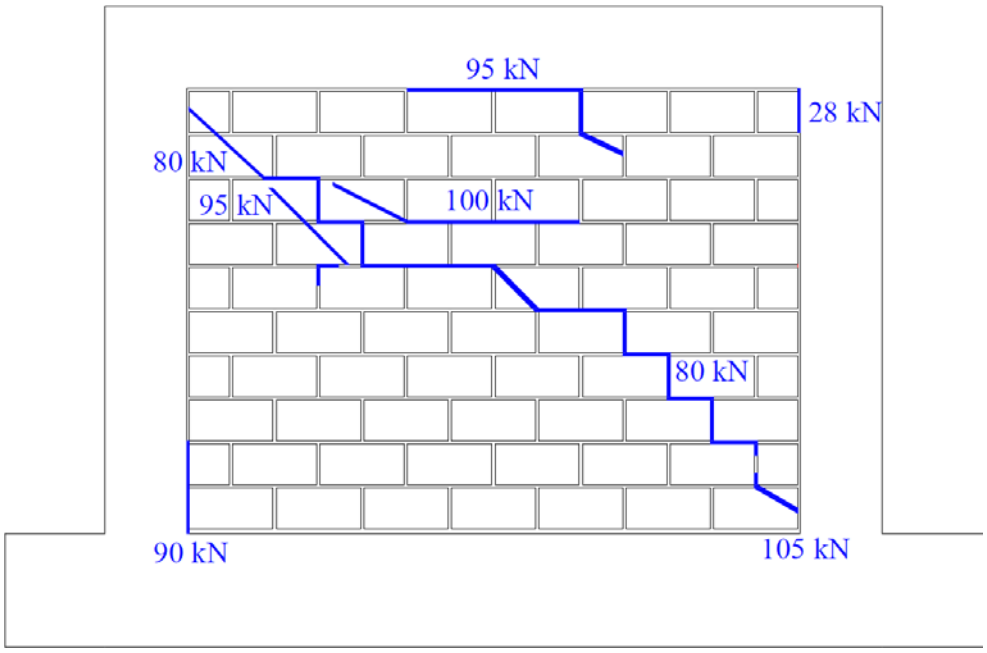

Figure 4.17 Crack Patterns of Specimen IF-RC-ID under In-Plane Loading

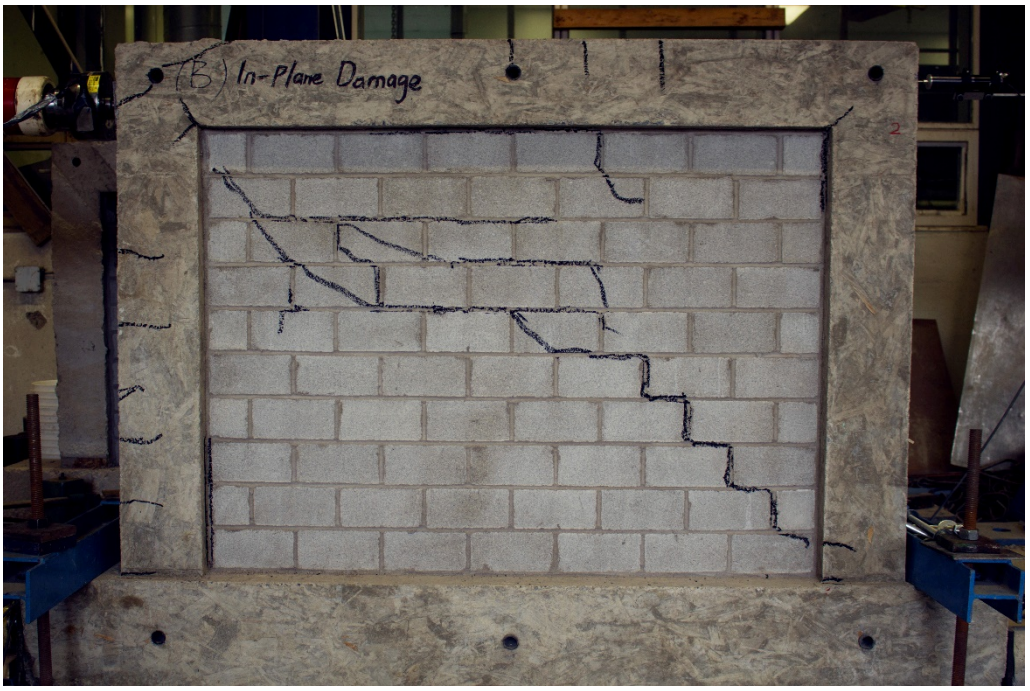

Figure 4.18 Prior In-Plane Damage for Specimen IF-RC-ID

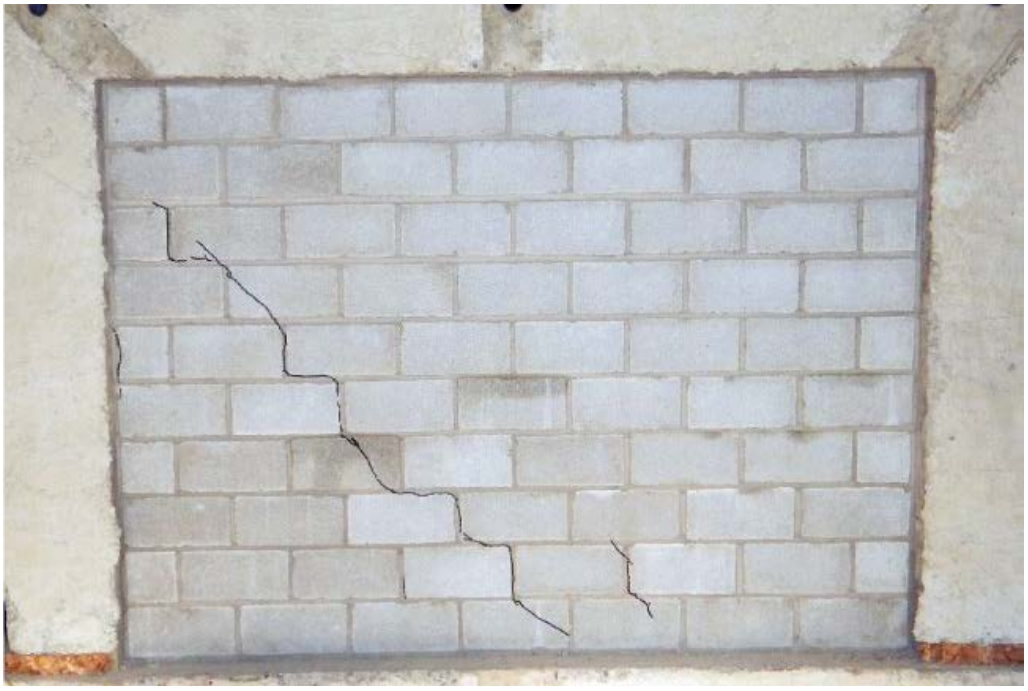

Figure 4.19 Prior In-Plane Damage for Specimen IF-D1 (Sepasdar 2017)

The load vs. out-of-plane displacement curve for the central LVDT (the one with the maximum recorded displacement) is plotted in Figure 4.20, and Figures 4.21 and 4.22 show the cracking pattern with corresponding out-of-plane loading. The specimen showed a linear behaviour up to about 6.6 kPa in the stage one, and the initial stiffness of the linear portion was about 21.0 kPa/mm. The first major crack caused by out-of-plane loading was developed at the pressure of about 28.6 kPa and out-of-plane displacement of 3.4 mm on the top right side of infill. At a pressure of about 32 kPa, a major horizontal crack was observed along the fifth layer bed joints from the top beam and the mortar along the interface between the top beam and infill began to crush. As load increased, the existing cracks gradually widened and new cracks also developed extending from the right top corner of the infill to the center of the infill. The specimen reached its ultimate strength at

the pressure of 37.6 kPa and the out-of-plane displacement of 7.7 mm, which represented the end of stage three. The final collapse of infill occurred at the pressure of 34.2 kPa (about 91% of ultimate load) with out-of-plane failure displacement of 10.6 mm. Similar to previous specimens, the collapse of the infill was resulted from web shear failure of the masonry blocks, as shown in Figure 4.23.

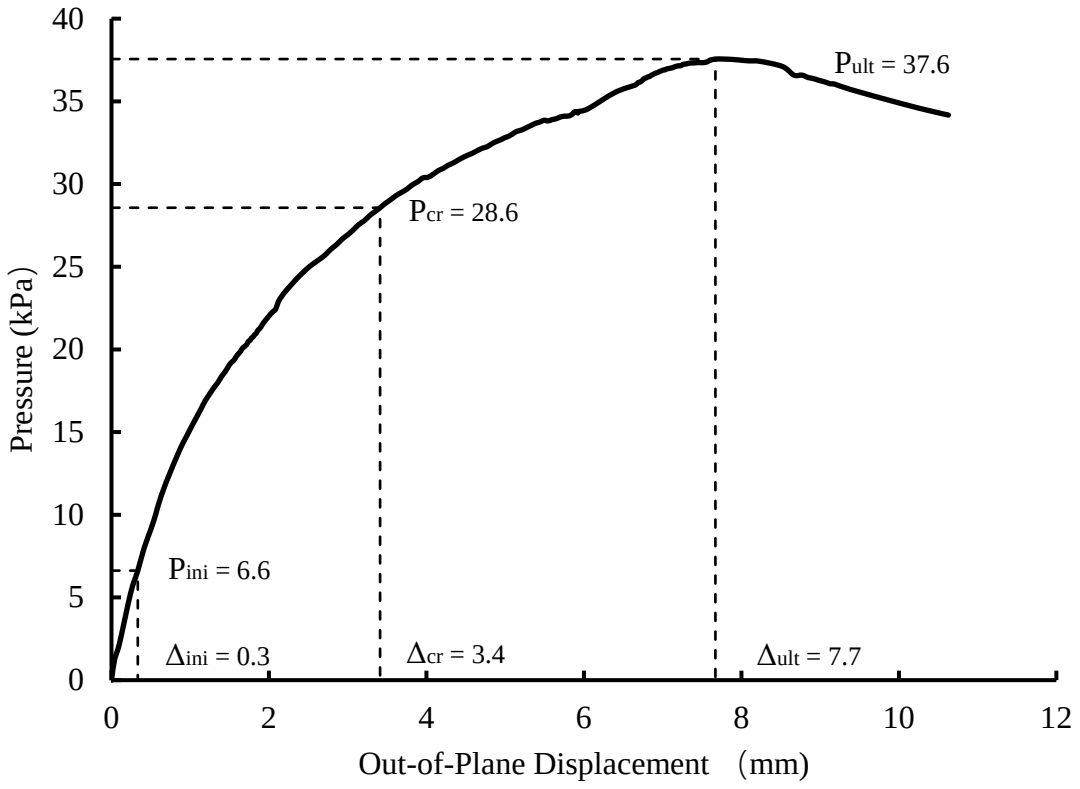

Figure 4.20 Pressure vs. Out-of-Plane Displacement of Specimen IF-RC-ID

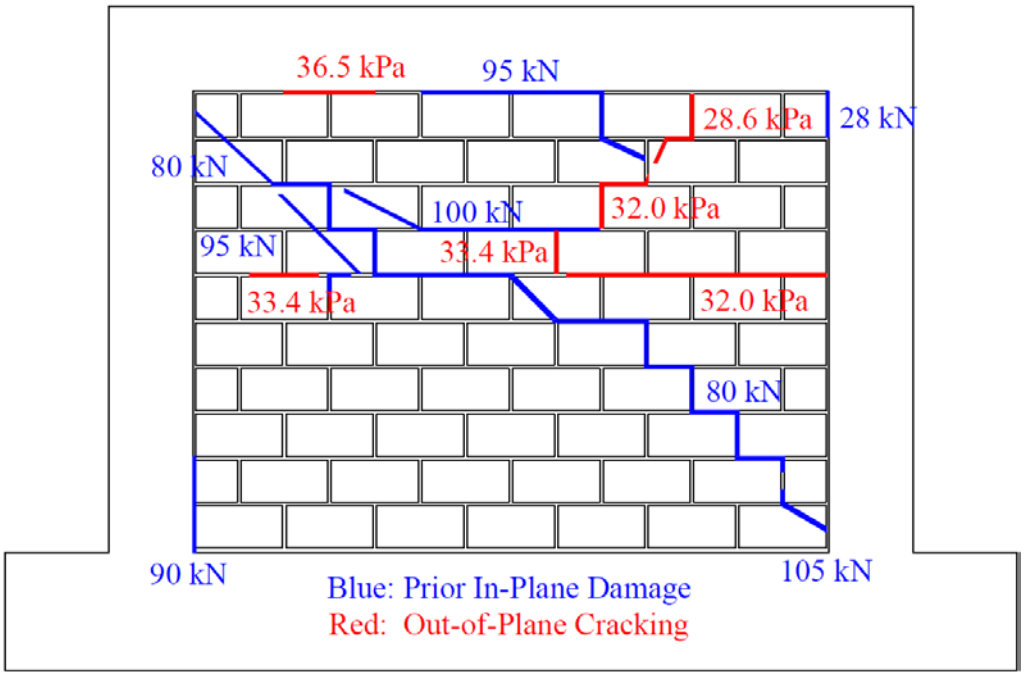

Figure 4.21 Crack Patterns of Specimen IF-RC-ID

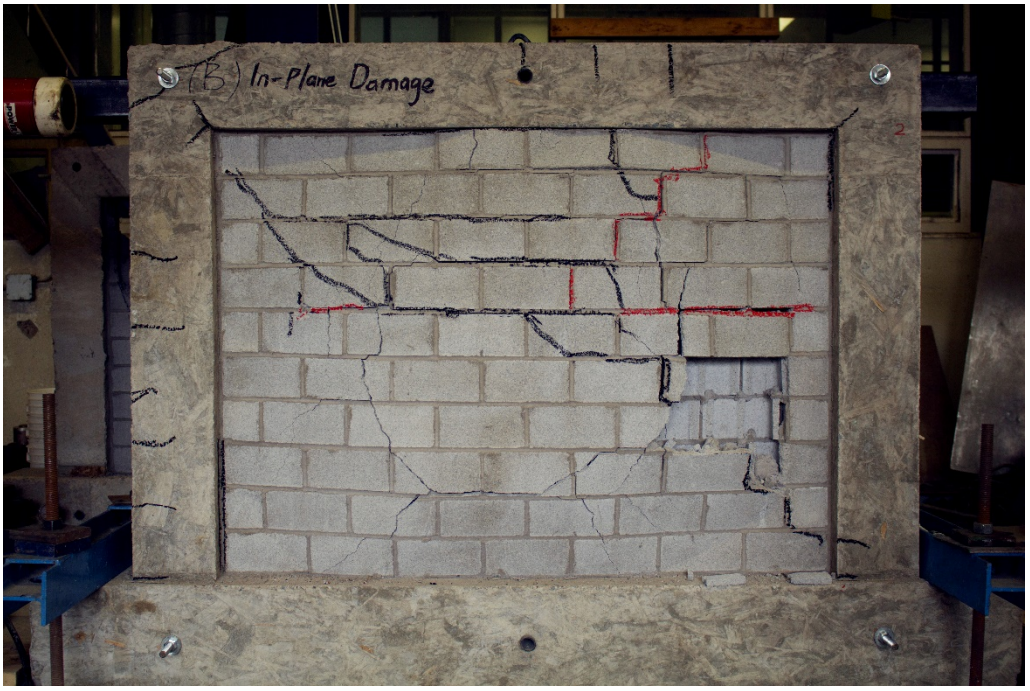

Figure 4.22 Failure Mode of Specimen IF-RC-ID on Leeward

Figure 4.23 Web Shear Failure of Masonry Units for Specimen IF-RC-ID

The displacement profile for the infill, as illustrated in Figure 4.24 and 4.25, shows that a symmetrical arching action was developed before the infill reached the cracking load. After that point, although arching in both directions were still evident, the deformation profile was no longer symmetrical and the top and left portion of the infill experienced greater deformation. This is believed to be attributed to pre-loading damage which caused one section of the infill weaker than others.

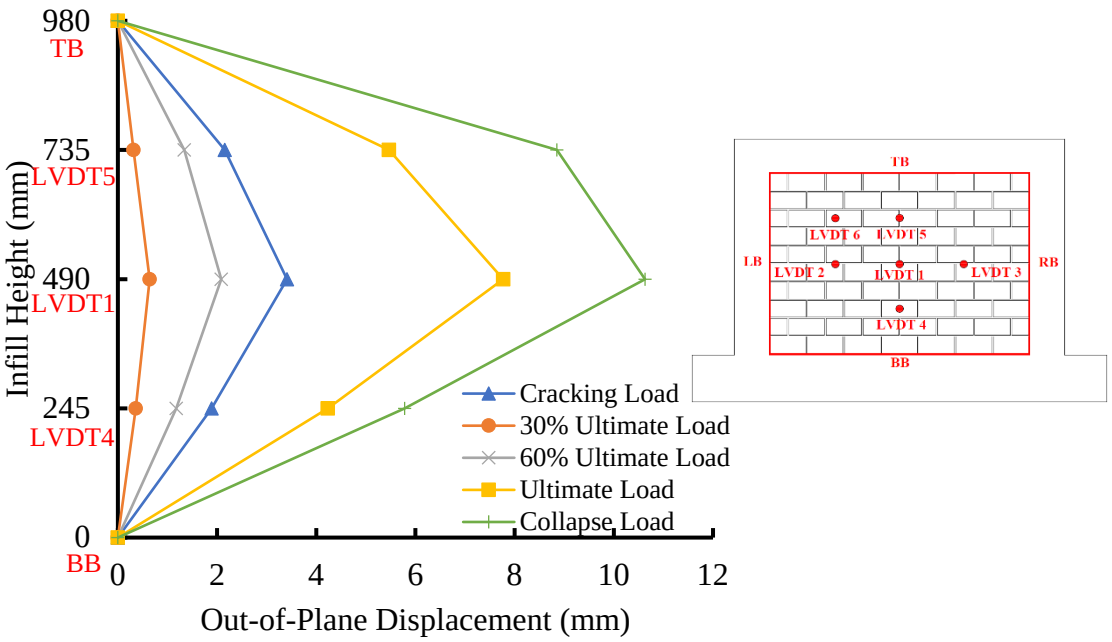

Figure 4.24 Displacement Curves of Specimen IF-RC-ID for Vertical LVDTs

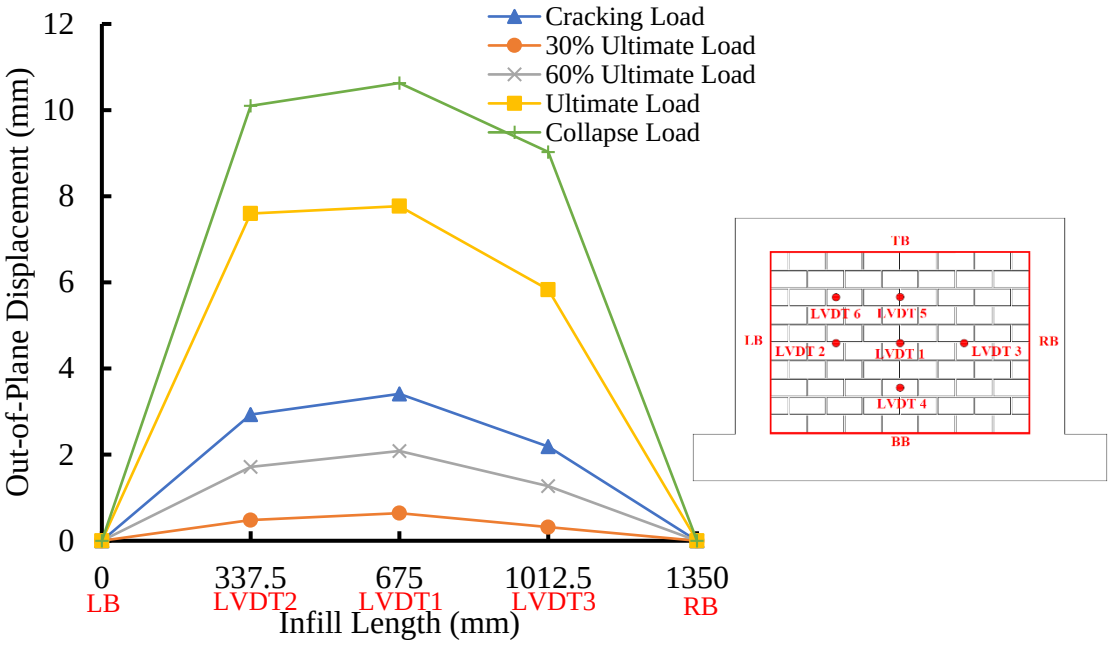

Figure 4.25 Displacement Curves of Specimen IF-RC-ID for Horizontal LVDTs

4.3.4 Specimen IF-RC-TG

The specimen had a 10 mm gap at the top beam-to-infill interface. The pressure vs. out-of-plane displacement curve for the central LVDT (the one with the largest recorded displacement) is plotted in Figure 4.26. The development of cracking pattern with the corresponding load and failure mode are shown in Figure 4.27 and 4.28, respectively. For this specimen, the curve did not show a clear separation of stage one from two, rather, it remained linear to the point of major cracking and beyond. When the load was increased to 4.3 kPa (about 23% of the ultimate load) corresponding to an out-of-plane displacement of 0.6 mm, a vertical crack was observed from the forth layer bed joint extending to the top beam as shown in Figure 4.27. The initial stiffness and cracking stiffness were then determined to be 7.2 kPa/mm. At the beginning of stage three, hairline diagonal cracks formed at the bottom of the vertical crack. With the increase of pressure, the diagonal cracks widened, and developed toward the bottom corners of the infill and developed along the interface between bocks and mortar. The cracking pattern is more or less similar to the yield line pattern for the infill with three sides supported. The infill reached its ultimate strength at the pressure of 18.5 kPa and out-of-plane displacement of 3.9 mm. After this point, the out-of-plane pressure began to drop but the infill appeared to be still stable, and at the pressure of 16.3 kPa (about 88% of ultimate load and out-of-plane displacement of 5.7 mm), the top portion of infill bulged out and more cracks (highlighted in red and blue) were

developed along the height of infill on both sides as seen in Figure 4.28. The test was then stopped and the final failure was deemed to have occurred. A close examination of failed specimen on the windward face as seen in Figure 4.29 showed that spalling of the faceshell of CMUs but the spalling was appeared to be a result of web shear through cracking.

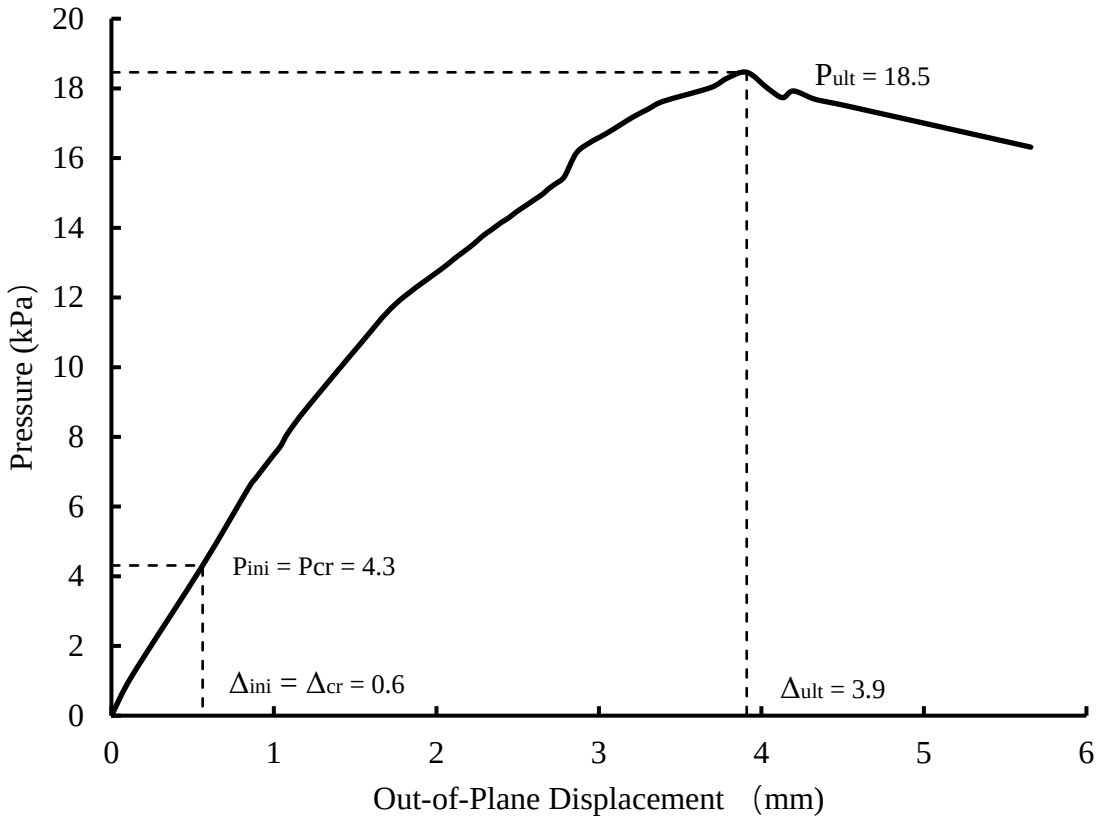

Figure 4.26 Pressure vs. Out-of-Plane Displacement of Specimen IF-RC-TG

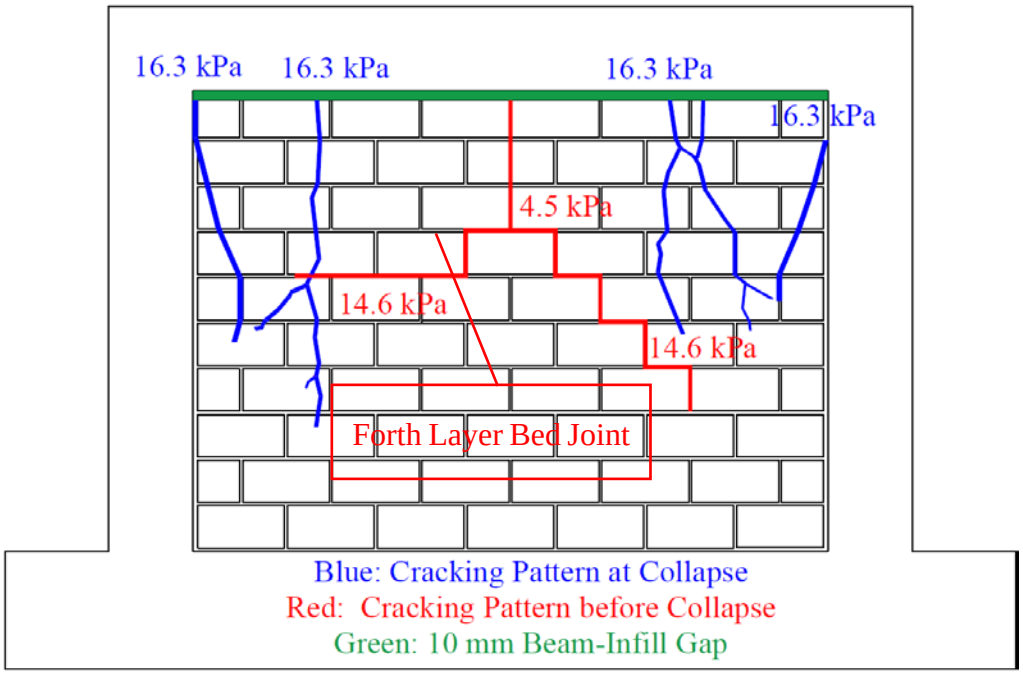

Figure 4.27 Crack Patterns of Specimen IF-RC-TG

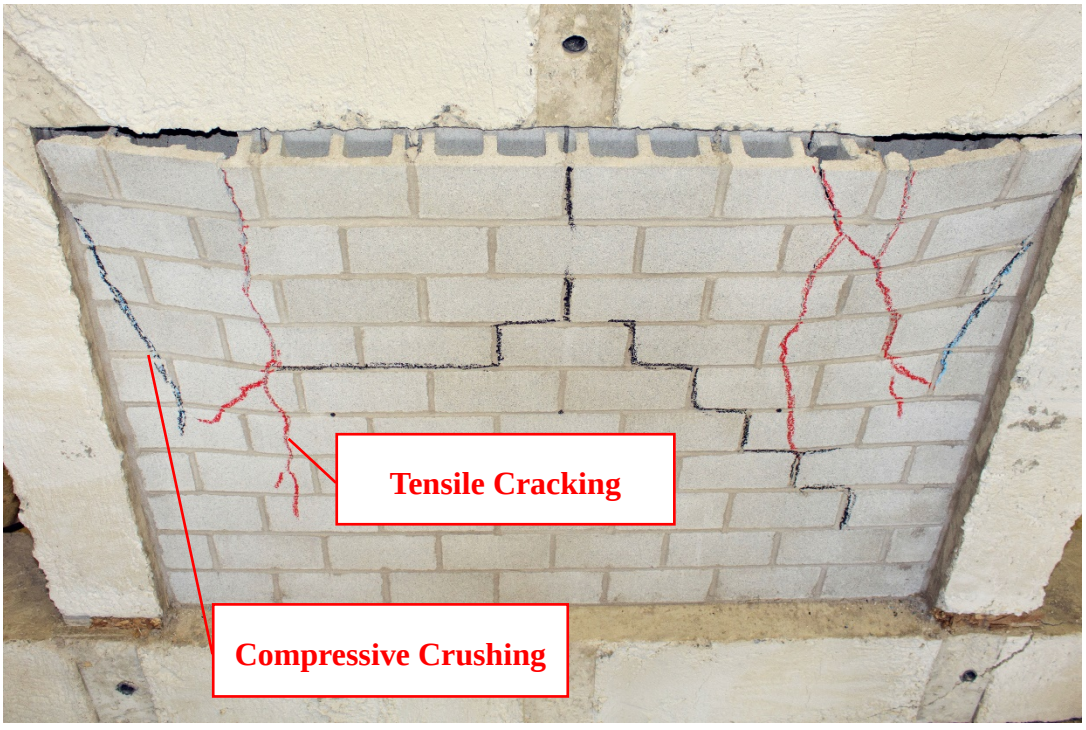

Figure 4.28 Failure Mode of Specimen IF-RC-TG on Leeward

Figure 4.29 Web Shear Failure of Masonry Units for Specimen IF-RC-TG

The displacement profiles through loading history are plotted in Figure 4.30 for vertical LVDTs and in Figure 4.31 for horizontal LVDTs. While horizontal displacements showed a symmetrical pattern with respect to the infill center, the deformation along the vertical direction was non-symmetrical and the magnitude of displacements decreased from the top beam to close to zero at the bottom. This indicates that arching action still developed in the horizontal span, but the effective arching did not develop in the direction of vertical span where the top beam was not engaged to provide a rigid support due to the presence of 10 mm top gap. As the contact between the infill and the bottom beam was maintained during the loading, the infill should be considered as supported on three sides and free at the top. This may explain the yield line like cracking pattern consistent with a typical slab with this

type of boundary condition. However, unlike a conventional slab yield line pattern where yield line is dependent on the tensile behaviour of the slab, the infill yield line is also dependent on the arching effect. Prior to the ultimate load, the maximum out-of-plane displacement was recorded at LVDT 5 (the center of the third course), and it was shifted to LVDT 6 (the top edge of infill) when the final failure of infill occurred, confirming that the top portion of the infill bulged out (lost stability) immediately after the ultimate load.

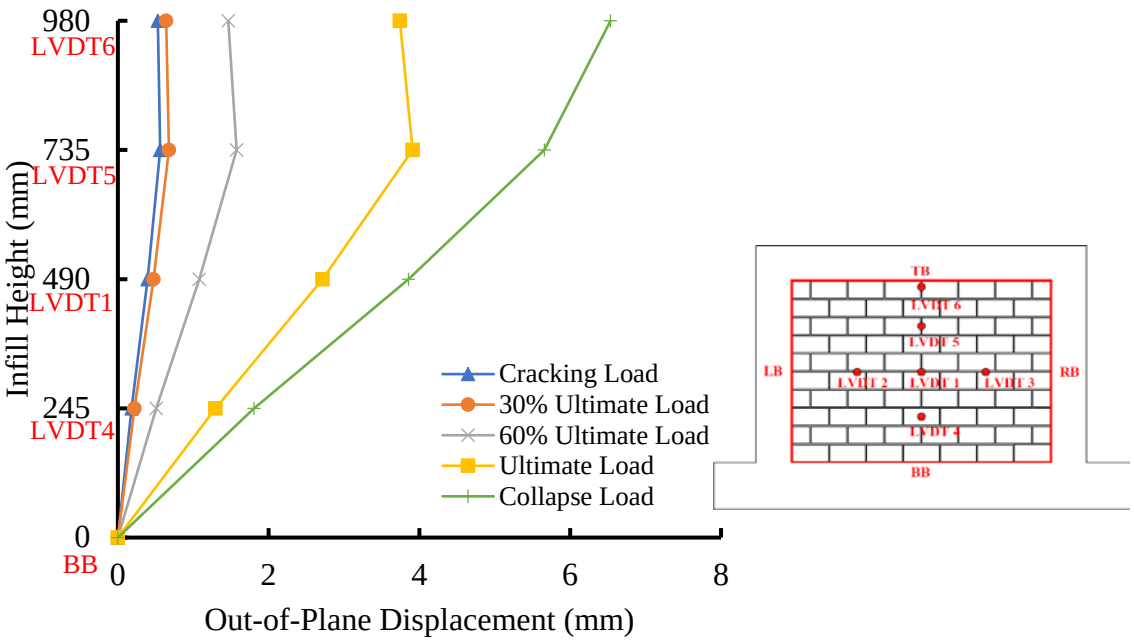

Figure 4.30 Displacement Curves of Specimen IF-RC-TG for Vertical LVDTs

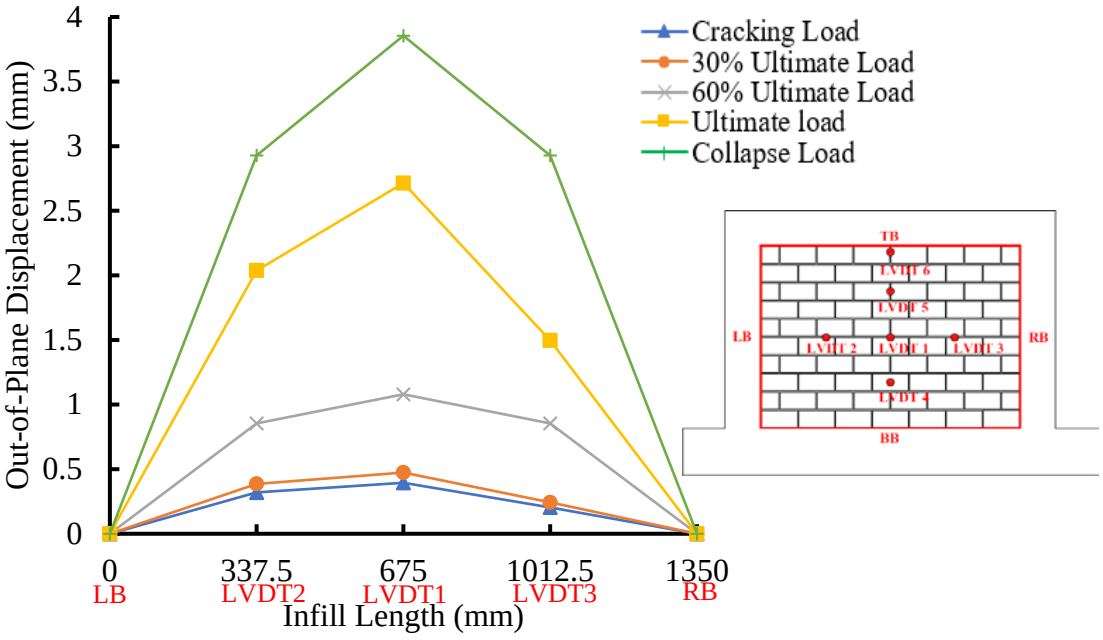

Figure 4.31 Displacement Curves of Specimen IF-RC-TG for Horizontal LVDTs

4.3.5 Specimen IF-RC-SG

This specimen had a 5 mm gap between the infill and columns of the frame on each side. Figure 4.32 plots the pressure vs. out-of-plane displacement curve for the central LVDT (the one with maximum recorded displacement), and Figure 4.33 illustrates the cracking pattern with corresponding loads. At the stage one, the specimen showed a linear behaviour with an initial stiffness of 19.3 kPa/mm. When the load increased to about 50% of the ultimate load (18.4 kPa), a horizontal crack was first observed at the mid-height of infill at an out-of-plane displacement of 1.6 mm, resulting in a cracking stiffness of 11.5 kPa/mm. The infill maintained more or less the linear behaviour during the development of cracks (from the end of stage one to end of stage two). At pressure of 33.5 kPa, the width of the horizontal crack widened to about 2 mm, and the vertical arching action was significant. Additionally, diagonal cracks developed and extended from the top corners of the infill to the center of the infill with the height of three blocks, and most of them were observed along the block-mortar interface. At pressure of 36.3 kPa, crushing of the mortar was observed at the top corners of the infill along a length of two and half blocks. The infill reached its ultimate strength at pressure of 36.5 kPa and out-of-plane displacement of 7.4 mm. At stage four, the dropping off portion of loading was small, and the infill collapsed at the pressure of 35.7 kPa (about 98% of ultimate load) with an out-of-plane displacement of 8.2 mm.

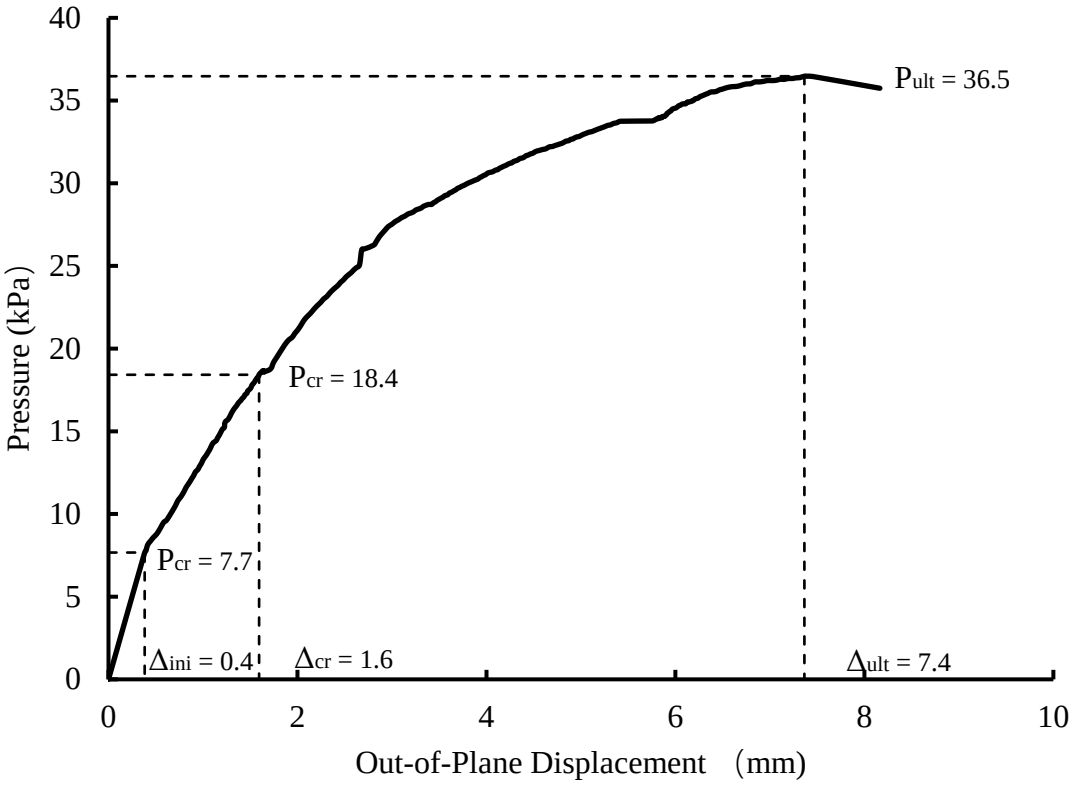

Figure 4.32 Pressure vs. Out-of-Plane Displacement of Specimen IF-RC-SG

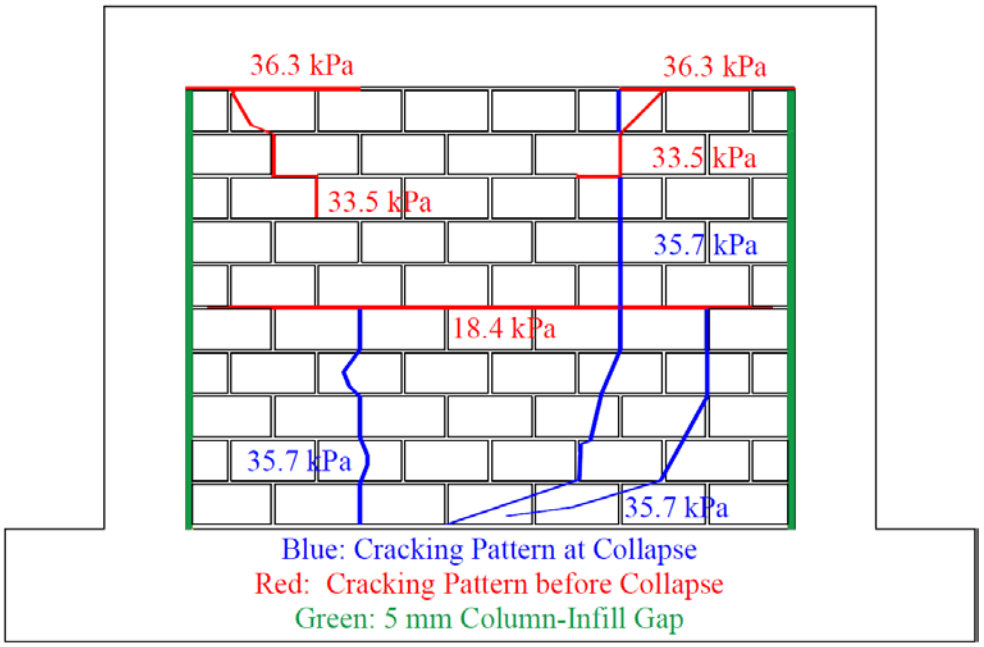

Figure 4.33 Cracking Patterns of Specimen IF-RC-SG

Figure 4.34 and Figure 4.35 show the final failure mode where significant cracking has caused separation of segment one. It was found that the column-to-infill gap remained throughout the loading history and deformation of the infill/frame did not fully close the gap. The out-of-plane displacement profiles at several levels through loading history are plotted in Figure 4.36 and Figure 4.37. The vertical arching was pronounced as evidenced in Figure 4.36 where deformation appeared to be symmetrical with respect to the center of infill throughout the loading history and deformation increased significantly prior to failure. On the other hand, the horizontal displacement profile (Figure 4.37) did not demonstrate marked displacement variation across the span, indicating that there was no marked arching in that direction. Combining with the discussion on specimen IF-RC-TG, it suggests that the presence of frame-to-infill gap has significant effect on the out-of-plane behaviour through changing the cracking pattern and failure mode.

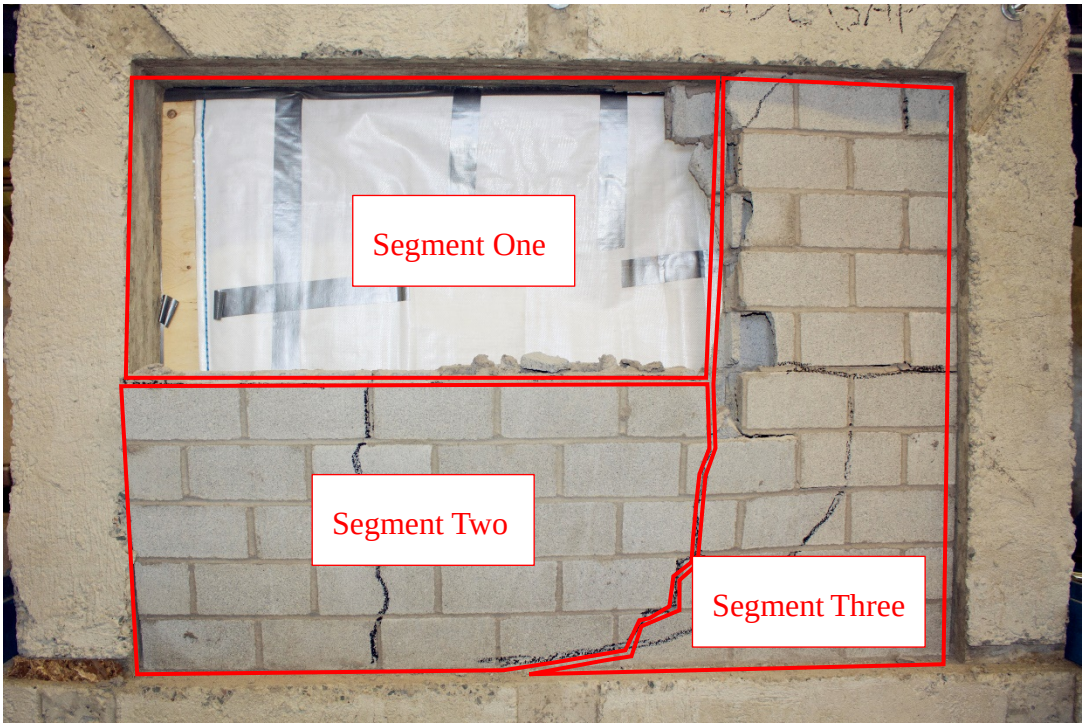

Figure 4.34 Failure Mode of Specimen IF-RC-SG on Leeward

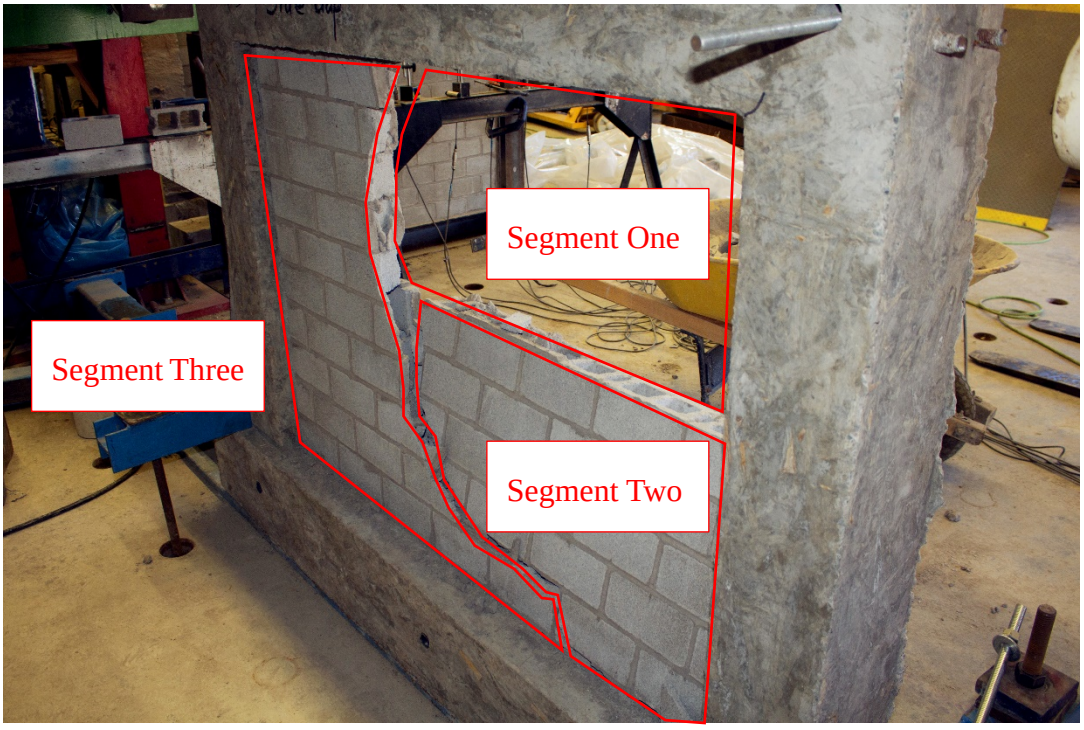

Figure 4.35 Failure Mode of Specimen IF-RC-SG on Windward

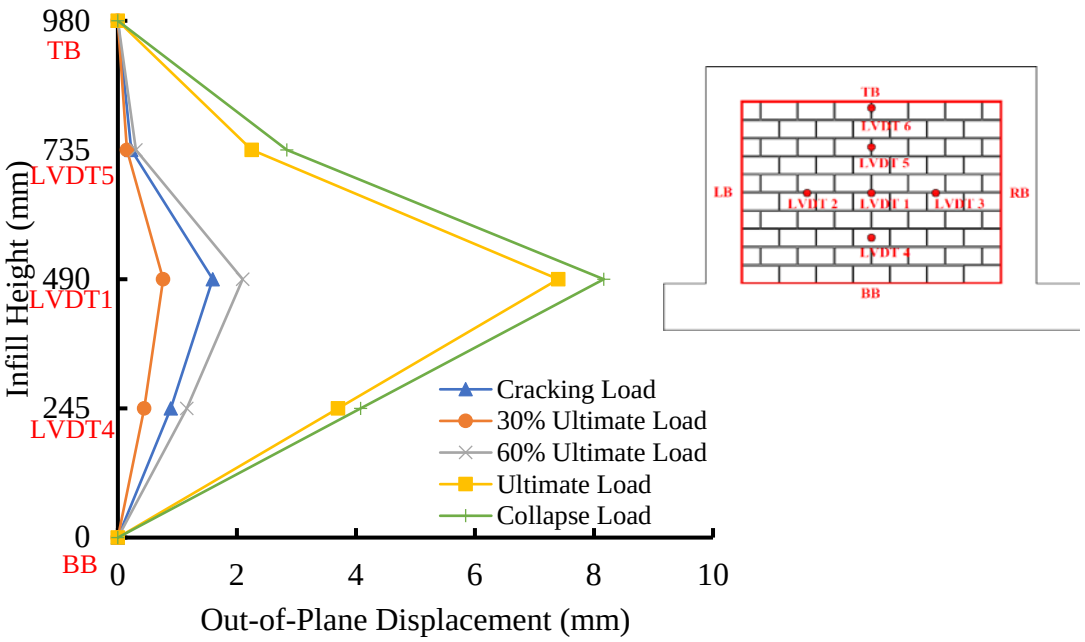

Figure 4.36 Displacement Curves of Specimen IF-RC-TG for Vertical LVDTs

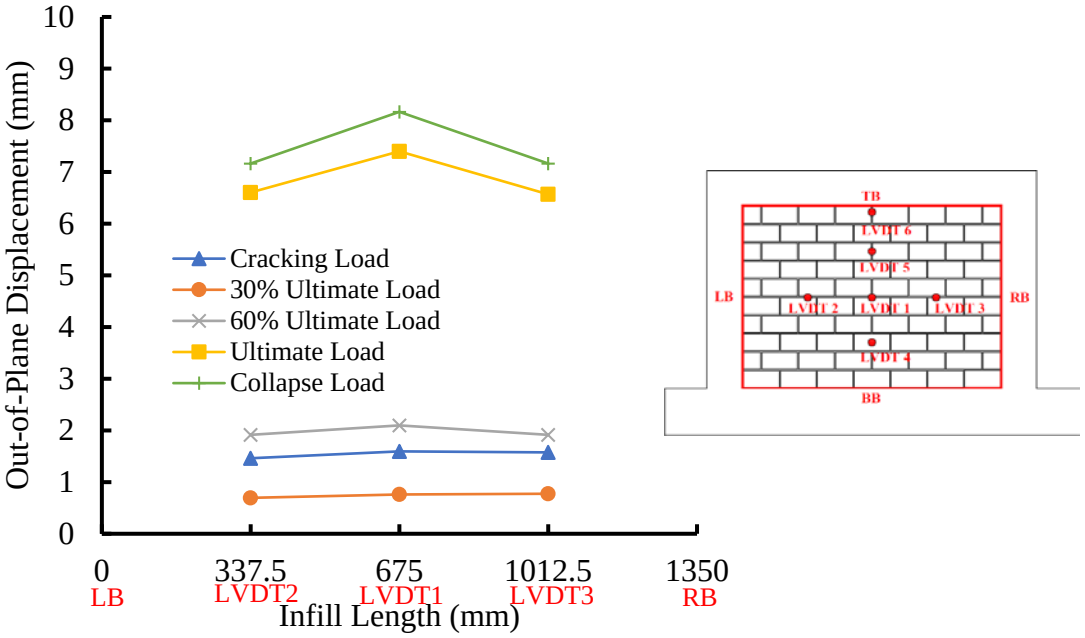

Figure 4.37 Displacement Curves of Specimen IF-RC-TG for Horizontal LVDTs

4.3.6 Specimen IF-S

The pressure vs. out-of-plane displacement curve for the infilled steel frame specimen is shown in Figure 4.38, and Figure 4.39 illustrates the cracking pattern with corresponding loads. At the stage one, this specimen behaved very stiff up to 7 kPa (about 20% of the ultimate load) with almost negligible displacement. Immediately after 7 kPa, a significant decrease in stiffness was evident. As the pressure continued to increase to about 16 kPa (about 47% of the ultimate load), a crack was developed along the fourth layer bed joint from the top beam with a length of five blocks. The diagonal cracks began to develop from the ends of the initial horizontal crack to the bottom corners of the infill in stage three. At load of about 26.3 kPa (about 77% of the ultimate pressure), a horizontal crack was developed at about the mid-height of infill with a length of four blocks, and the stiffness of the infill further decreased. A sudden drop on the load vs. out-of-plane displacement curve was observed at a load of about 30.6 kPa, but the curve resumed an increasing trend immediately thereafter. A major horizontal crack along the fifth bed joint from the top beam and diagonal cracks extending to the corners of the infill were developed at the load of 29.7 kPa. The specimen reached its ultimate strength at pressure of 34.3 kPa and out-of-plane displacement of 15.1 mm. The specimen failed suddenly and the main central section collapsed as shown in Figure 4.40.

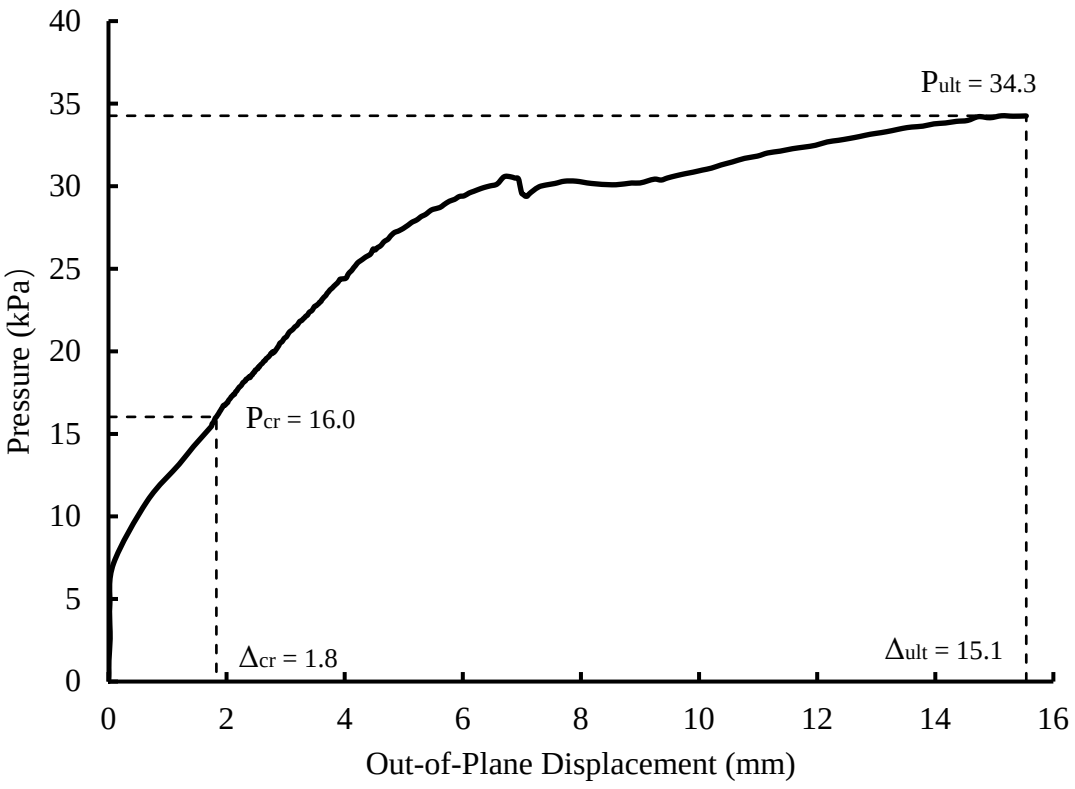

Figure 4.38 Pressure vs. Out-of-Plane Displacement of Specimen IF-S

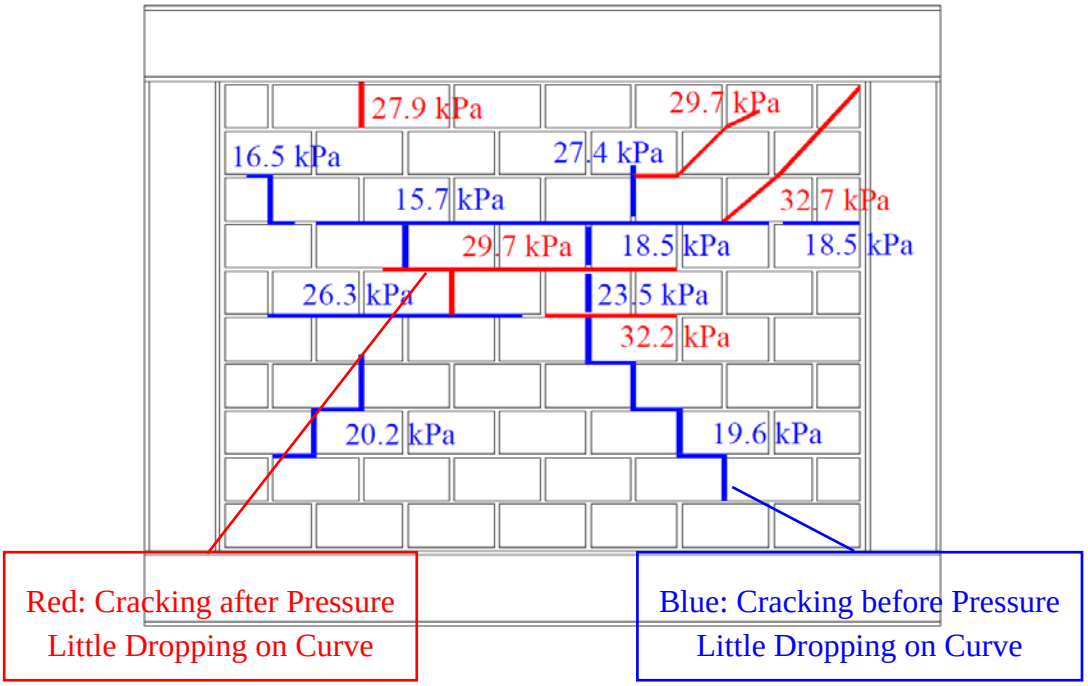

Figure 4.39 Crack Patterns of Specimen IF-S

Figure 4.40 Failure Mode of Specimen IF-S on Leeward

Similar to other specimens, most cracks were developed at the interfaces between blocks and mortar, and the collapse of the infill was resulted from web shear failure of the masonry blocks, as shown in Figure 4.41.

Figure 4.41 Web Shear Failure of Masonry Units for Specimen IF-S

The out-of-plane displacement profiles through loading history are plotted in Figure 4.42 and Figure 4.43 for vertical and horizontal LVDTs respectively. They show that the maximum recorded out-of-plane displacement was observed at the center of the infill with a value of about 15.5 mm, and two-way arching action was developed in this specimen as evidenced by the fully symmetrical displacement profile with respect to the vertical and horizontal center line.

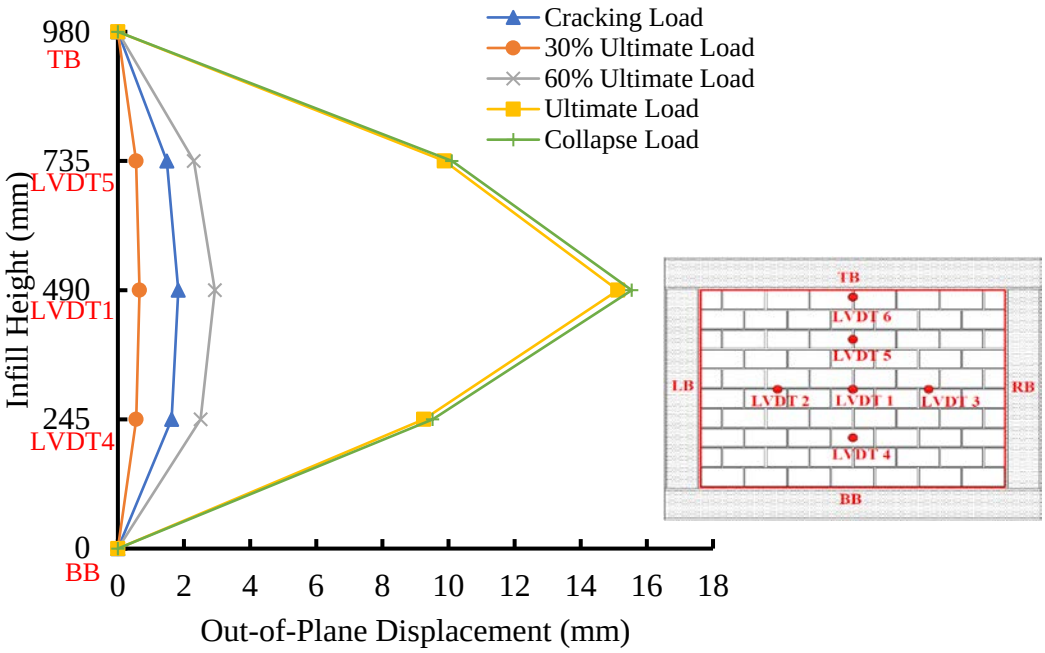

Figure 4.42 Displacement Curves of Specimen IF-S for Vertical LVDTs

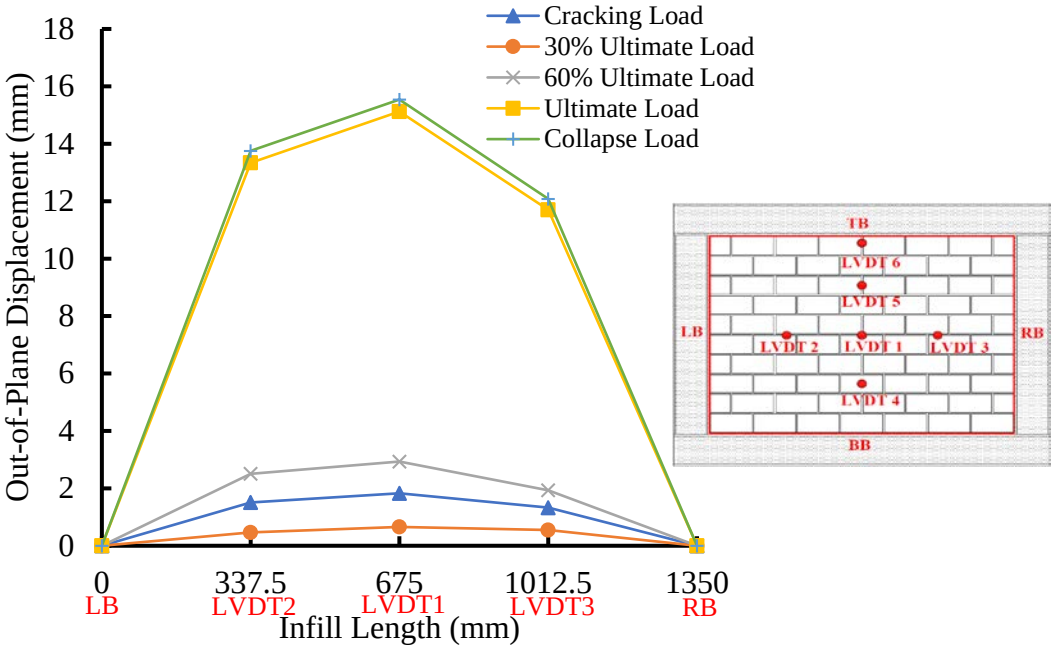

Figure 4.43 Displacement Curves of Specimen IF-S for Horizontal LVDTs

4.3.7 Summary of Infilled Frame Specimen Results

The test results of cracking load (P_{cr}), ultimate load (P_{ult}), failure load (P_{fail}) and their corresponding maximum recorded out-of-plane displacements on the infill for each specimen, are presented in Table 4.8. The initial stiffness (K_{ini}), cracking stiffness (K_{cr}) and ultimate stiffness (K_{ult}) are also summarized in the table. For specimen IF-RC-ID, at the in-plane loading stage, the applied lateral load prior to out-of-plane loading and cracking load when a major diagonal crack was observed are denoted as F_{app}, and F_{cr}, respectively. Their corresponding lateral displacement are denoted as δ_{app} and δ_{cr} respectively.

Table 4.8 Summary of Test Results of Infilled Specimen

Loading	Components	IF-RC-DO	IF-RC-ID	IF-RC-TG	IF-RC-SG	IF-S
Out-of-plane	P_{cr} (kPa)	19.7	28.6	4.3	18.4	16.0
	P_{ult} (kPa)	36.2	37.6	18.5	36.5	34.3
	P_{fail} (kPa)	35.4	34.2	16.3	35.7	34.3
	Δ_{cr} (mm)	1.2	3.4	0.6	1.6	1.8
	Δ_{ult} (mm)	7.9	7.7	3.9	7.4	15.1
	Δ_{fail} (mm)	8.6	10.6	5.7	8.2	15.5
	K_{ini} (kPa/mm)	25.0	21.0	7.2	19.3	83.2
	K_{cr} (kPa/mm)	16.4	8.4	7.2	11.5	8.9
	K_{ult} (kPa/mm)	4.6	4.9	4.7	4.9	2.3
In-plane	F_{cr} (kN)	-	80.7	-	-	-
	F_{app} (kN)	-	104.7	-	-	-
	δ_{cr} (mm)	-	7.2	-	-	-
	δ_{app} (mm)	-	13.4	-	-	-

For ease of reference, a summary of the test results obtained in the Sepasdar's study is also presented in Table 4.9.

Table 4.9 Summary of Test Results of Infilled Specimen (Sepasdar, 2017)

Loading	Components	IF-ND	IF-W-ND	IF-D1	IF-D2
Out-of-plane	P_{cr} (kPa)	26.8	23.7	14.6	24.8
	P_{ult} (kPa)	66.3	43.7	44.4	26.4
	P_{fail} (kPa)	66.3	40	42.9	26.0
	Δ_{cr} (mm)	0.5	0.6	0.3	7.6
	Δ_{ult} (mm)	12.5	4.3	6.6	9.9
	Δ_{fail} (mm)	12.5	6.75	8.1	11.0
	K_{ini} (kPa/mm)	58.1	55.8	51.8	6.3
	K_{cr} (kPa/mm)	53.6	39.5	48.7	3.3
	K_{ult} (kPa/mm)	5.3	10.2	6.7	2.7
In-plane	F_{cr} (kN)	-	-	107.4	113.3
	F_{app} (kN)	-	-	107.4	139.3
	δ_{cr} (mm)	-	-	6.5	8.7
	δ_{app} (mm)	-	-	6.5	26.4

4.4 Effect of Opening

Figure 4.44 plots the pressure vs. out-of-plane displacement curve of specimens IF-RC-DO, IF-ND and IF-W-ND, and the maximum recorded displacement was used in the plot. In general, the figure shows that presence of an opening, regardless of whether it be a window and door, results in a reduction in infill strength. Note that the openings in both specimens were covered with a relatively stiff plywood board during the test. It can then be assumed that the pressure acting on the board was transferred to the sides of the opening, so the area surrounding the opening resisted more pressure, which led to the reduction of the ultimate load the infill sustained. When comparing specimens IF-ND and IF-RC-DO, it is found that the infill door opening caused about 26% reduction on the cracking load and about 45% reduction on the ultimate load. When comparing specimens IF-RC-DO with IF-W-ND with a central window opening but a similar opening-to-infill area ratio (around 17.5%), the former attained about 17% less cracking and ultimate load. For the out-of-plane displacement, the specimen with the door opening showed more pronounced non-linearity and greater ductility than that with the window opening. The initial stiffness and cracking stiffness of specimen IF-RC-DO were less than 50% of those for specimen IF-W-ND. The comparison of cracking pattern and final failure mode of two specimens are shown in Figure 4.45 and Figure 4.46, respectively. It shows that openings of same size but different configuration result in changes in cracking pattern and failure mode. The first visible

cracking was observed at top corners of the opening, regardless of whether it be a window and door. In the case of the window opening, the cracks expanded towards top corners of the infill with the increase of pressure, and the cracking pattern and failure mode was more or less concentrated around the opening in a yield-line like manner and the rest of infill and boundary support from frame seemed to remain intact. However, in the case of the door opening, the cracking was more random and did not form any visible yield-line like pattern. The final failure pattern indicated a disintegration of the entire infill and the boundary with the frame was also lost where the top portion of the infill bulged out.

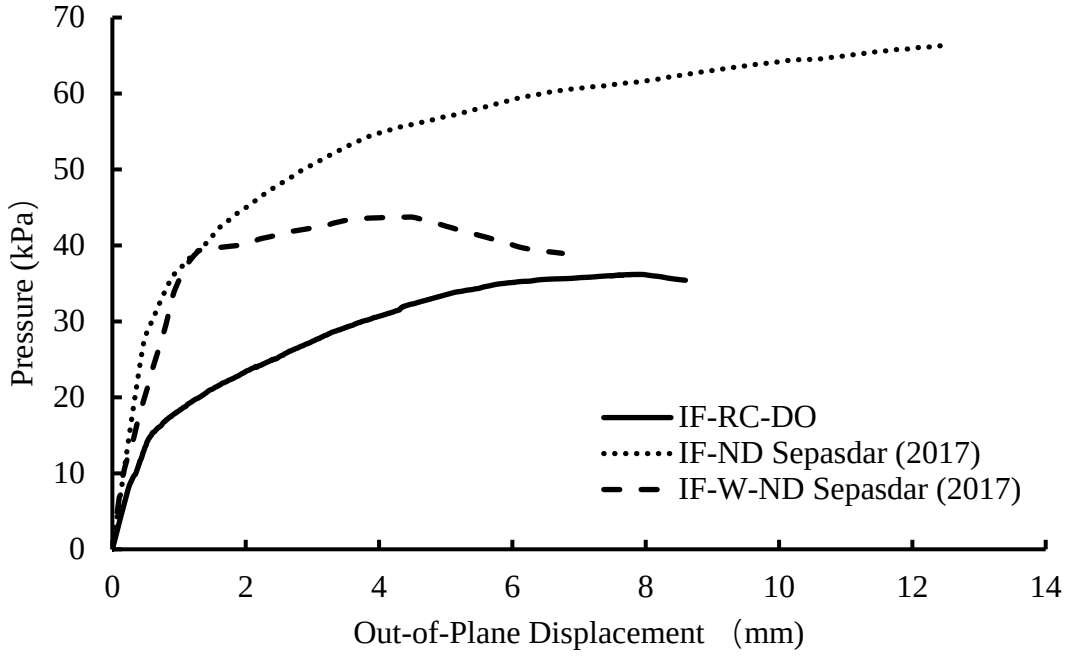

Figure 4.44 Pressure vs. Out-of-Plane Displacement of Specimens IF-RC-DO, IF-ND and IF-W-ND

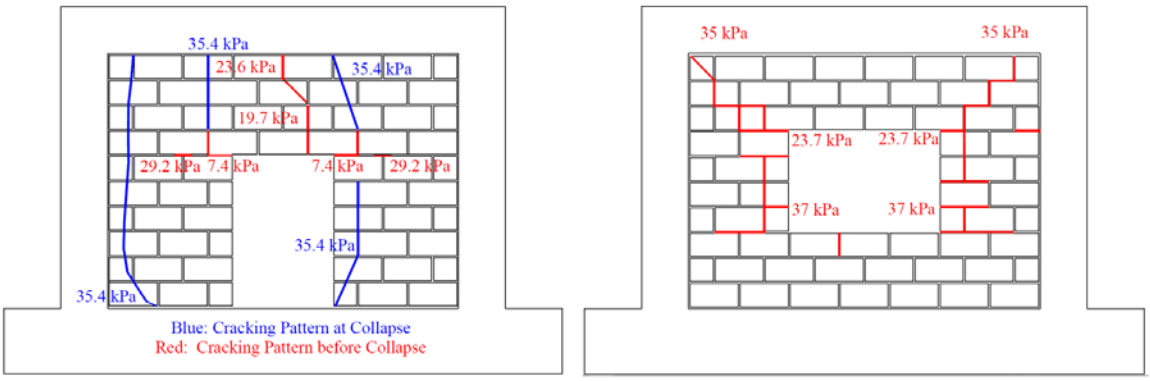

(a) Specimen IF-RC-DO (b) Specimen IF-W-ND

Figure 4.45 Cracking Pattern of Specimens IF-RC-DO and IF-W-ND

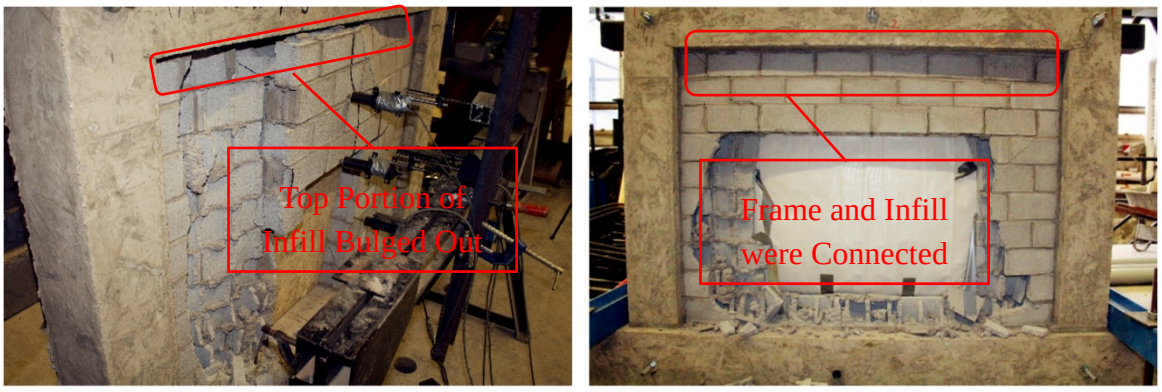

(a) Specimen IF-RC-DO (b) Specimen IF-W-ND

Figure 4.46 Failure Mode of Specimens IF-RC-DO and IF-W-ND on Leeward

4.5 Effect of Prior In-Plane Damage

The in-plane load vs. lateral displacement curves for specimens IF-D1, IF-D2, and IF-RC-ID are plotted in Figure 4.47. The physical damage of specimen IF-D1 at the applied lateral displacement was the onset of first major diagonal cracking while at the applied lateral displacement, specimen IF-D2 has reached its ultimate in-plane capacity with physical damage of masonry crushing at the loaded corners. Specimen IF-D2 was then subjected to

an applied lateral displacement in between.

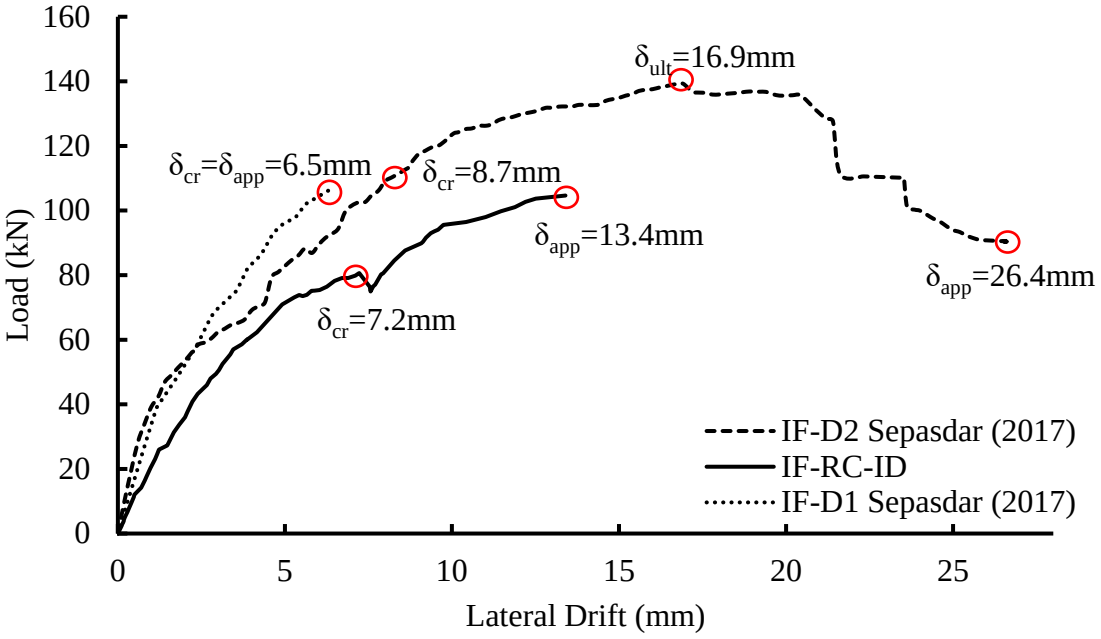

Figure 4.47 Load vs. In-Plane Displacement of Specimens IF-D1, IF-D2 and IF-RC-ID under In-Plane Loading

The pressure vs. out-of-plane displacement curves for center points (the point with the largest recorded displacement) of specimens IF-ND, IF-D1, IF-D2, and IF-RC-ID are plotted in Figure 4.48. It shows that the presence of in-plane damage results in reductions in both the out-of-plane ultimate load and displacement of the specimen. The increasingly earlier non-linearity of the response as in-plane damage increased indicates the prior damage resulted in an increasingly softer infill. Comparing to specimen IF-ND, the out-of-plane ultimate load and displacement of specimen IF-RC-ID was reduced by 43% and 38% respectively, and the initial stiffness and ultimate stiffness had 64% and 7.5% reductions respectively. The extents of reductions in the infill ultimate load is evidently related to the

level of damage. As the level of damage increased, the reduction also increased.

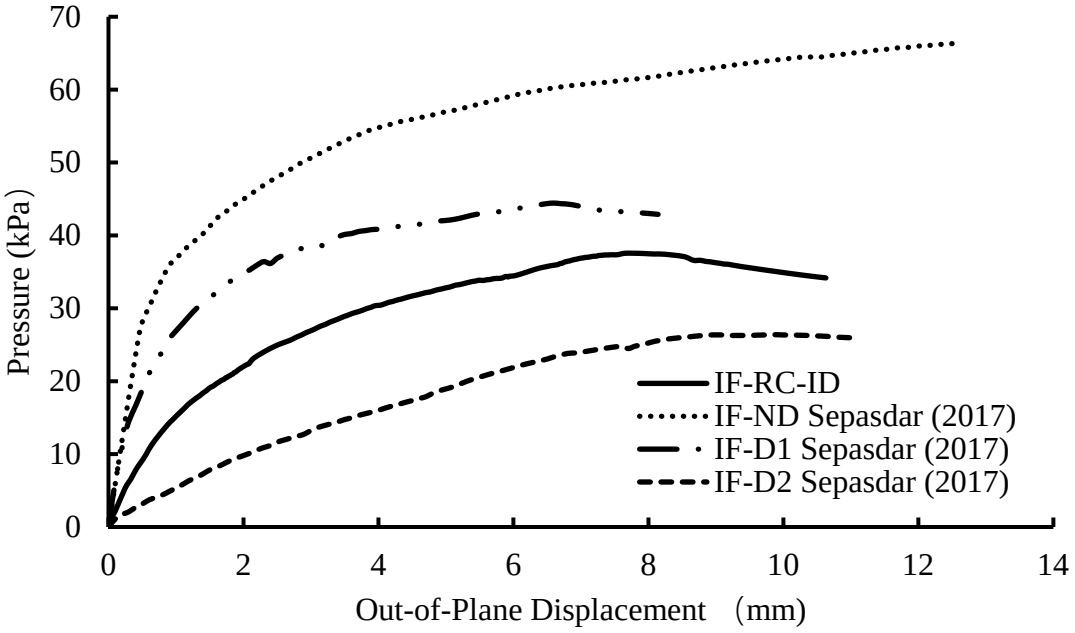

Figure 4.48 Pressure vs. Out-of-Plane Displacement of Specimens IF-ND, IF-D1, IF-D2 and IF-RC-ID

Combining results from this and the previous study, a relationship between prior in-plane damage level and out-of-plane ultimate load reduction of infills can be determined. Figure 4.49 and Figure 4.50 show this relationship with two definitions of prior damage. Figure 4.49 defines the prior damage level as the ratio of applied lateral displacement before out-of-plane loading (δ_{app}) to the lateral displacement at ultimate resistance of the specimen (δ_{ult}) whereas Figure 4.50 defines the prior damage directly using the in-plane drift levels (δ_{app}/h). It is found that in both cases, the ultimate out-of-plane strength of infill reduced with the increase of prior in-plane damage, and it seems that the ultimate strength of infill had a linear relation with the prior in-plane damage level.

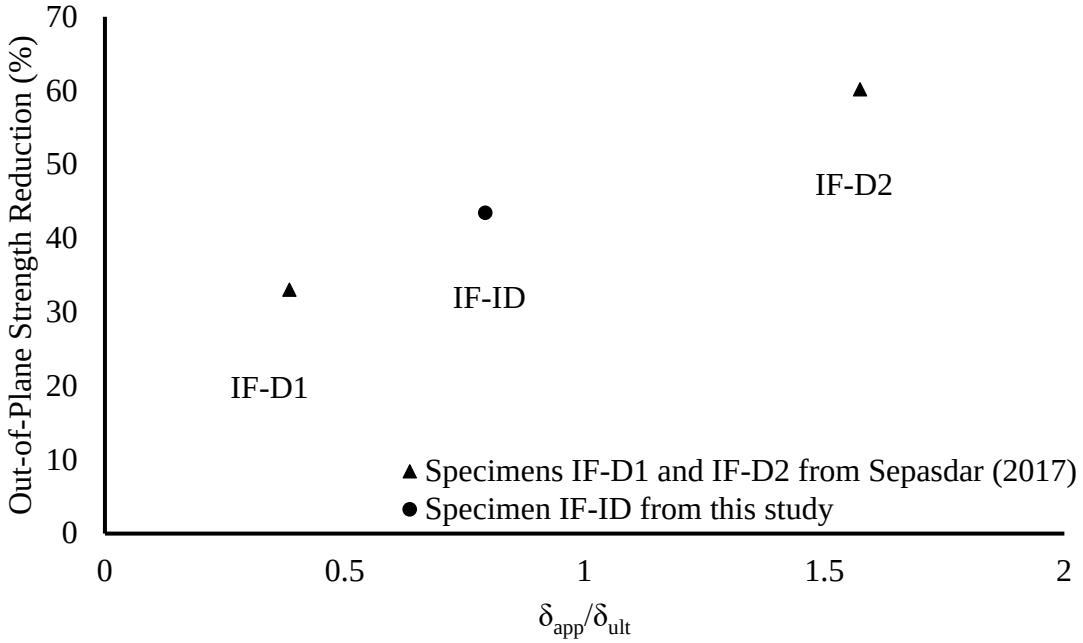

Figure 4.49 Relationship Between Prior In-Plane Displacement Ratio, $\delta_{app}/\delta_{ult}$, and Ultimate Strength Reduction

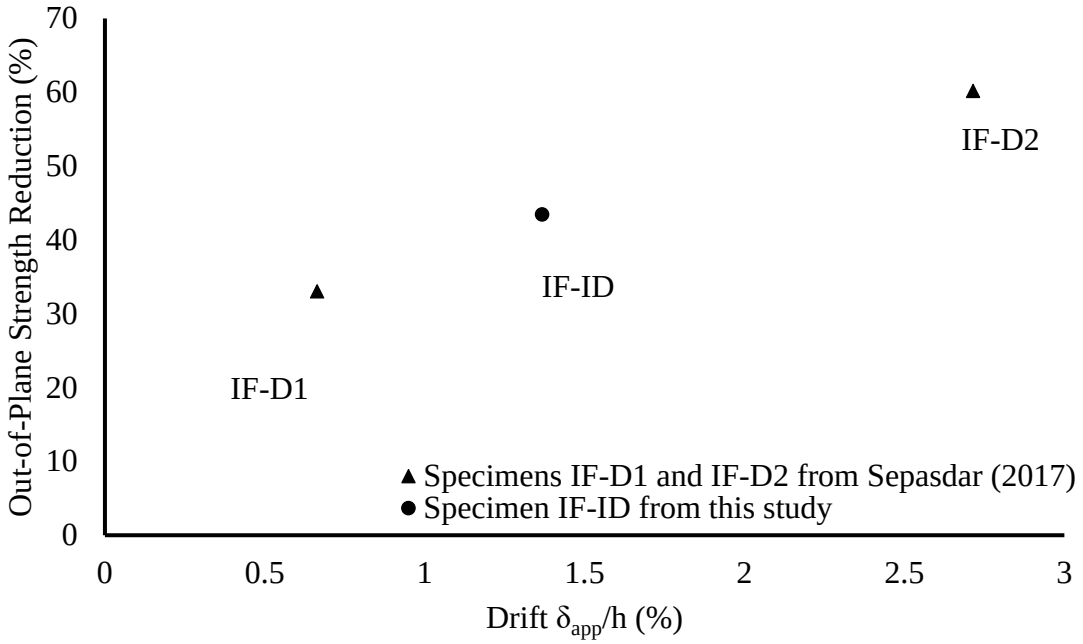

Figure 4.50 Relationship Between Prior In-Plane Drift, δ/h, and Ultimate Strength Reduction

4.6 Effect of Interfacial Gap

The infilled frames with the same total size of gaps (specimens IF-RC-TG and IF-RC-SG) and specimen IF-ND were used to evaluate the effect of the gap, and the pressure vs. out-of-plane displacement curves of these specimens are plotted in Figure 4.51. The out-of-plane displacement used in this case was the displacement recorded at the center of the infill at ultimate load. It shows that the presence of gaps, regardless of the location, results in a reduction in the infill out-of-plane strength. This is attributed to the fact that the presence of gap will reduce a potential two-way arching to one-way arching in the direction where the boundary support is available. It has been shown that two-way arching will result in a greater infill strength than one-way arching. The comparison of top gap vs. side gap shows that the gap at the top beam-infill interface is more detrimental to the infill strength than the side gap. As shown in Figure 4.51, for a 10 mm gap size, the top beam-infill location resulted in about 72% reduction in ultimate load whereas the column-infill location resulted in about 45% reduction in ultimate load. As described previously, the specimen with the top gap developed a cracking pattern similar to a yield line pattern for a three-side supported wall; and the specimen with the side gap still developed arching in the vertical span direction evidenced by the mid-height horizontal crack. It can be concluded that the presence of gap affects the infill strength through altering its failure mechanism. The infill is still capable of developing arching action even with gaps. For the given infill geometry,

the top beam-infill gap is more detrimental than the side column-infill gap.

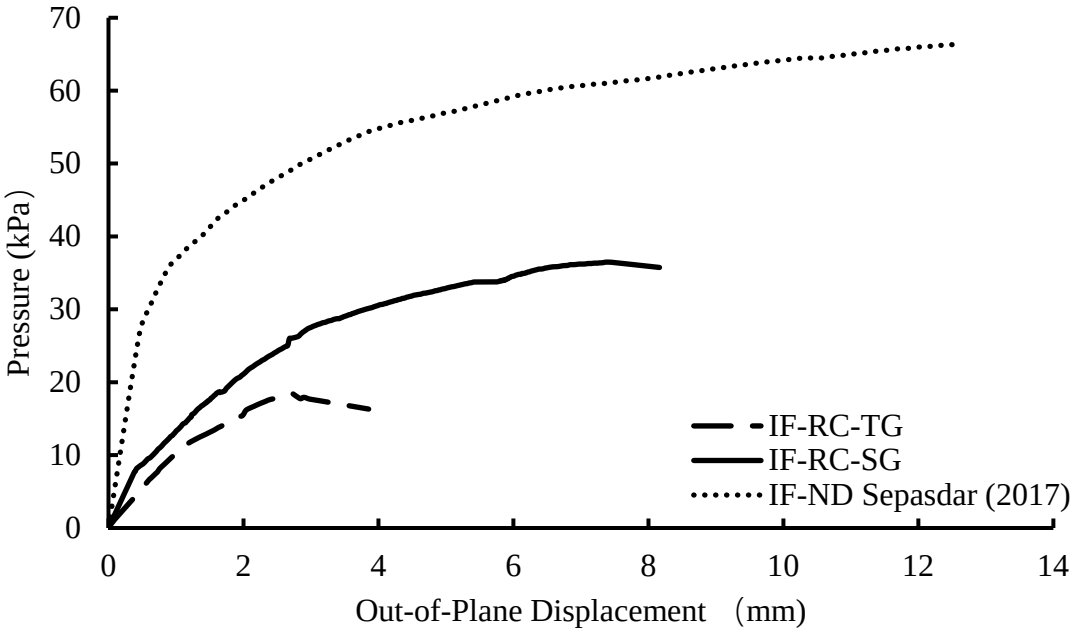

Figure 4.51 Pressure vs. Out-of-Plane Displacement of Specimens IF-ND, IF-RC-TG and IF-RC-SG

4.7 Effect of Boundary Frames

Figure 4.52 shows pressure vs. out-of-plane displacement curves for specimens IF-ND and IF-S, and the maximum recorded displacement was used (at the center of infill for both specimens). Except for the bounding frame, the specimen IF-S (bounded by a steel frame) was identical to specimen IF-ND (bounded by a RC frame). The figure shows that the infill bounded by the steel frame attained a 40% less cracking load and a 48% less ultimate load comparing with its RC frame counterpart. The more pronounced nonlinearity observed for specimen IF-S throughout almost the entire loading history suggests that the steel bounding

frame entails a softer infill system when subjected to out-of-plane loading. In particular, the cracking stiffness and ultimate stiffness of specimen IF-S decreased by about 83% and 57%, respectively comparing with specimen IF-ND. Interesting to note, however, is that the flexural stiffnesses (EI) of frame members of specimen IF-S and IF-ND were calculated to be 3.46×10^{12} N-mm^2 and 1.77×10^{12} N-mm^2, respectively. A stiffer frame (IF-S) corresponded to a lower strength. This seemingly anomaly may be attributed to three factors. One, the torsional stiffness (GJ) of frame members of specimen IF-S (7.81×10^9 N-mm^2) is lower than that of the RC frame (1.09×10^{12} N-mm^2). As illustrated in Figure 4.53, when a thrust force was exerted on the frame member from arching action, the force is acted on the flange of the frame (in the case of a steel frame) and this force could act on any point of the flange depending on the rotation of the wall segment. This may result in a more significant twisting effect on the steel W frame member than a solid rectangular concrete section. Secondly, the same force acting on the flange of the steel section transfers the force through significant bending action on the flange. Although the steel section as a whole has a larger flexural stiffness than the RC section, the flange itself is essentially a steel plate and its bending stiffness is much lower than a RC section. It is then believed that the combined twisting effect and configuration of the steel section lead to weakening of the rigidity of the frame member. This observation is particularly important as it suggests that the flexural rigidity of the entire member section alone is not sufficient to indicate its effectiveness in enabling arching action. Third, it is noted that the base beam of specimen IF-ND was

directly clamped to the floor, whereas the base beam of specimen IF-S was clamped to two W steel beams which were in turn secured to the floor. The latter setup allowed deflection and rotation of the base beam of the steel frame, which can compound the problem of an inherently low flexural stiffness of the steel frame.

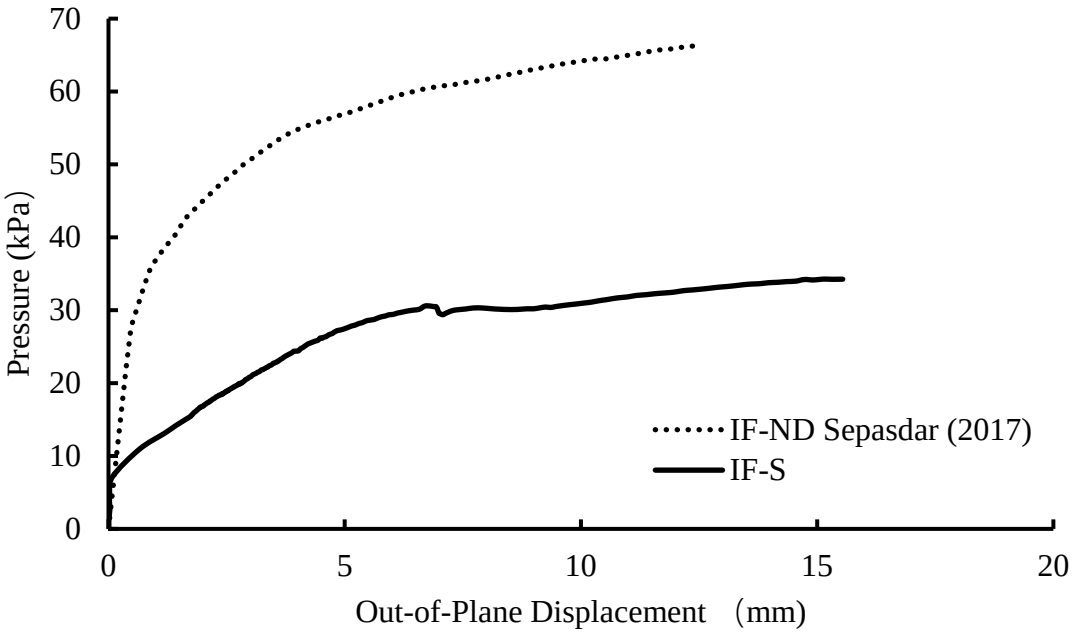

Figure 4.52 Pressure vs. Out-of-Plane Displacement of Specimens IF-ND and IF-S

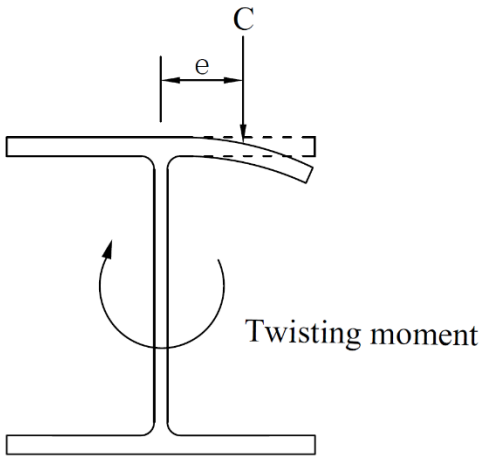

Figure 4.53 Thrust Force Acting on the Flange of the Steel Frame

CHAPTER 5 EVALUATION OF ANALYTICAL METHODS

5.1 INTRODUCTION

This chapter examines the performance of several existing analytical methods for calculation of infill out-of-plane strength and displacement using the experimental results. To have a more complete discussion, this evaluation also included the test results of Sepasdar's study.

The material and geometrical properties used in the evaluation are summarized in Table 5.1 for specimens in this study and in Table 5.2 for specimens in Sepasdar's study. In accordance with CSA S304-14, the modulus of elasticity of masonry (E_m) was calculated as $850f'_m$. The shear modulus (G) of the concrete and steel was calculated based on their respective Young's moduli assuming that the Poisson's ratio of the concrete and steel equals to 0.15 and 0.3, respectively. The uncracked moment of inertia of RC frame members (I_b and I_c) was calculated based on the transformed sections taking into account of the steel contribution.

Table 5.1 Material and Geometrical Properties of Specimens from This Study

ID	IF-RC-DO	IF-RC-ID	IF-RC-TG	IF-RC-SG	IF-S
t (mm)	90	90	90	90	90
h (mm)	980	980	980	980	980
l (mm)	1350	1350	1350	1350	1350
f'_m (MPa)	9.0	9.0	7.9	7.9	9.0
E_m (MPa)	7650	7650	6715	6715	7650
f'^*_j (MPa)	10.4	10.4	7.6	7.6	7.6
$E_b=E_c$ (MPa)	16911	16911	20357	16911	201172
$I_b=I_c$ (x10^6 mm^4)	104.7	104.7	104.7	104.7	17.2
$G_b=G_c$ (MPa)	7352.6	7352.6	8850.9	7352.6	77374
$J_b=J_c$ (x10^6 mm^4)	147.6	147.6	147.6	147.6	0.101

where f'^*_j is the compressive strength of mortar.

Table 5.2 Material and Geometrical Properties of Specimens from Sepasdar (2017)

ID	IF-ND	IF-W-ND	IF-D1	IF-D2
t (mm)	90	90	90	90
h (mm)	980	980	980	980
l (mm)	1350	1350	1350	1350
f'_m (MPa)	9.4	9.4	9.7	9.7
E_m (MPa)	7990	7990	8245	8245
f'_j (MPa)	20.4	20.4	21.6	21.6
$E_b=E_c$ (MPa)	16911	16911	16911	20357
$I_b=I_c$ (x10^6 mm^4)	104.7	104.7	104.7	104.7
$G_b=G_c$ (MPa)	7352.6	7352.6	7352.6	8850.9
$J_b=J_c$ (x10^6 mm^4)	147.6	147.6	147.6	147.6

5.2 STRENGTH EVALUATION

Chapter 2 presented the existing analytical methods for calculation of out-of-plane strength of a “regular” infill as well as several equations proposed for “irregularities” in infills such

as infill openings, prior in-plane damage, and interfacial gaps. For ease of reference, the following sections will provide a summary of the methods first and then the evaluation of the methods using experimental results as appropriate.

5.2.1 Comparison with Methods for "Regular" Infills

Table 5.3 summarizes the existing analytical methods for calculation of the out-of-plane strength of a "regular" infill using these methods. Except for BS 5628 (2005), the other methods are semi-empirical based on curve-fitting of results from either experimental or numerical studies. BS 5628 (2005) on the other hand, is based on the mechanics of arching action. The unknown term in that equation is the wall deflection. For design purposes, the wall deflection is suggested to be assumed zero. Table 5.4 presents the ratios of experimental to analytical ultimate strength (P_{ult}/P_{ana}) for "regular" specimens. For calculation using BS 5628, both zero and experimentally obtained wall deflection were used. To calculate the one-way arching strength, the predicted strength was based on the arching action along the direction with less length. For two-way arching strength calculation, the participation of arching in the other direction was considered using the same mechanics principle and assuming that the out-of-plane displacements developed in both directions were identical. A sample calculation for one-way and two-way arching strength using BS 5628 is presented in APPENDIX A.

Table 5.3 Analytical Methods for Out-of-Plane Strength for "Regular" Infills

Method	Out-of-Plane Strength	Note
BS 5628 (2005)	$w_f = \frac{8C}{h^2}(\gamma t - \Delta_0)$	$\gamma = 0.9$ Δ_0= Wall Delfection $C = \emptyset_m 0.85 f'_j (0.1t)$
MSJC 2013	$q_{ult} = 729(f'_m)^{0.75} t_{inf}{}^2 \left(\frac{\alpha_{arch}}{l_{inf}{}^{2.5}} + \frac{\beta_{arch}}{h_{inf}{}^{2.5}}\right)$	$\alpha_{arch} = \frac{1}{h_{inf}}(E_{bc} I_{bc} h_{inf}{}^2)^{0.25} \le 50$ $\beta_{arch} = \frac{1}{l_{inf}}(E_{bb} I_{bb} l_{inf}{}^2)^{0.25} \le 50$
FEMA 356 (2000)	$q_{ult} = \frac{0.7 f'_m \lambda_2}{\left(\frac{h_{inf}}{t_{inf}}\right)} \times 144$	h_{inf}/t_{inf} | 5 | 10 | 15 | 25 λ_2 | 0.129 | 0.060 | 0.034 | 0.013 Interpolation shall be used.
Dawe and Seah (1989)	For a panel supported on four sides: $q_{ult} = 800(f'_m)^{0.75} t^2 \left\{\frac{\alpha}{L^{2.5}} + \frac{\beta}{H^{2.5}}\right\}$	For a panel supported on four sides: $\alpha = \frac{1}{H}(EI_c H^2 + GJ_c tH)^{0.25} \le 50$ $\beta = \frac{1}{L}(EI_b L^2 + GJ_b tL)^{0.25} \le 50$
Angel (1994)	For a panel without prior in-plane damage $q = \frac{2f'_m}{\left(\frac{h}{t}\right)} R_1 R_2 \lambda$	$R_1 = 1$ $R_2 = 0.357 + 7.14 \times 10^{-8} EI \le 1$ $\lambda = 0.154 \exp\left(-0.0985 \frac{h}{t}\right)$
Klingner et al. (1996)	$q = \frac{8}{h^2 l}\left\{M_{yv}[(l-h) + h\ln(2)] + M_{yh}\left(\frac{x_{yv}}{x_{yh}}\right)\ln\left(\frac{1}{1-h/2}\right) l\right\}$	$M_{yv} = \frac{0.85 f'_m}{4}(t - x_{yv})^2$ $x_{yv} = \frac{t f'_m}{1{,}000E\left[1 - \frac{h}{2\sqrt{(h/2)^2 + t^2}}\right]}$
Moghaddam and Goudarzi (2010)	$q_r = \min\left\{\begin{array}{c} q_{cr} = \left[0.85 - \left(0.12 + \frac{0.045}{\alpha}\right)\frac{f_m}{E_m}\lambda^2\right]\frac{f_m}{\lambda^2} \\ q_{max} = \frac{0.18 E_m}{\left(0.12 + \frac{0.045}{\alpha}\right)\lambda^4} \end{array}\right\}$	$\alpha = \frac{K}{(E_m t l/h)}$ $K = \frac{384 E_f I_b}{l^3}$ $\lambda = h/t$

Table 5.4 Comparison of Experimental and Analytical Results for "Regular" Infills

ID	Test Result	Ratio of Experimental to Analytical Results (P_{ult}/P_{ana})									
		BS 5628 (2005)				MSJC 2013	FEMA 356 (2000)	Dawe and Seah (1989)	Angel (1994)	Klingner et al. (1996)	Moghaddam and Goudarzi (2010)
	Pult (kPa)	Assume $\Delta_0=\Delta_{exp}$		Assume $\Delta_0=0$							
		One-Way	Two-Way	One-Way	Two-Way						
IF-S	34.3	0.91	0.59	0.77	0.60	0.59	1.07	0.54	1.10	0.30	0.55
IF-ND	66.3	1.62	1.06	1.42	1.12	1.31	1.98	1.18	2.04	0.56	1.03

Table 5.4 shows that of the exiting methods, no one provides consistent estimate of infill strength for both bounding frames. One method may be accurate for one type of bounding frames, but performs poorly for the other type of frames. When steel bounding frames are considered, it seems that FEMA 356 and Angel (1994) provide the best estimate with a P_{ult}/P_{ana} slightly above unity, indicating a reasonably accurate and conservative estimate. The first principles method (BS 5628) overestimates the infill strength in general, but more significantly if two-way arching action is considered. The use of experimental wall deflection data vs. zero although improves the estimate but does not change the trend of overestimating. When RC frames are considered, the methods proposed by Moghaddam and Goudarzi (2010) and Dawe and Seah (1989) performed best with P_{ult}/P_{ana} greater than but close to unity. Unlike the steel bounding frame case, the first principles method (BS 5628) for RC frames underestimates the strength regardless of whether the experimental deflection data or zero is used. The inconsistency in the performance of BS 5628 method show that the basic first principle method is not adequate to reflect effect of boundary

frames.

The methods proposed in MSJC 2013 and Dawe and Seah (1989) are formulated in a similar way with the exception that the former formulation removed the term of torsional stiffness of the frame member. It is then not surprising that two methods provide similar estimates. The rationale for removal of torsional effect is that the torsional stiffness term in the formulation is mathematically small in comparison to the flexural stiffness term. While the elimination of torsional effect might be reasonable for steel bounding frames (inherently weak in torsion), the more significant deviation of MSJC 2013 from the experimental data than Dawe and Seah's method for RC frames seems to suggest that the removal of torsional stiffness term should be cautioned.

The methods proposed by FEMA 356 (2000) and Angel (1994) are formulated in a similar way where the former (formulated in imperial units) simplified the equation proposed by the latter. Thus, both methods provide similar estimates. Interesting to note though is that FEMA 356 permits the consideration of arching action provided that the flexural stiffness of frame members exceeds a value of 1.03×10^{13} N-mm^2, whereas Angel's method considers the frame stiffness effect through a factor R_2 which only accounts for stiffness between 5.7×10^{12} and 2.6×10^{13} N-mm^2. In this study, the flexural stiffnesses of both the steel frame and the RC frame members are below the above specified limits but both has shown evident arching action from experimental observations. In addition, the performance of both

methods differed significantly with one (steel bounding frame) being reasonably accurate and the other (RC frame) being grossly conservative.

While considering two-way arching action, the method proposed by Klingner et al. (1996) was based on idealized cracking patterns of infills (similar to yield line patterns) under out-of-plane load. Experimental cracking patterns (described previously) have shown that infill cracks patterns could be quite different from an idealized yield line pattern. This will significantly skew the analytical result, and in this case, result in marked overestimation.

The method proposed by Moghaddam and Goudarzi (2010) provided overestimation in strength for steel frames with an experimental-to-analytical ratio of 0.55 but a reasonably accurate estimate for RC frames with an experimental-to-analytical ratio of 1.03. It is noted that the Moghaddam and Goudarzi's method was based on the experimental results of infilled RC frames. And clearly, the equation loses its accuracy when used for steel bounding frames.

5.2.2 Comparison with Methods for Infills with Opening

Table 5.5 summarizes the method for consideration of infill openings in the out-of-plane strength calculation.

Table 5.5 Analytical Methods for Out-of-Plane Strength for Infill with Opening

Method	Out-of-Plane Strength	Note
Flanagan and Bennett (1999)	For a panel with opening $q = \left(1 + F_r\left(A_o/A_p\right)\right)(q')$	Blast resistant door opening: $F_r = -2.73$ Blast resistant window opening: $F_r = -3.07$ Non-blast resistant door opening: $F_r = 1.36$ Non-blast resistant window opening: $F_r = -1.00$ q' = out of strength of infill without opening

It should be pointed out that there is only one equation (Flanagan and Bennett's equation) available for the treatment of infill openings. It was originally developed by Mays et al. (1998) and used to estimate the out-of-plane strength for concrete walls with opening. The opening effect is considered in a linear function of opening-to-infill area ratio $q/q' = 1 + F_r (A_o/A_p)$ where F_r is the factor for opening type.

Table 5.6 presents the q/q' ratios from both experimental and analytical results for infill specimens with openings. Since the openings were covered with a plywood board, they were considered as blast-resisting in the calculation. This method gives reasonably good estimate for the effect of door openings but underestimates the effect of window openings

to a larger degree (20% difference). Interesting to note is that the method suggests different F_r factors for door and window blast-resistant openings and assigns a higher negative F_r for window openings. Thus, for the same opening-to-infill area ratio, out-of-plane strength of infills with a door opening is greater than the infill with a window opening. However, in fact the infill with door opening experimentally resisted less out-of-plane loading than the infill with window opening.

Table 5.6 Comparison of Experimental and Analytical Results for Infills with Openings

ID	A_o/A_p	Test Results		Flanagan and Bennett (1999)
		P_{ult} (kPa)	$(q/q')_{exp}$	$(q/q')_{ana}$
IF-ND	-	66.3	-	-
IF-RC-DO	0.17	36.2	0.55	0.52
IF-W-ND	0.17	43.7	0.66	0.46

5.2.3 Comparison with Methods for Infills with Prior In-Plane Damage

The method proposed by Angel (1994) considers the effect of in-plane damage on the out-of-plane strength through a prior in-plane damage reduction factor R_1, as shown in Table 5.7. The R_1 factor is defined as a function of damage indicator $\delta/2\delta_{cr}$ where δ is the maximum lateral deflection experienced by the specimen and δ_{cr} is the displacement at the cracking load.

Table 5.7 Analytical Methods for Out-of-Plane Strength for "Prior In-Plane Damaged" Infill

Method	Out-of-Plane Strength	Note
Angel (1994)	$q = \frac{2f'_m}{(\frac{h}{t})} R_1 R_2 \lambda$	$R_1 = 1$ if $\delta/(2\delta_{cr}) < 0.5$ (infill not cracked) Otherwise, $R_1 = \left[1.08 - 0.015\left(\frac{h}{t}\right) - 0.00049\left(\frac{h}{t}\right)^2 + 0.000013\left(\frac{h}{t}\right)^3\right]^{\frac{\delta}{2\delta_{cr}}}$ $R_2 = 0.357 + 7.14 \times 10^{-8} EI \leq 1$ $\lambda = 0.154 \exp\left(-0.0985\frac{h}{t}\right)$

To isolate the effect of prior damage from effect of slenderness and frame stiffness, the comparison was conducted using normalized strength where the strength of specimens with prior damage was normalized by the control specimen without prior damage and the result is presented in Table 5.8.

Table 5.8 Comparison of Experimental and Analytical Results for Infills with Prior In-Plane Damage

ID	$\delta/2\delta_{cr}$	Prior In-Plane Damage Strength Reduction Factor (R_1)	
		Test Result	Angel (1994)
IF-D1	0.50	0.67	0.94
IF-RC-ID	0.93	0.57	0.88
IF-D2	1.53	0.4	0.82

As shown in Table 5.8, Angel's reduction factors (R_1) are all greater than the experimental reduction factors on average by 33%, which indicates that the method by Angel (1994) grossly underestimates the effect of prior in-plane damage on the out-of-plane strength of infill. Also noted is that the deviation between the experimental and the Angel's reduction factors increases as the level of prior in-plane damage increases. As Angel's equation was proposed based on analytical results through curve fitting, the experimental results do not seem to support the equation.

Recalling that in Chapter 4, a correlation between the prior in-plane damage and the reduction of infill out-of-plane strength was presented based on the results obtained in this study. The literature survey yielded one more experimental result obtained by Furtado et al. (2016). Including this specimen, the out-of-plane strength reduction vs. the prior in-plane damage level defined as ($\delta_{app}/\delta_{ult}$) is shown in Figure 5.1. In the case of specimen inf_3 the maximum lateral deflection (δ_{app}) experienced by the specimen was 15 mm, and the ultimate in-plane deflection (δ_{ult}) of the specimen was 7.5 mm.

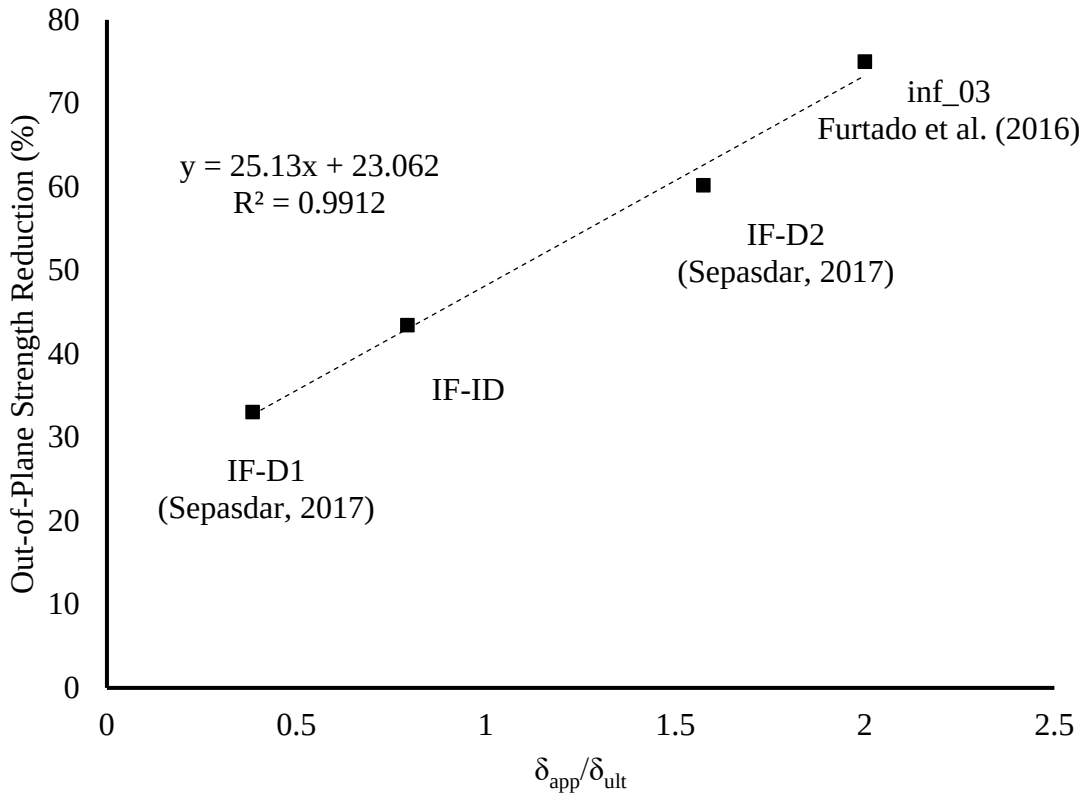

Figure 5.1 Relationship Between Prior In-Plane Displacement Ratio, $\delta_{app}/\delta_{ult}$, and Ultimate Strength Reduction

It appears that a more or less linear relationship exists between prior in-plane damage level and ultimate strength reduction. An expression of this relationship can be expressed as follows with the coefficient of determination (R^2) of 0.99.

$$R_{in} = 25.13\frac{\delta_{app}}{\delta_{ult}} + 23.062 \qquad [5\text{-}1]$$

where R_{in} is the proposed prior in-plane damage reduction factor.

The expression is developed based on four specimens. To provide a better representation

of prior in-plane damage reduction factor, more studies on the effect of prior in-plane damage are needed.

5.2.4 Comparison with Methods for Infills with Interfacial Gap

Table 5.9 summarizes the methods for calculation of the out-of-plane strength of an infill with interfacial gaps. The three available methods consider the gap effect in a different manner. BS 5628's method simply relies on geometric relationship of a three-hinge arch in equilibrium after the deflection closes the gap. Dawe and Seah's method applies only to the top beam to frame gap situation. It treats the infill as a three-side supported and one-side free panel subjected to out-of-plane loading. MSJC 2013's method is similar to the Dawe and Seah's method in essence but only considers the infill with gaps in one-way arching action in the direction where the contact is available. Table 5.10 presents the ratios of experimental to analytical ultimate strength (P_{ult}/P_{ana}) for infill specimens with gaps. For the method proposed by BS 5628, the maximum gap that can exist and still allow arching to develop is first calculated and they were determined to be 26.8 mm for top gaps. The gap size for specimens IF-RC-TG was 10 mm which met the specified limit and the arching action can be developed. In the case of side gaps, since the infill was still in tight contact with the frame in the vertical direction, the arching action would then develop in that direction. In other words, the infill with side gaps can be treated as a standard one-way arching infill in the vertical direction. The calculations can be found in APPENDIX C. Note

that both theoretical Δ_g and experimentally obtained Δ_{exp} were used in the BS 5628 equation for comparison.

Table 5.9 Analytical Methods for Out-of-Plane Strength for Infill with Gap

Method	Out-of-Plane Strength	Note
BS5628	Max. gap that could exit in infill: $g \le \frac{4(\gamma t)^2}{l}$ $\Delta_g = \frac{g(l-g)}{4\gamma t}$ $w_f = \frac{8C}{h^2}(\gamma t - \Delta_0)$	$\gamma = 0.9$
Dawe and Seah (1989)	For a panel supported on three sides and free at the top: $q_{ult} = 800(f'_m)^{0.75} t^2 \alpha / L^{2.5}$	$\alpha = \frac{1}{H}(EI_c H^2 + GJ_c tH)^{0.25} \le 75$
MSJC 2013	$q_{ult} = 729(f'_m)^{0.75} t_{inf}{}^2 (\frac{\alpha_{arch}}{l_{inf}{}^{2.5}} + \frac{\beta_{arch}}{h_{inf}{}^{2.5}})$	For infill with top gap, $\beta = 0$ For infill with side gap, $\alpha = 0$ $\alpha = \frac{1}{h}\left(E_c I_c h_{inf}{}^2\right)^{0.25} \le 50$ $\beta = \frac{1}{l}(E_b I_b l^2)^{0.25} \le 50$

Table 5.10 Comparison of Experimental and Analytical Results for Infills with Gap

ID	Test Result	Ratio of Experimental to Analytical Results (P_{ult}/P_{ana})			
		BS 5628 (2005)			
	P_{ult} (kPa)	Assume $\Delta_0=\Delta_g$ One-Way	Assume $\Delta_0=\Delta_{exp}$ One-Way	Dawe and Seah (1989)	MSJC 2013
IF-RC-TG	18.5	0.72	0.48	1.04	1.15
IF-RC-SG	36.5	0.94*	0.99	1.13	1.26

* Δ_0=0 for side gaps

Table 5.10 shows that BS 5628 method overestimates the strength of gapped infills in

general. The overestimation is significant when the top gap specimen is concerned and to a much lesser degree (almost accurate) for the side gapped specimen. It can be concluded from these observations that 1) BS 5628 method, derived originally for one-way arching, might be suitable for side gapped specimens as they are essentially one-way arching specimens; 2) BS 5628 method, is not suitable for top gapped specimens as they are essentially supported on three sides.

Dawe and Seah's method provided the accurate estimate of the out-of-plane strength for the infill with top gap with an experimental-to-analytical ratio of 1.04. The yield line pattern suggested by this method compared well with the experimental observation. While formulated similarly to Dawe and Seah's method, MSJC 2013 method considered only one-way arching of a gapped infill, regardless of the size of the gap. It is thus reasonable to observe a similar underestimation only to a greater degree than Dawe and Seah's method. The advantage of the MSJC method is its applicability to both top and side gaps but both methods do not provide any guidelines on the size of the gap. More data is in need to make further assessment on whether this level of accuracy will be maintained for different gap sizes and gap locations.

5.3 DISPLACEMENT EVALUATION

A summary of exiting analytical methods for calculation of out-of-plane displacement is

presented in Table 5.11.

Table 5.11 Analytical Methods for Out-of-Plane Displacement

Method	Out-of-Plane Displacement	Note
Flanagan and Bennett (1999)	$\frac{\Delta_{ult}}{h} = \frac{0.002\left(\frac{h}{t}\right)}{1+\sqrt{1-0.002\left(\frac{h}{t}\right)^2}}$	Valid for h/t ratios up to 25
Klingner et al. (1996)	$x_{yv} = \frac{tf'_m}{1{,}000E\left[1-\frac{h}{2\sqrt{(h/2)^2+t^2}}\right]}$	For one-way vertical arching For one-way horizontal arching: h is replaced with l

Table 5.12 lists comparison results in terms of ratios of experimental to analytical values ($\Delta_{ult}/\Delta_{ana}$) including Sepasdar's and current studies. These are displacements corresponding to the ultimate load.

Table 5.12 Summary of Out-of-Plane Displacement Evaluation

ID	Test Result	Ratio of Experimental to Analytical Results ($\Delta_{ult}/\Delta_{ana}$)	
	Δ_{ult} (mm)	Klingner et al. (1996)	Flanagan and Bennett (1999)
IF-RC-DO	7.9	0.65	0.72
IF-RC-ID	7.7	0.64	0.70
IF-RC-TG	3.9	0.32	0.35
IF-RC-SG	7.4	0.61	0.67
IF-S	15.1	1.25	1.37
IF-ND	12.5	1.04	1.14
IF-W-ND	4.3	0.36	0.39
IF-D1	6.6	0.55	0.60
IF-D2	9.9	0.82	0.90

The two methods provide a more or less same trend. It appears that for all "irregular" infills, both methods overestimate the deflection to an average experimental-to-analytical ratio of

0.59. It can be concluded that the two methods are not suitable for evaluating infills with "irregularity". On the other hand, two methods performed better for "regular" infills with experimental-to-analytical ratio close to but greater than unity, indicating a conservative estimate. Between the two methods, the one by Klingner et al. (1996) provided the better estimate. This may be attributed to the fact that Klingner et al.'s equation considered the effect of masonry compressive strength and modulus of elasticity on the out-of-plane displacement whereas Flanagan and Bennett's equation is only dependent on the infill slenderness. However, neither methods takes into account the effect of the bounding frame. The experimental observation showed that the specimen IF-S developed more out-of-plane displacement than the specimen IF-ND. It suggests that the bounding frame could affect the out-of-plane displacement of infill. It is then worthwhile for future research to investigate how to incorporate the above described factors into the displacement calculation.

5.4 DUCTILITY

Ductility is the measure of a structure's ability to undergo deformation beyond yield level while maintaining most of its load carrying capacity. The greater ductility of structure, the greater reduction of the design seismic force. In seismic design codes (NBCC 2015), the ductility factor is used to design the reduction in seismic force, and NBCC 2015 permits the design seismic load is reduced by a factor of 1 to 5 depending on the type of seismic resisting systems, and the typical ductility factor used in design for unreinforced masonry is 1.0. However, there is no provision to provide specified value or formulation for the ductility factor of masonry infilled wall under out-of-plane load.

As the experimental results showed that most of out-of-plane displacement was developed after the infill reached its 60% strength, it is reasonable to define the out-of-plane ductility factor (R) as the ratio of the out-of-plane displacement at ultimate load to the out-of-plane displacement corresponding to 60% of the ultimate load, as expressed in Eqn [5-2].

$$R = \frac{\Delta_{ult}}{\Delta_{0.6Pult}} \qquad [5\text{-}2]$$

Table 5.13 summaries the out-of-plane ductility factor (R) calculated using Eqn [5-2] for each specimen in the current and Sepasdar's studies. As shown in Table 5.13, the ductility factor of all masonry infilled frames is greater than 2.0 with an average value of 4.9, which is much greater than the specified ductility factor of 1.0 for unreinforced masonry structure

in NBCC 2015.

Table 5.13 Summary of the Ductility for Each Specimen

ID		P_{ult} (kN)	Δ_{ult} (mm)	$0.6P_{ult}$ (kN)	$\Delta_{0.6Pult}$ (mm)	R
Current Study	IF-RC-DO	36.2	7.9	21.7	1.6	4.9
	IF-RC-ID	37.6	7.7	22.4	2.1	3.7
	IF-RC-TG	18.5	3.9	11.1	1.6	2.4
	IF-RC-SG	36.5	7.4	21.9	2.1	3.5
	IF-S	34.3	15.1	20.6	2.9	5.2
Sepasdar (2017)	IF-ND	66.3	12.5	39.8	1.4	8.9
	IF-W-ND	43.7	4.3	26.2	0.7	6.1
	IF-D1	44.4	6.6	26.6	1.0	6.6
	ID-D2	26.4	9.9	15.8	3.9	2.5

It was also found that the ductility factor of the infilled RC frame is 1.7 times that of the infilled steel frame. This is attributed to the fact that the RC frame provides stiffer boundary support and thus greater arching action which enabled the infill to experience more deflection before failure. This indicates that contrary to the conventional thinking where steel frames are more ductile then RC frames, when the out-of-plane loading is concerned, RC frames outperforms the steel frames. When the in-plane prior damage is concerned, the out-of-plane ductility factor of infill decreases as the in-plane damage level increases and an approximate exponentially decreasing trend is shown in Figure 5.2. As the infill is intended to act as lateral load resisting element, the interaction of in-plane and out-of-plane forces, especially in a seismic event, needs to be considered in design.

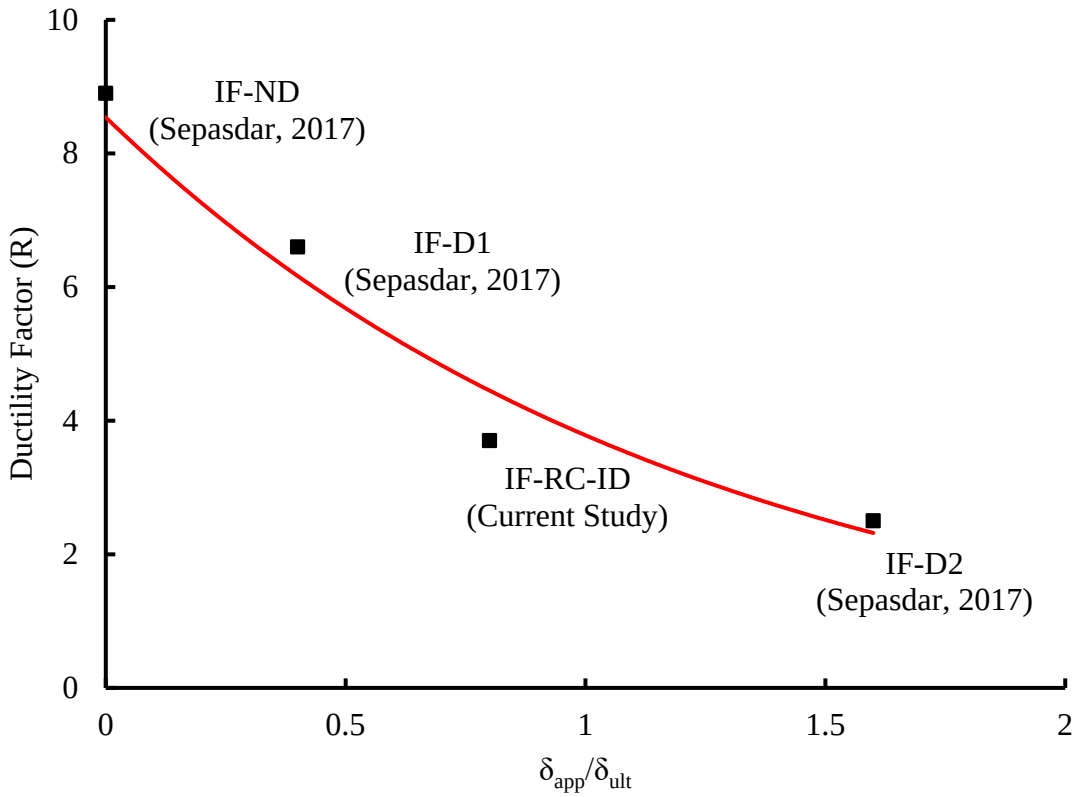

Figure 5.2 Relationship Between Prior In-Plane Displacement Ratio, $\delta_{app}/\delta_{ult}$, and Ductility Factor

CHAPTER 6 SUMMARY AND CONCLUSIONS

6.1 SUMMARY

This study was conducted as an integral part of an on-going research framework on the out-of-plane behaviour of masonry infilled frames. The main objective of this study was to further investigate the out-of-plane behaviour and strength of masonry infills with a focus on the effect of infill openings, frame-to-infill interfacial gaps, prior in-plane damage, and bounding frames. Five infilled frame specimens including four masonry infilled RC frames and one masonry infilled steel frame were subjected to uniform distributed out-of-plane loading to failure. All the masonry infills were fabricated with the same geometry but with different parameters, and the masonry infills were constructed using half scaled standard 200 mm concrete masonry units. Four RC frame specimens included one having a door opening accounting for 17.6% of the infill area, one having prior in-plane damage and two having frame-to-beam interfacial gaps. The steel frame specimen served as a control specimen to be compared with the RC frame control specimen. During the test, the general behaviour, cracking and failure pattern, load vs. displacement curve, and out-of-plane displacement profile throughout loading history were recorded. The effect of opening, frame-to-infill interfacial gaps, prior in-plane damage, and bounding frames was presented and discussed. The validity of several analytical methods proposed by various researchers as well as those specified in the current American and Canadian masonry standards for out-

of-plane strength and displacement were assessed using the experimental results.

6.2 CONCLUSIONS

The following conclusions are drawn from this study:

Failure mode under out-of-plane loading:

- All specimens tested under out-of-plane loading had a sudden and volatile failure characterized by out-of-plane collapse of the infill. The initiation of the collapse was identified as web shear failure of the masonry units.

- The studied parameters (infill opening, interfacial gap, prior in-plane damage) were shown to cause changes in the cracking and failure pattern from a “regular” specimen.

Effect of opening:

- Comparing with the infill without opening, the door opening (17.6% of the infill area) resulted in about 26% reduction in the cracking load and about 45% reduction in the ultimate load under out-of-plane loading.

- Comparing with the infill with a window opening of a similar opening area, the infill with door opening attained 17% less ultimate load, indicating a door configuration is more detrimental to the infill strength than a window configuration.

Effect of prior in-plane damage:

- Compared with the infill with no prior damage, the prior damage sustained from in-plane loading resulted in a reduction in the out-of-plane strength of the infill. The more severe the prior damage, the greater the reduction.
- Combining the results from this and an earlier study, an approximately linear relationship exists between the out-of-plane ultimate strength reduction and the prior in-plane damage level.

Effect of interfacial gap:

- Comparing with the infill without interfacial gaps, the presence of gaps, whether at the frame-to-beam or frame-to-column interfaces, resulted in reductions in infill strength although to different degrees. A 10 mm gap caused about 72% reduction in strength when it was at the frame-to-beam interface and 45% reduction when it was at frame-to-column interface. A frame-to-beam gap appeared to be more detrimental than a frame-to-column gap.
- The cracking pattern of specimen with the top gap was similar to a yield line pattern of a wall being three-side supported and one-side free, and the specimen with the side gap developed arching action in the vertical span direction.

Effect of boundary frames:

- Comparing with the masonry infilled RC frame specimen, the infill bounded by a steel frame resulted in a 40% less cracking load and a 48% less ultimate load under out-of-plane loading. The RC frame was shown to result in larger infill deflection and thus ductility than the steel frame.

Evaluation of analytical methods:

- For "regular" specimens (with no opening, no gaps, no prior damage), none of the methods is able to produce consistently accurate estimate for both RC and steel frame specimens. For RC frames, the methods proposed by Moghaddam and Goudarzi (2010) and Dawe and Seah (1989) performed better with P_{ult}/P_{ana} greater than but close to unity. For steel frames, the methods proposed by FEMA 356 and Angel (1994) are considered better methods.

- For "irregular" specimens with parameters, Angel's method for considering in-plane prior damage and Flanagan and Bennett's method for considering infill openings showed significant disparity with the experimental results; whereas methods by Dawe and Seah and MSJC for interfacial gap consideration performed better.

It is cautioned that more physical results covering more variations of parameters are in need to provide a thorough assessment of performance of existing methods. However, the inadequacy of existing methods in providing treatment of out-of-plane behaviour and

strength has been demonstrated through available data.

REFERENCES

Akhoundi, F., Vasconcelos, G., Lourenco, P., Silva, L. (2016). Out-of-plane response of masonry infilled RC frames: Effect of workmanship and opening. *16th International Brick and Block Masonry Conference*, Pádua, Italy.

Abrams, D. P., EERI, M., Angel, R., Uzarski, J., (1996). Out-of-plane strength of unreinforced masonry infill panels. *Earthquake Spectra*, 12(4)825-844.

Anderson, H., (1984). Arching action in transverse laterally loaded masonry wall panels. *The Structural Engineer,* 62B(1)12-23.

Angel, R. (1994). Behavior of reinforced concrete frames with masonry infill walls. Ph.D. Dissertation, the University of Illinois at Urbana-Champaign.

ASTM A370 (2012). Standard Test Methods and Definitions for Mechanical Testing of Steel Products. ASTM International, West Conshohocken, PA.

ASTM C1314 (2016). Standard test methods for compressive strength of masonry prisms. ASTM International, West Conshohocken, PA.

ASTM C140/C140M (2016). Standard test methods for sampling and testing concrete masonry units and related units. ASTM International, West Conshohocken, PA.

ASTM C143/C143M (2015). Standard test method for slump of hydraulic-cement concrete. ASTM International, West Conshohocken, PA.

ASTM C270 (2014). Standard specification for mortar for unit masonry. ASTM international, West Conshohocken, PA.

ASTM C39/C39M (2016). Standard test method for compressive strength of cylindrical concrete specimens. ASTM International, West Conshohocken, PA.

ASTM E8 (2008). Standard test methods for tension testing of metallic materials. ASTM International, West Conshohocken, PA.

Bennett, R. M., Fowler, J.J., and Flanagan, R. D. (1996). Shaking table testing of structural clay tile infilled frames. *1996 North American Masonry Conference*.

BS 5628 (2005). Code practice for Use of masonry: Structural use of unreinforced masonry. British Standard Institution, BSI, London.

CAN/CSA A165 (2015). CSA standards on concrete masonry units. Mississauga, ON, Canada: Canadian Standard Association.

CAN/CSA A179-04 (2014). Mortar and grout for unit masonry**.** Mississauga, ON, Canada: Canadian Standard Association.

CAN/CSA A23-3 (2014). Design of concrete structures. Mississauga, ON, Canada: Canadian Standard Association.

CAN/CSA S304-14 (2014). Design of masonry structures. Mississauga, ON, Canada: Canadian Standard Association.

Chen, X. (2016). Numerical study of the in-plane behaviour of concrete masonry infills bounded by steel frames. Doctoral Thesis, Dalhousie University.

Dafnis, A., Kolsch, H., and Reimerdes, H. (2002). Arching in masonry walls subjected to earthquake motions. *Journal of Structural Engineering,* ASCE,128(2): 153-159.

Dawe, J. L., and Seah C. K. (1989). Out-of-plane resistance of concrete masonry infilled panels. *Canadian Journal of Civil Engineering*, 16:854-864.

Drysdale, R.G., and Hamid, A.A. (2005). Masonry structures: behaviour and design. Mississauga, Ontario: Canadian Masonry Design Centre.

Federal Emergency Management Agency (FEMA). (2000). NEHRP guideline for the seismic rehabilitation of buildings. FEMA-356, Building Seismic Safety Council, Washington, D.C.

Flanagan, R. D., and Bennett, R. M. (1993). Uniform lateral load capacity of infilled frames. *1994 ASCE Structure Congress*.

Flanagan, R. D., and Bennett, R. M. (1999). Arching of masonry infilled frames: comparison of analytical methods. Practice Periodical on Structural Design and Construction, ASCE, 4(3):105-110.

Furtado, A., Rodrigues, and H., Arêde, A. (2016). Experimental evaluation of out-of-plane capacity of masonry infill walls. *Journal of Engineering Structures,* ELSEVIER, 111:48-63.

Gabrielsen, and Kaplan K. (1976). Arching in masonry walls subjected to out-of-plane forces. NBS Building Science Series 106, National Workshop on Earthquake Resistant Masonry Construction.

Gabrielsen, B., and Wilton C. (1974). Shock tunnel tests of arched wall panels. Report No 7030-19 URS Research Company, San Mateo, Ca.

Gabrielsen, B., Wilton C., and Kaplan K. (1975). Response of arching walls and debris from interior walls caused by blast loading. Report No 7030-23, URS Research Company, San Mateo, Ca.

Henderson R. C., Fricke K. E., and Jones W. D. (2003). Summary of a large- and small-scale unreinforced masonry infill test Program. *Journal of Structural Engineering*, ASCE, 129(12): 0733-9445.

Hu, C. (2015). Experimental study of the effect of interfacial gaps on the in-plane behaviour of masonry infilled RC frames. Master Thesis, Dalhousie University.

Klingner, R. E., Rubiano, N. R., Bashandy, T. R., and Sweeney, S. C. (1996). Evaluation and analytical verification of shaking table data from infilled frames. Part 2: Out of plane behavior. *Proceeding 7th North American Masonry Conference*, 521–532.

Masonry Standard Joint Committee (2013). Building code requirements for masonry structures. ACI 530/ASCE 5/TMS 402, American Concrete Institute, Detroit.

Mays, G. C., Hetherington, J. G., and Rose, T. A. (1998). Resistance deflection functions for concrete wall panels with openings. *Journal of Structural Engineering,* ASCE, 124(5):579–587.

McDowell, E. L., McKee, K. E., and Sevin, E., (1956). Arching action theory of masonry walls. *Journal of the Structural Division*, Proceeding of ASCE, 82(2)915-1-915-18.

Misir, I.S., Ozcelik, O., Girgin, S.C., Yucel, U. (2015). The behavior of infill walls in RC frames under combined bidirectional loading. *Journal of Earthquake Engineering,* 00:1-28.

Moghaddam, H., and Goudarzi, N., (2010). Transverse resistance of masonry infills. *Journal of Structural Engineering*, ASCE, 107(4)461-467.

Monk, C.B. (1958). Resistance of structural clay masonry to dynamic forces. Research Report No.7, Structural Clay Products Research Foundation, Geneva, Illinois.

NBCC (2015). National building code of Canada. Institute for Research in Construction, NRCC, Ottawa, Ontario.

Porto, F.d., Guidi, G., Benetta, M.D., and Verlato, N. (2013) Combined in-plane/out-of-plane Experimental Behaviour of Reinforced and Strengthened Infill masonry walls. *12th Canadian Masonry Symposium*.

Sepasdar, R. (2017). Experimental investigation on the out-of-plane behaviour of concrete masonry infilled frames. Master Thesis, Dalhousie University.

APPENDIX A SAMPLE CALCULATION OF INFILLS

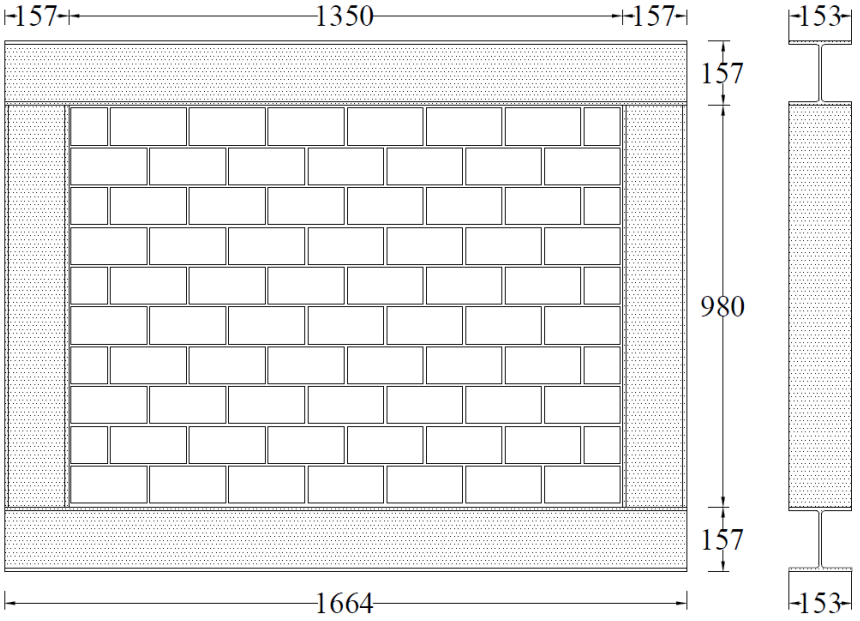

Figure A.1 Infilled Frame Specimen IF-S (unit: mm)

Specimen IF-S was taken as the example for the sample calculation.

Infill Properties:

t = 90 mm h = 980 mm l = 1350 mm

Concrete block with Type N mortar, and the flexural tensile strength of masonry is estimated based on CSA S304-14 (2014)

f'_m = 9.0 MPa E_m = 7650 MPa γ = 0.9 (according to the suggestion in BS 5628)

f_{tn} = 0.3 MPa (flexural tensile strength of masonry normal to bed joints)

f_{tp} = 0.55 MPa (flexural tensile strength of masonry parallel to bed joints)

Frame Properties:

E_f = 201172 MPa G_f = 77373.9 MPa F_y = 402 MPa

$I_b = I_c = 1.72x10^7$ mm^4 $J_b = J_c = 1.01x10^5$ mm^4

Arching Action Analysis:

Several analytical methods have been developed by various researchers to compute the out-of-plane strength of masonry infills. The following presents sample out-of-plane strength calculations using three methods by Dawe and Seah (1989), Angel (1994) and BS 5628 first principle mechanics.

1. Dawe and Seah's method (1989):

$$q_{ult} = 800(f'_m)^{0.75}t^2(\alpha/L^{2.5} + \beta/H^{2.5})$$

$$= 800 \times 9.0^{0.75} \times 90^2(43.5/1350^{2.5} + 37.1/980^{2.5}) = 63.5 \text{ kPa}$$

where

$$\alpha = \frac{1}{H}(EI_cH^2 + GJ_ctH)^{0.25}$$

$$= \frac{1}{980}(201172 \times 1.72 \times 10^7 \times 980^2$$

$$+ 77374 \times 1.01 \times 10^5 \times 90 \times 980)^{0.25} = 43.6$$

$$\beta = \frac{1}{L}(EI_b L^2 + GJ_b tL)^{0.25}$$

$$= \frac{1}{1350}(201172 \times 1.72 \times 10^7 \times 1350^2$$

$$+ 77374 \times 1.01 \times 10^5 \times 90 \times 1350)^{0.25} = 37.1$$

2. Angel's method (1994):

The specimen IF-S did not have prior in-plane damage, so the prior in-plane damage reduction factor (R_1 = 1.0). As discussed in Chapter 5, the flexural stiffness of bounding frame in specimens IF-S is less than the limit of 1.03×10^{13} N-mm^2, so it is assumed that the flexural stiffness reduction factor (R_2) equals 0.357.

$$q = \frac{2f'_m}{(\frac{h}{t})} R_1 R_2 \lambda = \frac{2 \times 9.0}{(\frac{980}{90})} \times 1.0 \times 0.357 \times 0.05269 = 31.1 \text{ kPa}$$

where

$$\lambda = 0.154\exp\left(-0.0985\frac{h}{t}\right) = 0.154\exp\left(-0.0985\frac{980}{90}\right) = 0.053$$

3. Mechanics of Rigid Arching Analysis:

The zero out-of-plane wall displacement (Δ_0 = 0) was suggested in for calculation of the out-of-plane strength of infill. The Δ_0, however, in the following equation is an estimate of deflection amount due to wall axial shortening.

1) One-way Arching Action:

$$\varepsilon_m^v = \frac{f'_m}{E_m} = \frac{9.0}{7650} = 0.00118$$

$$g_0^v = \varepsilon_m^v \times h = 0.00118 \times 980 = 1.15$$

$$\Delta_0 = \frac{g_0^v \times h}{4 \times \gamma \times t} = \frac{1.153 \times 980}{4 \times 0.9 \times 90} = 3.49\text{mm}$$

$$C_v = \emptyset_m \times f'_m \times (1-\gamma) \times t = 1 \times 0.85 \times 9.0 \times (1-0.9) \times 90 = 68.9\text{kN/m}$$

$$w_v = \frac{8C}{h^2}(\gamma t - \Delta_0) = \frac{8 \times 68.9}{980^2}(0.9 \times 90 - 3.49) = 44.5\ \text{kPa}$$

2) Two-way Arching Action:

As mentioned previously, Drysdale and Hamid (2005) proposed that the extent at which the horizontal arching participates in load carrying capacity was calculated considering that the out-of-plane displacement for arching in both direction was identical. So, the out-of-plane displacement for vertical arching was also used to calculate the participation of horizontal arching action.

$$g_0^h = \frac{4 \times \Delta_0 \times \gamma \times t}{l} = \frac{4 \times 3.49 \times 0.9 \times 90}{1350} = 0.84\text{mm}$$

$$\varepsilon_m^h = \frac{g_0^h}{l} = \frac{0.84}{1350} = 0.00062$$

$$f_c = \varepsilon_m^h \times E_m = 0.00062 \times 7650 = 4.74\text{MPa}$$

$$C_h = \emptyset_m \times f_c \times (1-\gamma) \times t = 1 \times 0.85 \times 4.76 \times (1-0.9) \times 90 = 36.3\text{kN/m}$$

$$w_h = \frac{8C_h}{l^2}(\gamma t - \Delta_0) = \frac{8 \times 36.3}{1350^2}(0.9 \times 90 - 3.49) = 12.3\ \text{kPa}$$

Total out-of-plane strength is calculated as:

$$w = w_h + w_v = 44.5 + 12.3 = 56.8\ \text{kPa}$$

The above calculation is repeated using experimentally obtained out-of-plane wall displacement ($\Delta_0 = \Delta_{exp}$) in the strength equation as follows.

3) One-way Arching Action:

$$C_v = \emptyset_m \times f'_m \times (1-\gamma) \times t = 1 \times 0.85 \times 9.0 \times (1-0.9) \times 90 = 68.9\text{kN/m}$$

$$w_v = \frac{8C}{h^2}(\gamma t - \Delta_0) = \frac{8 \times 68.9}{980^2}(0.9 \times 90 - 15.1) = 37.8\ \text{kPa}$$

4) Two-way Arching Action:

$$g_0^h = \frac{4 \times \Delta_0 \times \gamma \times t}{l} = \frac{4 \times 15.1 \times 0.9 \times 90}{1350} = 3.6\text{mm}$$

$$\varepsilon_m^h = \frac{g_0^h}{l} = \frac{3.6}{1350} = 0.0027$$

$$f_c = \varepsilon_m^h \times E_m = 0.0027 \times 7650 = 20.5\text{MPa}$$

As the corresponding horizontal compressive stress of masonry was larger than the actual compressive stress of masonry, so the $f_c = f'_m = 9.0$ MPa was suggested in design for calculation of the out-of-plane strength of infill.

$$C_h = \emptyset_m \times f_c \times (1-\gamma) \times t = 1 \times 0.85 \times 9.0 \times (1-0.9) \times 90 = 68.9\text{kN/m}$$

$$w_h = \frac{8C_h}{l^2}(\gamma t - \Delta_0) = \frac{8 \times 68.9}{1350^2}(0.9 \times 90 - 15.1) = 19.9\ \text{kPa}$$

Total out-of-plane strength is calculated as:

$$w = w_h + w_v = 37.8 + 19.9 = 57.7\ \text{kPa}$$

Flexural Analysis:

Moment of inertia of the wall for bending in the vertical direction is:

$$I_m = \frac{bh^3}{12} - \frac{b(t - t_e)^3}{12} = \frac{10^3 \times 90^3}{12} - \frac{10^3 \times (90 - 2 \times 17)^3}{12} = 4.61 \times 10^7 \frac{mm^4}{m}$$

where t_e is the thickness of the face shell for the block.

The section modulus of the wall is:

$$S_m = \frac{I_m}{t/2} = \frac{4.61 \times 10^7}{90/2} = 1.02 \times 10^6 \frac{mm^3}{m}$$

1. Flexural action analysis for cracking load:

$$q = \frac{f_{tn} S_m}{h^2/8} = \frac{0.3 \times 1.02 \times 10^6}{980^2/8} = 2.55 \text{ kPa}$$

2. Yield line analysis:

The analysis of panel simply supported on four sides using yield line method is used to estimate the out-of-plane strength of the infill, and the Figure A. 2 shows the idealized yield line pattern of specimen IF-S.

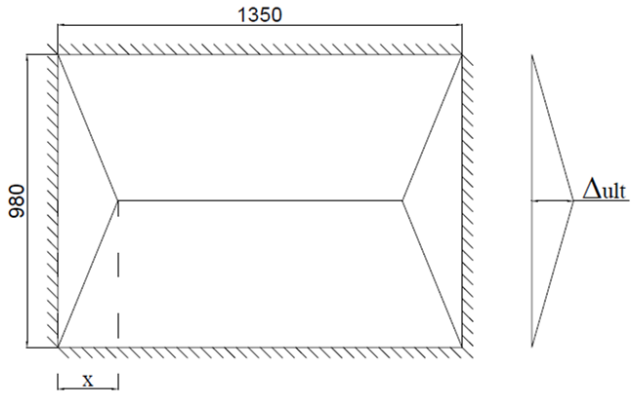

Figure A.2 Yield Lines of Specimen IF-S (unit: mm)

The moment resistant of the wall is:

$$M_{rh} = f_{tp}S_m = 0.65 \times 1.02 \times 10^6 = 0.66\frac{kN \cdot m}{m}$$

$$M_{rv} = f_{tn}S_m = 0.3 \times 1.02 \times 10^6 = 0.31\frac{kN \cdot m}{m}$$

In this calculation, the out-of-plane uniformly distributed load (q) and x can be calculated by realizing that external work and internal work are the same. The external work is equal to the out-of-plane load (q) multiplied by the out-of-plane displacement (Δ_{ult}), and the internal work is equal to the moment per unit length parallel and normal to bed joints (M_{rh} and M_{rv}) multiplied by the corresponding rotations.

$$2q\frac{490x}{2}\frac{\Delta_{ult}}{3} + 2q\frac{490x}{2}\frac{\Delta_{ult}}{3} + q[490(1350 - 2x)]\frac{\Delta_{ult}}{2} = 2M_{rv}\frac{\Delta_{ult}}{490}x + 2M_{rh}\frac{\Delta_{ult}}{x}490 + M_{rv}(1350 - 2x)\frac{\Delta_{ult}}{490}$$

Δ_{ult} is removed from both sides of the equation. The distance (x) is the value that results in smallest out-of-plane load. Therefore, it can be calculated by substituting M_{rv} and M_{rh} into the above equation, rearranging the equation base on the out-of-plane load (q), differentiating q with respect to x and set it to zero, and then solving for x. The minimum out-of-plane load (q) occurs at x = 694.3 mm, and results in a value of 8.2 kPa.

APPENDIX B SAMPLE CALCULATION ON FILLET WELDING DESIGN

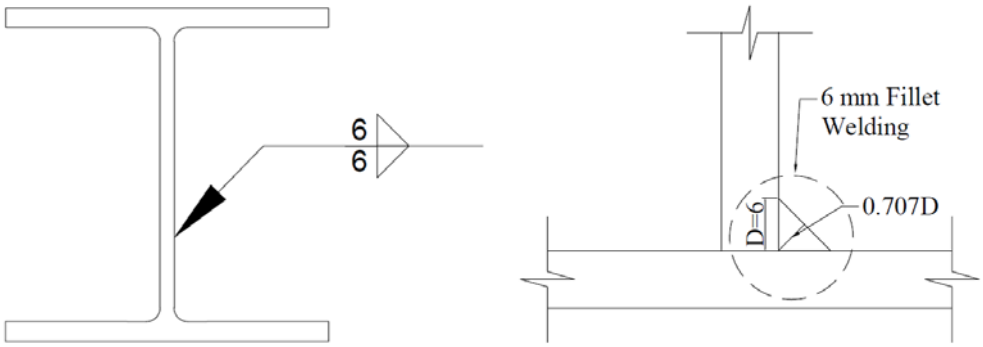

Figure B.1 Details of Beam-Column Fillet Welding

The method proposed by BS 5628 (2005) is used to determine the maximum out-of-plane load that the fillet welding connection can resist.

Electrode properties:

X_u = 490 MPa

Welding properties:

D = 6 mm

Effective area of the effective throat the weld:

$$A_w = \frac{\sqrt{2D^2}}{2} \times L = 0.707DL = 0.707 \times 6 \times 1$$

Assumption One: Only the beam of frame carried the out-of-plane load

The length of welding is:

$$L_{w-t} = L_{w-w} + L_{w-f} = 266.8 + 250.8 = 517.6 \text{ mm}$$

where $L_{w\text{-}w}$ and $L_{w\text{-}f}$ represent the length of welding on web and flange, respectively.

The shear resistant of the fillet welding per mm is:

$$V_r = 0.67\emptyset_w A_w X_u (1 + 0.5\sin^{1.5}\theta) M_w$$

$$= 0.67 \times 0.67 \times 0.707 \times 6 \times 1 \times 490 \times (1 + 0.5\sin^{1.5}90) \times 1.0$$

$$= 1.4\text{kN/mm}$$

The total shear resistant of the fillet welding for two beam-column connections is:

$$V_{r-total} = 2 \times V_r \times L_{w-t} = 2 \times 1.4 \times 517.6 = 1453.2\text{ kN}$$

Assume that the shear resistance of the fillet welding is equal to the thrust force acting on the beam, so the thrust force per unit length (C) is:

$$C = \frac{V_{r-total}}{l} = \frac{1453.2}{1.35} = 1073.4\text{ kN/m}$$

The maximum out-of-plane load corresponding to the shear resistant of the fillet welding and the assumption of 0 mm out-of-plane displacement of infill is:

$$w_h = \frac{8C}{h^2}(\gamma t - \Delta_o) = \frac{8 \times 1073.4}{980^2}(0.9 \times 90 - 0) = 724\text{ kPa}$$

<u>Assumption Two</u>: Only the column of frame carried the out-of-plane load

The shear resistant of the fillet welding per mm in transverse direction is:

$\theta_1 = 90^o$ which represents the orientation of the weld segment under consideration.

$\theta_2 = 90^o$ which represents the orientation of the weld segment in the joint that is nearest to 90^o.

$$V_r = 0.67\emptyset_w A_w X_u (1 + 0.5\sin^{1.5}\theta) M_w$$

$$= 0.67 \times 0.67 \times 0.707 \times 6 \times 1 \times 490 \times (1 + 0.5\sin^{1.5}90) \times 1.0$$

$$= 1.4\text{kN/mm}$$

where $M_w = \frac{0.85+\theta_1/600}{0.85+\theta_2/600} = \frac{0.85+90/600}{0.85+90/600} = 1.0$

The shear resistant of the fillet welding per mm in longitudinal direction is:

$\theta_1 = 0^o$ which represents the orientation of the weld segment under consideration.

$\theta_2 = 90^o$ which represents the orientation of the weld segment in the joint that is nearest to 90^o.

$$V_r = 0.67\emptyset_w A_w X_u (1 + 0.5\sin^{1.5}\theta) M_w$$

$$= 0.67 \times 0.67 \times 0.707 \times 6 \times 1 \times 490 \times (1 + 0.5\sin^{1.5}0) \times 0.85$$

$$= 0.79 \text{ kN/mm}$$

where $M_w = \frac{0.85+\theta_1/600}{0.85+\theta_2/600} = \frac{0.85+0/600}{0.85+90/600} = 0.85$

The total shear resistant of the fillet welding for two beam-column connections is:

$$V_{r-total} = 2 \times V_r \times L_{w-t} = 2 \times (1.4 \times 250.8 + 0.79 \times 266.8) = 1123.8 \text{ kN}$$

Assume that the shear resistance of the fillet welding is equal to the thrust force acting on the column, so the thrust force per unit length (C) is:

$$C = \frac{V_{r-total}}{h} = \frac{1123.8}{0.98} = 1146.7 \text{ kN/m}$$

The maximum out-of-plane load corresponding to the shear resistant of the fillet welding

and the assumption of 0 mm out-of-plane displacement of infill is:

$$w_h = \frac{8C}{h^2}(\gamma t - \Delta_0) = \frac{8 \times 1146.7}{1350^2}(0.9 \times 90 - 0) = 407.7 \text{ kPa}$$

Summary:

According to the arching action analysis based on BS 5628 (2005), it is found the out-of-plane load that the weld connection can resist is much larger than the out-of-plane load that the infill can resist.

APPENDIX C CALCULATION FOR INFILL WITH GAP

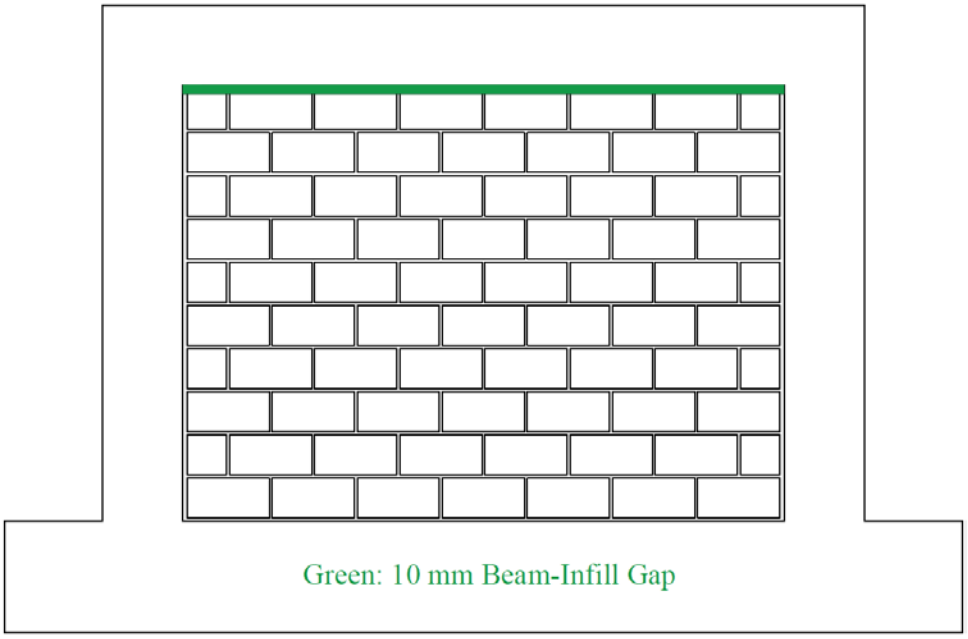

Figure C.1 Infilled Frame Specimen IF-RC-TG

The following presents a sample calculation of out-of-plane strength for gapped infills based on first principle mechanics.

Infill Properties:

t = 90 mm h = 980 mm l = 1350 mm g = 10 mm

f'_m = 7.9 MPa γ = 0.9 (according to the suggestion in BS 5628)

Maximum Gap:

The maximum gap that could exist in vertical direction is:

$$g \leq \frac{4(\gamma t)^2}{l} = \frac{4(0.9 * 90)^2}{980} = 26.8\text{mm}$$

The maximum gap that could exist in horizontal direction is:

$$g \leq \frac{4(\gamma t)^2}{l} = \frac{4(0.9 * 90)^2}{1350} = 19.4\text{mm}$$

Since the gap in this study is less than the allowable limit, the arching action will develop.

Mechanics of Rigid Arching Analysis:

1. The out-of-plane wall displacement ($\Delta_0 = \Delta_g$) corresponding to interfacial gap was used to calculate the out-of-plane strength of infill.

$$\Delta_g = \frac{gl}{4\gamma t} = \frac{10 \times 980}{4 \times 0.9 \times 90} = 30.2\text{mm}$$

$$C_v = \emptyset_m \times f'_m \times (1 - \gamma) \times t = 1 \times 0.85 \times 7.9 \times (1 - 0.9) \times 90 = 60.4\text{kN/m}$$

$$w_v = \frac{8C}{h^2}(\gamma t - \Delta_0) = \frac{8 \times 60.4}{980^2}(0.9 \times 90 - 30.2) = 25.5\ \text{kPa}$$

2. The experimental out-of-plane wall displacement ($\Delta_0 = \Delta_{exp}$) was used to calculate the out-of-plane strength of infill.

$$C_v = \emptyset_m \times f'_m \times (1 - \gamma) \times t = 1 \times 0.85 \times 7.9 \times (1 - 0.9) \times 90 = 60.4\text{kN/m}$$

$$w_v = \frac{8C}{h^2}(\gamma t - \Delta_0) = \frac{8 \times 60.4}{980^2}(0.9 \times 90 - 3.9) = 38.8\ \text{kPa}$$